An evaluation of new particle formation events in Helsinki during a Baltic Sea cyanobacterial summer bloom

Roseline C. Thakur[1], Lubna Dada[1,2,3], Lisa J. Beck[1], Lauriane L.J. Quéléver[1], Tommy Chan[1], Marjan Marbouti[1,12], Xu-Cheng He[1], Carlton Xavier[1], Juha Sulo[1], Janne Lampilahti[1], Markus Lampimäki[1], Yee Jun Tham[1,11], Nina Sarnela[1], Katrianne Lehtipalo[1,4], Alf Norkko[8,9], Markku Kulmala[1,5,6,7], Mikko Sipilä[1], Tuija Jokinen[1,10]

[1]Institute for Atmospheric and Earth System Research/Physics, Faculty of Science, 00014 University of Helsinki, Helsinki, Finland.
[2]School of Architecture, Civil and Environmental Engineering, École Polytechnique Fédérale de Lausanne, Lausanne, Switzerland
[3]Laboratory of Atmospheric Chemistry, Paul Scherrer Institute, 5232 Villigen PSI, Switzerland
[4]Finnish Meteorological Institute, Helsinki, Finland.
[5]Aerosol and Haze Laboratory, Beijing Advanced Innovation Center for Soft Matter Science and Engineering, Beijing University of Chemical Technology, 100089 Beijing, China.
[6]Joint International Research Laboratory of Atmospheric and Earth System Sciences, Nanjing University, 210023 Nanjing, China.
[7]Lomonosov Moscow State University, Faculty of Geography, 119991, Moscow, GSP-1, 1 Leninskiye Gory.
[8]Tvärminne Zoological Station, University of Helsinki, J.A. Palméns väg 260, FI-10900 Hangö, Finland
[9]Baltic Sea Centre, Stockholm University, Stockholm, Sweden
[10]Climate & Atmosphere Research Centre (CARE-C), The Cyprus Institute, P.O. Box 27456, Nicosia, CY-1645, Cyprus.
[11]School of Marine Sciences, Sun Yat-Sen University, Zhuhai 519082, China.
[12] Department of Electronics and Nano-engineering, Aalto University, 00076 Aalto, Finland.

Correspondence to: roseline.thakur@helsinki.fi

Abstract

Several studies have investigated New Particle Formation (NPF) events from various sites ranging from pristine locations, including ~~(boreal)~~ forest sites to urban areas. However, there is still a dearth of studies investigating NPF processes and subsequent aerosol growth in coastal yet semi-urban sites, where the tropospheric layer is a concoction of biogenic and anthropogenic gases and particles. The investigation of factors leading to NPF becomes extremely complex due to the highly dynamic meteorological conditions at the coastline especially when combined with both continental and oceanic weather conditions. Herein, we engage a comprehensive study of particle number size distributions and aerosol-forming precursor vapors at the coastal semi-urban site in Helsinki, Finland. The measurement period, 25 June 2019–18 August 2019, was timed with the recurring cyanobacterial summer bloom in the Baltic Sea region and coastal regions of Finland. Our study recorded several regional/local NPF and aerosol burst events during this period. Although the overall anthropogenic influence on ~~Sulfuric~~ sulfuric ~~Acid~~ acid (SA) concentrations was low during the measurement period,

Formatted: Superscript

Formatted: Font: 12 pt, Not Bold, Font color: Auto, English (United States), Border: : (No border), Pattern: Clear

Formatted: Font: 12 pt, Not Bold, Font color: Auto, English (United States), Border: : (No border), Pattern: Clear

Formatted: Font: 12 pt, Not Bold, Font color: Auto, English (United States), Border: : (No border), Pattern: Clear

Formatted: Default Paragraph Font

we observed that the regional or local NPF events, characterized by SA concentrations in the order of 10^7 molecules per cm^{-3} occurred mostly when the air mass travelled over the land areas. Interestingly, when the air mass travelled over the Baltic Sea, an area enriched with Algae and cyanobacterial blooms, high ~~Iodic~~ iodic ~~Acid~~ acid (IA) concentration coincided with an aerosol burst or a spike event at the measurement site. Further, SA-rich bursts were seen when the air mass travelled over the Gulf of Bothnia, enriched with cyanobacterial blooms. The two most important factors affecting aerosol precursor vapor concentrations, and thus the aerosol formation, were speculated to be (1) the type of phytoplankton species and intensity of bloom present in the coastal regions of Finland/ Baltic Sea and (2) the wind direction. During the events, most of the growth of sub-3 nm particles was probably due to SA, rather than IA or MSA, however much of the particle growth remained unexplained indicative of the strong role of organics in the growth of particles, especially in the 3–7 nm particle size range. Further studies are needed to explore the role of organics in NPF events and the potential influence of cyanobacterial blooms in coastal locations.

Keywords: coastal environment, particle growth, methane sulfonic acid, cyanobacterial summer bloom, sulfuric acid, iodic acid

1 Introduction

New particle formation (NPF) and growth of aerosols are regional processes occurring globally introducing a substantial aerosol load into the atmosphere. NPF has been observed in different environments, including pristine (Asmi et al., 2016; Jang et al., 2019; Jokinen et al., 2018), polluted boundary layers and urban areas (Kulmala et al., 2021; Kulmala et al., 2017; Manninen et al., 2010; Kulmala et al., 2016; Wang et al., 2017; Cai and Jiang, 2017; Deng et al., 2020; Yao et al., 2018; Du et al., 2021; Yan et al., 2021), boreal forests (Buenrostro Mazon et al., 2016; Dada et al., 2017; Kulmala et al., 2013; Kyrö et al., 2014; Leino et al., 2016; Nieminen et al., 2014; Rose et al., 2018), tropical forests (Artaxo et al., 2013; Wimmer et al., 2018) and mountain tops (Bianchi et al., 2016, 2020). Few studies have investigated NPF processes in a coastal environment although the coastal NPF research started quite early. The investigation of coastal aerosol events dates back to 1978, when the measurements of total aerosol number concentration were carried out at the Tasmanian coast (Bigg and Turvey, 1978). After that atmospheric nucleation was observed in the Southern hemisphere around the Antarctic coastline (O'Dowd et al., 1997), in Mace Head (Flanagan et al., 2005; McFiggans et al., 2004; O'Dowd et al., 2002), in coastal regions of China and Spain (Yu et al., 2019; Mc Figgans et al., 2010; Mahajan et al., 2011) and in open water regions of North East Greenland (Dall'Osto et

al., 2018). Most of these studies have identified biogenic emissions from marine algae as the main precursors driving the new particle formation in a perfect coastal setting.~~.~~

The measurements of gaseous precursors, meteorology and biogenic influences are important to study the coastal NPF, which may lead to the formation of coastal/marine clouds. Coastal clouds are the drivers of many coastal ecosystem (~~Manzoniet al 2012,~~ Carbone et al., 2013, Emery et al., 2018, Lawson et al., 2018). Any impact or fluctuations in the cloud formation may impact several other processes of the fragile coastal ecosystem. These coastal clouds demonstrate a high sensitivity to CCN (He et al., 2021) and they have a significant impact on the radiation budget because they have a high infrared emission and albedo when compared to the dark water bodies down below. In this study we highlight the type of NPF processes and their drivers in a semi-urban-coastal setting where the atmosphere could be a mixture of anthropogenic and biogenic emissions. Unlike the above mentioned previous studies which were mostly carried out in a perfect coastal environments where NPF would be most likely affected by the biogenic emissions, this study helps to evaluate the impact of urban emissions Vs coastal emissions on NPF and at large the cloud formation processes.

Formatted: Pattern: Clear (White)

Formatted: Line spacing: 1,5 lines

Formatted: Pattern: Clear (White)

Formatted: Pattern: Clear (White)

Formatted: Pattern: Clear (White)

Formatted: Pattern: Clear (White)

It is well documented that sulfuric acid (henceforth SA) is an important precursor to NPF in most environments (Almeida et al., 2013; Kulmala et al., 2013; Croft et al., 2016; Jokinen et al., 2017; Kirkby et al., 2011; Sipilä et al., 2010). The advancement in aerosol research, revealed that a binary system of SA and water is not sufficient to produce particles in ambient atmospheric conditions without stabilizing compounds (Benson et al., 2008; Duplissy et al., 2016; Kirkby et al., 2011). More recently, it has been found that a ternary system involving SA-ammonia-water or SA-amines-water yield much higher nucleation rates as compared to the binary system (Kulmala et al., 2000; Benson et al., 2008; Almeida et al., 2013; Glasoe et al., 2015; Kürten et al., 2016). In addition to these systems, organic compounds which are highly oxygenated - thus less volatile- have been found to contribute to secondary organic aerosol (SOA) mass in forested areas, mountain tops and anthropogenically influenced field sites (Ehn et al., 2014; Pierce et al., 2011; Riipinen et al., 2012; Zhang et al., 2009; Heikkinen et al. 2020; et al., 2020) and laboratory experiments have shown that they can contribute also to the first steps of NPF (Simon et al., 2020; Lehtipalo et al., 2018; Kirkby et al., 2016; Tröstl et al., 2016) .

Furthermore, another important molecular class, iodine as well as its related oxidized species play a crucial role in NPF especially in coastal areas (Allan et al., 2015; Mahajan et al., 2009; Raso et al., 2017; Sipilä et al., 2016) and in pristine marine locations (Baccarini et al., 2020; Beck et al., 2021; He et al., 2021). Some previous studies have reported the emissions of I_2 from the macroalgae at coastal sites (Huang et al., 2010; Peters et al., 2005; Saiz-Lopez and Plane, 2004).

Several studies from coastal sites like Roscoff, France (Mahajan et al., 2009; McFiggans et al., 2010), Mace Head, Ireland (O'Dowd et al., 2002) and other European coastlines (Mahajan et al., 2011; Saiz-Lopez et al., 2012) have reported iodine species initiating NPF. The reported events can be considered as aerosol burst events with high aerosol concentration and having exceptionally high initial growth rates (GR) (O'Dowd et al., 2002; McFiggans et al., 2004; Mahajan, et al., 2011). The study from the Roscoff coast suggests that the daytime emissions of I_2 ~~(~~produced by macroalgae~~)~~ during low tides drives the particle formation (McFiggans et al., 2010). The iodine oxides and/or oxoacids formed by the biogenic emissions from the micro- and macroalgae near the coastal regions are capable of self-clustering, which could form new particles with a diameter <3 nm and sometimes with a high gas concentration reaching up to 10^6 cm^{-3} or even more. Recent studies have shown that ion-induced ~~iodic acid~~IA nucleation proceeds at the kinetic limit and the overall nucleation rates (ion-induced nucleation + neutral nucleation) driven by iodine oxoacids (~~iodic acid, HIO_3~~IA and iodous acid, HIO_2) are high, even exceeding the rates of well-known precursors of NPF (He et al., 2021b, 2021a): ~~sulfuric acid~~SA with roughly 100 pptv ammonia under similar conditions (Sipilä et al., 2010). The rapid photolysis of I_2, (< 10 s), produces I atoms above the ocean surface and can be detected in high concentrations close to the source region (McFiggans et al., 2010). However, the compounds with longer lifetimes such as CH_3I (two days) provide a source of iodine throughout the troposphere (Saiz-Lopez et al. 2012).

~~Another important gaseous precursor of NPF, SA, could have different sources in Helsinki (Dada et al., 2020b; Väkevä et al., 2000).~~ Dimethyl sulfide (DMS) oxidation by OH radical in the daytime and by nitrate radical in the nighttime yields other aerosol precursor gases, such as methane sulfonic acid (henceforth, MSA) and SA (Barnes et al., 2006), which play a crucial role in the NPF processes. In a marine coastal environment, MSA concentrations, which are typically lower than those of SA, could be as low as 10% of SA concentration and could maximally reach 100% of SA concentration (Eisele and Tanner, 1993), yet MSA is a potential candidate to participate in the atmospheric nucleation and growth processes (Beck et al., 2021). The stability of heterogeneous MSA clusters have been studied in laboratory and modelling studies (Chen et al., 2020, 2015, 2016) but no study has yet documented MSA clusters in the ~~field. The~~field. The limited NPF studies in the semi-urban coastal regions and the dynamic coastal ~~atmospheric chemistry~~ meteorology drives the motivation of this research~~.~~. Another motivation for this research is that, till date ~~No~~ no detailed studies on the impact of biogenic emissions on ~~of~~ NPF events in Finland were done before ~~taking into account biogenic precursor gases near~~ in ~~the coast of Finland~~ despite the fact that extensive cyanobacteria blooms occur every year in the Baltic Sea region and neighboring water bodies (including Finnish lakes) (Kahru and Elmgren 2014), which could be a significant source of iodine

species, SA and MSA. ~~In addition, there is a lack of studies reporting the MSA concentrations in the atmosphere of Finland.~~ Increasing temperatures and the excessive nutrient load in the Baltic Sea promote algal growth (Kuosa et al., 2017; Suikkanen et al., 2007, 2013). According to HELCOM (Baltic Marine Environment Protection Commission), the Baltic Sea has warmed 0.3° C per decade, however after 1990 significantly faster at 0.6° C per decade and in Finnish coastal areas the warming is even faster with a 2° C increase since 1990 (Humborg et al. 2019). The amount of blue-green algae (i.e. cyanobacteria) has shown a statistically significant increase in open sea areas in the Gulf of Finland, Sea of Åland and the Sea of Bothnia in the last 40 years (Kahru and Elmgren, 2014). ~~Although nutrient pollution has showed a decreasing trend (Andersen et al., 2017), growing oxygen deficient waters recirculate nutrients and perpetuate cyanobacterial blooms (Funkey et al., 2014).~~ The increase in frequency and intensity of cyanobacterial blooms would increase the potential emission of biogenic gases changing the composition of the overlying atmosphere and the atmosphere of the neighboring sites, depending on the meteorological conditions. ~~Thus, this study was undertaken to understand particle formation processes, when the air plume is a mixture of anthropogenic as well as biogenic gases and particles as in the coastal semi-urban location in Helsinki, Finland.~~

~~Investigating the origin and chemistry of NPF events in an urban coastal setting could be quite challenging since precursor vapors of nucleation are likely a mixture of both anthropogenic and biogenic vapors from different sources. Further, pre-existing particles in the atmosphere affect the occurrence of NPF events by acting as sink for precursor gases and freshly formed particles preventing the latter from further growth.~~ In this semi-urban coastal setting the concentration of gaseous precursors and aerosol size distribution may be ~~These parameters, in turn, are~~ influenced by the local meteorological parameters such as wind direction, wind speed, (air mass) turbulences especially at the surface layer of the lower atmosphere. Coastal locations are dynamic environments with rapid changes in meteorological parameters, also making the study of NPF more challenging. ~~The meteorological condition could likely govern the removal of particles from the air stream preventing the growth of newly formed particles.~~

In this study, we aim at a thorough evaluation of aerosol precursor molecules with a detailed (NPF events) analysis during the cyanobacterial bloom period, in the coastal-city of Helsinki, Finland, from June to August (summer) 2019. ~~In addition, there is a lack of studies reporting the MSA concentrations in the atmosphere of Finland.~~This work evaluates the role of phytoplankton blooms and meteorological parameters in the NPF events observed during the measurement period. We also identify the major precursor vapor(s) and molecular clusters found during the aerosol events. Here, we formulate the hypothesis that gaseous precursors formed from the biogenic emissions from the surrounding marine areas could play an important role in the nucleation processes in Helsinki.

Formatted: Not Highlight
Formatted: Not Highlight
Formatted: Not Highlight
Formatted: Not Highlight
Formatted: Not Highlight
Formatted: Not Highlight
Formatted: Not Highlight
Formatted: Not Highlight
Formatted: Not Highlight
Formatted: Not Highlight
Formatted: Normal, Indent: First line: 2,3 cm

Although Helsinki is a coastal area yet the role of marine emissions on ~~New Particle Formation~~NPF processes has not been studied before.

2 Measurement Site and Methodology

~~To understand the chemical composition of the precursor vapors emitted from various sources around the site, the Chemical ionization Atmospheric Pressure interface-Time Of Flight mass spectrometer (CI-APi-TOF) was operated from the 4th floor laboratory of the Physicum building, Kumpula campus, University of Helsinki (60° 12' N, 24° 58' E ; 49m , a.m.sl). The other aerosol and trace gases instruments were operated at the SMEAR III station which is 180 m away from the mass spectrometric measurement site (Station for Measuring Ecosystem-Atmosphere Relation (SMEAR III), 60.20° N, 24.96° E; 25 m a.s.l.).~~

2.1 Measurement Site

The measurement sites are surrounded by coastal water bodies (<4km, Vanhankaupunginselkä), forests (<3km) and road connecting to the main city (<300m) as seen in figure 1. Overall Helsinki is located on a relatively flat land on the coast of the Gulf of Finland. The Helsinki Metropolitan area is about 765 km^2 with approximately one million inhabitants, counting together the city of Helsinki and the neighboring cities of Espoo, Vantaa, and Kauniainen. The climate in southern Finland can be classified as either marine or continental depending on the air-flows and pressure systems. Either way, the weather is milder than typically at the same latitude (60°N) mainly due to the Atlantic Ocean and the warm Gulf Stream.

Formatted: Indent: First line: 0 cm

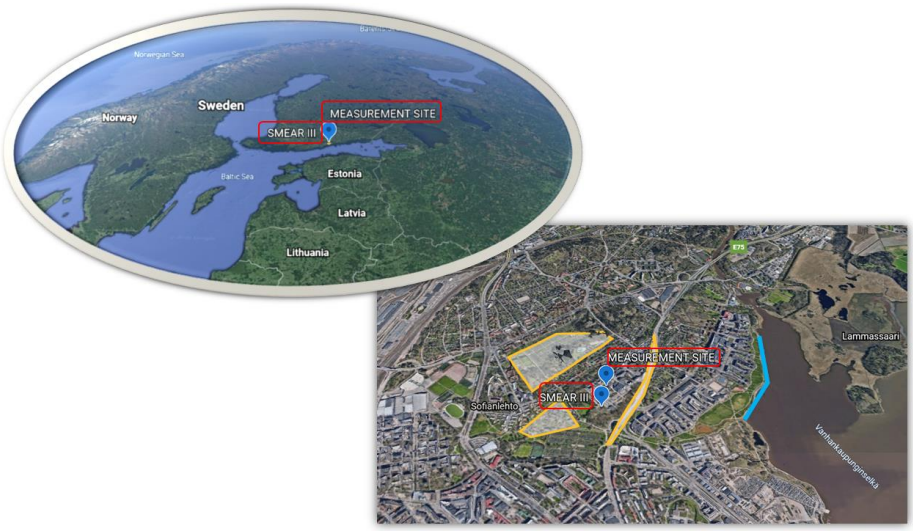

Figure 1: Map showing the two locations included in the study where instruments were operated (upper left panel). The yellow polygons on the left side of the measurement locations (on the lower right panel) shows forest/park with little or no traffic (West and Northwest, 300 m from the measurement site). The yellow double lines on the right of the measurement locations is the traffic area or the main road (E75) leading to the Helsinki city center (250 m east of the measurement site). The blue lines depict the coastline after which the lakes and coastal waters of Gulf of Finland start (1 km to the east from the measurement site) © Google Earth 2019

The site and measurement period (25 June 2019–18 August 2019) selected for this particular study are unique since this semi-urban location could be influenced by emissions from the recurring summertime blooms in the Baltic sea and the neighboring coastal regions. ~~We hypothesize that the biogenic emissions from summertime cyanobacterial blooms in the Baltic Sea and the neighboring water bodies could influence the new particle formation processes at this semi-urban location. The blooms in the Baltic Sea region are recurring phenomena during the summer.~~As per the SYKE press release (2019) the northern part of the Baltic Sea's main basin, entrance to the Gulf of Finland and south of the Åland Islands, were enriched with blue-green algae (cyanobacteria). The bloom lasted from June-August 2019. In coastal areas, bloom was mostly spotted in the Archipelago Sea, Gulf of Finland, Bothnian Sea and the Quark. The bloom situation developed rapidly and spatially highly variable, even over short distances. The fragmented nature of the coastal areas and changing wind and water currents makes the algal bloom conditions highly dynamic. ~~Increasing temperatures and the excessive nutrient load in the Baltic Sea promote algal growth (Kuosa et al., 2017; Suikkanen et~~

Formatted: Indent: First line: 0,63 cm

Field Code Changed

~~al., 2007, 2013). According to HELCOM (Baltic Marine Environment Protection Commission), the Baltic Sea has warmed 0.3° C per decade, however after 1990 significantly faster at 0.6° C per decade and in Finnish coastal areas the warming is even faster with a 2° C increase since 1990 (Humborg et al. 2019). The amount of blue-green algae (i.e. cyanobacteria) has shown a statistically significant increase in open sea areas in the Gulf of Finland, Sea of Åland and the Sea of Bothnia in the last 40 years (Kahru and Elmgren, 2014). Although nutrient pollution has showed a decreasing trend (Andersen et al., 2017), growing oxygen deficient waters recirculate nutrients and perpetuate cyanobacterial blooms (Funkey et al., 2014). The increase in frequency and intensity of cyanobacterial blooms would increase the potential emission of biogenic gases changing the composition of the overlying atmosphere and the atmosphere of the neighboring sites, depending on the meteorological conditions.~~

Field Code Changed

Field Code Changed

Field Code Changed

~~2.1~~ 2.2 Main Instruments

Formatted: Font: Bold

Formatted: Normal, No bullets or numbering

To understand the chemical composition of the precursor vapors emitted from various sources around the site, the Chemical ionization Atmospheric Pressure interface-Time Of Flight mass spectrometer (CI-APi-TOF) was operated from the 4th floor laboratory of the Physicum building, Kumpula campus, University of Helsinki (60° 12' N, 24° 58' E ; 49m , a.m.sl). The other aerosol and trace gases instruments were operated at the SMEAR III station which is 180 m away from the mass spectrometric measurement site (Station for Measuring Ecosystem-Atmosphere Relation (SMEAR III), 60.20° N, 24.96° E; 25 m a.s.l.).

The Atmospheric Pressure interface-Time Of Flight (APi-TOF) mass spectrometer is the state-of-the-art instrument for gas phase chemical composition investigations including aerosol precursor characterizations. Here the instrument is coupled with a nitrate based-chemical ionization (CI) inlet in order to measure neutral gas-phase molecules that are clustered and charged with a reagent ion. In our study we used inlet design as described by Eisele and Tanner (1993) and Kurten et al. (2011) and further used by Jokinen et al., 2012. The Time Of Flight (TOF) mass analyzer can detect molecules with masses up to 2000 Th with a mass resolution of 3600 Th/Th. More details on the working principle of the instrument and calibrations can be found in earlier studies (Junninen et al., 2010, Jokinen et al., 2012; Kürten et al., 2014). The sampled air was drawn in through a 1 m-long, "¾" diameter stainless steel tube with an average flow rate of 10 L~~l~~pm. In this study, the chemical ionization was done via nitrate ions (NO_3^-) through X-ray exposure of nitric acid (HNO_3, flow rate: 3 mL~~l~~pm), saturating the sheath air flow entering the CI (flow rate: 30 L~~l~~pm), the inlet flow of 10 L~~l~~pm was reached by using a 40 L~~l~~pm total flow. The instrument was calibrated prior to the experiment according to (Kürten et al., 2012) resulting in a calibration factor of 1.45×10^9 molecule

per normalized unit signal including the diffusion losses in the inlet line.

The resulting data (i.e. obtained signals) were averaged to 60 min before the mass calibration step performed through the MATLAB based program tofTools (Junninen et al., 2010). SA, MSA, IA concentrations are calculated after normalizing them with the reagent ions (NO_3^- and $(HNO_3)NO_3^-$) ~~The final concentration of the gases were derived~~ using the equation mentioned in Jokinen et al., 2012. The uncertainty range of the measured concentrations reported in this study is estimated to be −50%/+100% and the limit of detection, LOD: 4×10^4 molecules cm^{-3} (Jokinen et al., 2012). HOMs and IA have been estimated to be charged similarly at the kinetic limit as SA (Ehn et al., 2014; Sipilä et al., 2016), so the calibration factor for them should be similar, but please note, that the concentration of other compounds than SA can be highly uncertain due to different ionizing efficiencies, sensitivities and other unknown uncertainties. If MSA, IA or HOMs do not ionize at the kinetic limit these concentrations could be underestimated and thus, the concentrations reported in here should be taken as low limit values.~~Uncertainties of absolute concentration measured by CI-APi-TOF are estimated to be in the order of ±50%, while the uncertainties of relative changes in the concentration are smaller than 10% (Ehn et al., 2014). SA, MSA, IA concentrations and~~ The normalized signals of specific HOMs ~~(all figures presented in SI)~~ found in the study are calculated using high resolution peak fitting data. Please note that the concentration of ~~all~~ highly oxygenated molecules (HOM monomers and dimers) ~~sum (monomers and dimers) concentrations~~ were calculated from the ~~Unit~~ unit ~~Mass~~ mass ~~Resolution~~ resolution ~~(UMR)~~ data. ~~The~~

Neutral cluster and Air Ion spectrometer (NAIS, Airel Ltd., Estonia, Manninen et al., 2010; Mirme and Mirme, 2013) was used to measure the number size distribution of both positive and negative ions between 0.8 nm and 42.0 nm (electric mobility diameter). The NAIS also measures the number size distribution of total particles (neutral ~~and naturally charged~~) between 2.5–42.0 nm. ~~It uses two identical differential mobility analyzers (DMA, (Knutson and Whitby, 1975)) for simultaneous measurement of positive and negative ions.~~ NAIS consists of two multichannel electrical mobility analyzer columns (DMA's) operating in parallel. The columns differ by the polarity of the ions measured, but are otherwise identical (Mirme and Mirme, 2013) in operation. However they may differ in the transfer functions after calibration.The calibration procedure for the DMAs is presented in Mirme and Mirme, 2013. The ion mode measurements are corrected as in Wagner et al., 2016)".The flow rate of the instrument is 60 ~~lpm~~ Lpm which is split into 30 ~~lpm~~ Lpm for each DMA. The instrument was installed in the SMEAR III station. The data was recorded every 2 s.

Larger particles of 36~~–~~820 nm were measured using a twin differential mobility particle sizer (DMPS) (Aalto et al., 2001). The instrument was installed in the SMEAR III station. The time resolution of data is 10 minutes.

Formatted: Subscript

Formatted: Superscript

Formatted: Pattern: Clear

Formatted: English (United States)

Formatted: English (United States)

Formatted: Font: (Default) Times New Roman, Font color: Auto

Formatted: Font: (Default) Times New Roman, Font color: Auto

The size distribution of 1–3 nm particles was measured by a Particle Size Magnifier (PSM, Airmodus Ltd., Finland; Vanhanen et al., 2011) in series with a condensation particle counter (Airmodus Ltd., Finland). The PSM was operated by scanning the flow 0.1–1.3 lpm (continuously changing the saturator flow rate) which allows determining the 1–3 nm particle concentration and calculation of particle size distribution. The data was recorded for each second and the duration of each scan was fixed to 240 s. The raw data inversion was carried out through the kernel method (Chan et al., 2020; Lehtipalo et al., 2014). The raw data of the PSM employed a pretreatment filter that calculates the correlation between the observed particle concentration and the saturator flow rate of a single scan and discards scans with significant non-correlation or negative correlation (Chan et al., 2020).

Details about the Back-trajectory calculations, Chl*a* data analysis, meteorological and other calculations of parameters such as growth rates and formation rates are explained in the SI.

Formatted: Indent: First line: 2,3 cm

Formatted: Font: Italic

~~**2.2 Back trajectory calculations**~~

~~Back trajectories of the different NPF event days were calculated using the data from the Global data Assimilation System (GDAS) as input into the NOAA Hybrid Single-Particle Lagrangian Integrated Trajectory (HYSPLIT) model (http://www.arl.noaa.gov/ready/, Rolph et al., 2017; Stein et al., 2015). We used the isentropic trajectories as they incorporate vertical transport components. The 24 h back trajectories were calculated at an arrival height of 100 m a.g.l. The new trajectory starts every 6 hours. The frequency (%) of trajectory was calculated with the following equation (Eq. (1)).~~

~~$$\text{Traj. Freq.} = \frac{100 \times number\ of\ trajectories\ passing\ through\ each\ grid\ square}{number\ of\ trajectories} \quad (1)$$~~

~~The trajectory analysis was also performed using the Lagrangian particle dispersion model Flexpart v10.4 (Pisso et al., 2019; Stohl et al., 2005) mainly to assess the residence times of the air masses. Flexpart is a stochastic model used to compute trajectories of hypothetical particles, based on mean as well as turbulent and diffusive flow (Pisso et al., 2019). We have used Flexpart along with ECMWF ERA-Interim wind fields which has a spatial resolution of 1°×1° at three hour temporal resolution (Pisso et al., 2019). Flexpart was used to simulate 3-day backward trajectories starting from the particle release point located at SMEAR III (24.5° E, 60.1° N) for the event days. The residence times were normalized for clarity in the all the figures and is shown on a scale of 0 to 1 (Results are included in the supplementary information).~~

~~**2.3 Meteorological and other supporting data**~~

The meteorological data such as wind speed, wind direction, temperature, pressure, relative humidity and other supporting datasets e.g chlorophyll (Chl-*a*), SO_2, O_3 concentration and sea level information was additionally used to interpret the NPF events and support the observations of this work (See table S1 for details). The Chl-*a* satellite images were mapped through the GlobColour level-3. The GlobColour level-3 mapped products present merged data from SeaWIFS, MERIS, MODIS AQUA, VIIRS (0'Reily et al., 2000) sensors to provide robust and high coverage data for Chl-*a* measurements. The merging processes are described in Mangin, 2017. In this study, weighted average method (AVW) for retrieving daily Chl-*a* concentration (mg m^{-3}) for latitude: 45 °N to 80 °N and longitude: 20 °W to 60 °E was used. The GlobColour level-3 binned products have a resolution of 1/24° at the equator (i.e. around 4.63 km) for global products (Mangin, 2017).The details of these additional supporting data given in SI (Table S1).

2.4 Formation and growth rate calculations

The growth rates (GR) were calculated based on the 50% appearance time method using the NAIS ion data from both polarities, depending on the better quality polarity (Dada et al., 2020a; Dal Maso et al., 2016; Lehtipalo et al., 2014). This method uses particle number concentration at different size bins (D*p*), which are recorded as a function of time. The "appearance time" of particles of size D*p* is the time when their number concentration reaches 50% of its maximum value during the NPF event. To estimate the maximum GR (kinetic) that can be explained by the condensation of certain vapors, two parametrization methods were used, first by Nieminen et al., 2010 for IA and MSA and the second by Stolzenburg et al., 2020 for SA. The growth estimation from SA condensation recently provided by Stolzenburg et al., 2020 also takes into account the hydration of SA particles and dipole-dipole enhancement which is responsible for increasing the collision rate between neutral molecules and neutral particles. As these parameters were not known for IA and MSA, we used the method by Nieminen et al. (2010) for them. The growth due to MSA could be slightly overestimation by this method (Beck et al., 2021) since the parameterization is based on the assumption of irreversible condensation, but MSA rapidly partitions between gas and particle phases if suitable meteorological conditions prevail. The calculated kinetic GR was compared with the total measured particle GR to determine the contribution of each vapor to the growth process (discussed in further sections).

The formation rate of the total particles of diameter 1.5 nm is calculated using the time derivative of the particle number concentration measured using the PSM in the size range 1.5–3 nm. The formation rate was corrected for the coagulation losses and growth out of the bin following the method explained by Kulmala et al. 2012. The formation rate of the charged particles was calculated from the time derivative of ions measured using the NAIS in ion mode in size range 1.5–3 nm from

~~both polarities. The formation rate of ions was corrected for coagulation sink, growth outside of the bin, ion-ion recombination and ion-neutral attachment as previously discussed in Kulmala et al. 2012.~~

~~**2.5 Condensation sink**~~

~~The condensation sink (CS) plays an important role in understanding aerosol dynamics. This parameter determines how fast gas molecules will condense on the pre-existing particles (Dal Maso et al., 2002; Kulmala et al., 2005, 2012). In this study, CS has been calculated by using the DMPS data, according to Pirjola et al., 1999.~~

Formatted: Font: Not Italic

Commented [TRC1]: condensation sink has been completely removed from the MS.

3. Results and discussions

3.1 Meteorological parameters and cyanobacterial bloom during the study.

3.1.1 Meteorological Parameters

The meteorological parameters, especially the wind speed, wind direction and ambient temperature, varied significantly during the study period. The time format in the entire study is UTC+02:00 h. This study period includes the hottest summer days of Finland in year 2019. The average temperature during 17–28 July (the warmest period) was 21.6° C with a maximum temperature of 31.6° C recorded on the 28 July (Fig. 2). Temperature starts to decrease after 29 July. The average temperature in August was 16.5° C with a maximum temperature of 21.9° C recorded on 5 August 2019.

The wind direction was highly variable during June-July period. The wind direction in July was mostly from the sectors 270°–320° (West-Northwest) and 90°–150° (East-South East). In August, the wind gained more stability and was dominantly blowing from 180°–270° (South-West) (Fig. 2). The wind speed also showed high variability in June-July. The wind speeds during June and early weeks of July were mostly >6.5 m s^{-1}, followed by a bit calmer mid-July (mostly <=4 m s^{-1}) with preceding high winds in end of July until mid-August (gusts of winds > 5.2 m s^{-1}) (Fig. 2). However, the average wind speeds in both the months was 3 m s^{-1}. The average daylight hours in July were 17-18 hours with the daytime hours between 04:00–22:00 h which starts to decrease in August to 15–16 hours of daylight per day (05:00 h – 21:00 h) as per the Global radiation data obtained from SMEAR III station for the study period. Therefore, the actual nighttime hours in our measurement site can considered from 23:00 h–03:00 h during Finnish summers.

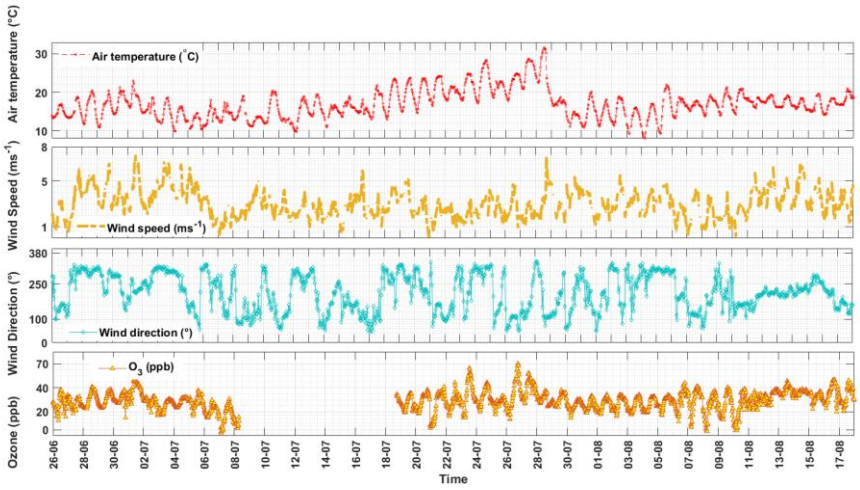

Figure 2: Time series of meteorological parameters and O_3 (data from SMEAR III station, 30-minute averaged) during the study period.

3.1.2 Cyanobacterial bloom conditions during the study

The Baltic Sea (defined from 53° N to 66° N latitude and from 10° E to 30° E longitude inclusive of Gulf of Bothnia, Gulf of Finland and Gulf of Riga) is characterized by usually two algal blooms occurring in early Spring (mostly diatoms) and a ~~Summer~~ summer bloom increasingly dominated by cyanobacteria (blue green algae). The summer bloom period selected for this study was typically characterized by cyanobacteria. When these microscopic cyanobacteria multiply and aggregate, they are seen as blue-green patches or scum-like layers over the surface of lakes and marine waters. The warm early summer temperatures (during June) resulted in a cyanobacterial bloom (Finnish national monitoring; SYKE press release, 2019). However, the weather conditions in end of July began changing with high winds causing the cyanobacteria to be highly mixed in the water column, which reduced bloom intensity at the sea surface to lower than normal mean cyanobacterial biomass (mean biomass of cyanobacteria, 105 µg L^{-1}, Kownacka et al., 2020) in end of July and August (SYKE press release, 2019). However the average biomass of cyanobacteria in 2019 (196 µg L^{-1}, Kownacka et al., 2020) was slightly higher than the average. Subsequently, temperatures were lower in August as compared to June and July and windier as compared to other summer months. These windy conditions kept the lake cyanobacteria well mixed in the water. The northern Baltic Sea, including the Gulf of Finland, the Southern parts of the Åland islands and even the Bothnian Sea occasionally observed massive blooms of cyanobacteria during June-August 2019. However, the bloom intensity of

Formatted: Superscript

Formatted: English (United States)

cyanobacteria at the coastal areas were intermittent and changed rapidly due to the spatial complexity of the coastline and variable winds and currents.

These cyanobacterial blooms are generally dominated by three taxa, *Nodularia spumigena* , *Aphanizomenon* sp. and *Dolichospermum* sp. (Knutson et al., 2016; Kownacka et al., 2020). In the Baltic Sea, these cyanobacteria actually contribute the most to the total pelagic nitrogen fixation (Klawonn et al., 2016). Other potential primary producers emitting vapors are the littoral macroalgae growing along the shallow coastline. For example, the perennial macroalgae, *Fucus vesiculosus* covers large areas of the coastal areas of Baltic Sea, where they support very high biomass and high productivity (Attard et al., 2019). Low sea levels (0.2–0.8 m, wave height at Suomenlinna aaltopoiju station, https://en.ilmatieteenlaitos.fi/wave-height) were recorded in mid-July (11 July 2019–27 July 2019) during the period when high temperatures (20° C and above) prevailed (Fig.2) in our study region. During these conditions, contributors to emissions might be a mix of both coastal macroalgae and open sea microalgae, which are mostly the cyanobacteria. There is a possibility that reasonably, large extents of coastal macroalgae, including *F. vesiculosus*, were exposed to direct sunlight (in shallow waters or low tide conditions) during the decay of the blooms during mid-August (when the bloom intensity was low, SYKE press release, 2019), hence making this time window favorable for observing potentially high emissions in gas phase from macroalgae, in addition to the emissions from cyanobacterial blooms. However, in the semi-urban/coastal setting of this measurement site, there could be various other parameters, which also could play a role in determining the concentrations of the biogenic emissions; for example the wind speed and wind direction. The atmosphere in this semi-urban coastal location is itself a cocktail of various vapors, oxidants and particles, which would affect the quantification, source apportionment and characterization of the biogenic emissions.

Field Code Changed

Formatted: English (United States)

Formatted: Pattern: Clear

3.2 Precursor vapor concentrations and their sources

The measured daytime precursor vapor concentrations showed a regular diurnal cycle consistent with the photochemical production of SA and IA in 90% of the days in this study. SA, key precursor of atmospheric NPF, is formed mainly by reaction of sulphur dioxide with OH-radicals, which is predominantly controlled by the photochemical cycles (e.g. Sipilä et al., 2010; Jokinen et al., 2017). The ~~mean (whole day)~~daily mean concentration of SA in July and August were almost similar, ~~was 3~~2.98 × 10^6 molec. cm^{-3} ~~and 2.67 × 10^6 molec. cm^{-3} respectively~~. The mean concentration is slightly lower as~~than~~ compared to the concentrations of SA measured in Helsinki street canyon ~~reported by very recent study measured in a Helsinki street canyon~~, 1×10^7 molec. cm^{-3} (Olin et al., 2020) but similar to the SA concentration measured at the SMEAR III station in 2018 (Okuljar et al., 2021). In

the study of Olin et al., 2020, SA concentrations were greatly affected by vehicular traffic as the site is situated at a busy street canyon. The SMEAR III is considered as a background site much less affected by vehicular traffic (Okuljar et al., 2021). In comparison to other locations, the daytime SA concentration in pristine Antarctic region has been reported from 10^5 up to 10^7 molec. cm^{-3} (Mauldin et al., 2001, Jokinen et al., 2018), 10^6 molec. cm^{-3} in remote continental, remote marine and forest regions and 10^7 molec. cm^{-3} in urban and rural agricultural lands using the same technique as in here (Berresheim et al., 2000; Kuang et al., 2008; Petäjä et al., 2009; Kurtén et al., 2011; Zheng et al., 2011; Chen et al., 2012; Jokinen et al., 2012; 2017, Kürten et al., 2014; Bianchi et al., 2016; Baalbaki et al., 2021; Dada et al., 2020~~b~~). It has been well documented that SA contributes to aerosol formation and growth processes (Boy et al., 2008; Eisele et al., 2006; Fiedler et al., 2005; Iida et al., 2008; Sarnela et al., 2015; Jokinen et al., 2018; Kürten et al., 2015, 2016; Mauldin et al., 2001; Paasonen et al., 2010; Wang et al., 2011; Weber et al., 1998, 1999; Yao et al., 2018; Dada et al., 2020~~b~~). Most of these studies are conclusive that SA concentration in the atmosphere depends on the anthropogenic and biogenic activities around the site.

In the coastal marine boundary layer, the MSA concentration is typically 10–100% of that of SA (Berresheim et al., 2002; Eisele and Tanner, 1993). Until recently, no studies have been found to report MSA and IA concentrations in coastal/urban setting of Finland. The ~~mean (whole day)~~daily mean concentration of MSA in July and August was almost similar, 4×10^5 molec. cm^{-3}. The mean concentration of IA in July and August was 1~~.27~~ × 10^6 molec. cm^{-3} and 3~~2.69~~ × 10^6 molec. cm^{-3}, respectively, showing two times increase in IA concentrations in August (Fig. S1). A similar increase in IA concentrations from summer to autumn were observed in the Arctic Ocean, where the increase in IA was attributed to the freezing onset of the pack ice and increase in ozone concentrations (Baccarini et al., 2020). However, here the increase is mainly due to the change in the air mass arriving at the experimental site, enriched with biogenic emissions from the blooms. For the same period, the CI-API~~-~~TOF data shows exceptionally high concentrations of highly oxygenated organic molecules (HOMs), with monomer concentrations (300–450 amu) of 10^8 molec. cm^{-3} and HOM dimer concentrations (450–600 amu) of 10^8 molec. cm^{-3} as well (Fig.S2).

~~In more details, the~~ The IA concentration rises one order of magnitude, from 10^6 to 10^7 during the 11–17 August, when the wind direction changes abruptly (from 280°–360°to 180°–230° , marine air mass, Fig. 3). We found that during the marine air (180°–230°, South Easterly, over Gulf of Finland and South westerly, over Northern Baltic sea) influence over the study region the average noontime maximum of SA, IA is on the order of 10^7 molec. cm^{-3} and MSA is around 10^6 molec. cm^{-3} (Fig. 3). This is one order of magnitude higher concentration than when the wind was from over land (Fig. 3).

The highest concentration, 3~~.2~~ × 10^7 molec. cm^{-3} of IA was observed when the wind is coming from the Baltic sea sector, whereas the highest SA concentrations (~ 3~~.0~~ × 10^7 molec. cm^{-3}) was observed~~we observe~~ when air mass travelled over the countries of Estonia and Russia crossing Gulf of Finland before entering the measurement site (land+sea region). The connection between the aerosol precursors and the wind direction can be observed in the cases where the wind direction changes rapidly. The highest IA concentration was recorded when the wind direction changes after the 4 August, 180°–230° (the Baltic Sea region). The change in wind direction was clearly reflected in a reversal of the concentration trends of SA and IA (Fig. 3). It was observed that the winds coming from 80°–180° or 250°–280° (land-sea region, Fig. 3) were SA rich air masses. This comprises of the landmasses of south and northeastern Finland, Northern Russia, part of Gulf of Finland and Estonia and North-North western part of Finland including a part of northernmost Gulf of Bothnia. The sector 0°–90° or 280°–360° (land, Fig. 3) consists mostly of urban cities.

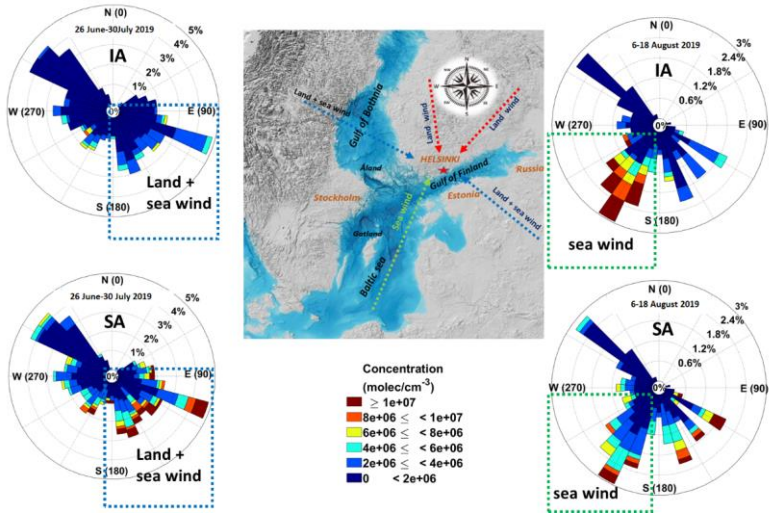

Figure 3: Windroses showing the variability in the concentration of gases with wind direction during the study period. Percentages on the concentric circles denote the frequency of winds from different directions. The spokes are color coded as per the concentration of the gas from the particular direction. The numbers in the parenthesis within the windroses refer to the wind direction in degrees.

During the entire study period, when the air plume passed over the northern Baltic Sea region and the wind speed was high enough (> 4m s^{-1}) high concentrations of IA was observed. While IA can be exclusively sourced from the marine and biogenic emissions (Mahajan et al., 2011; O'Dowd et al.,

2002; Sipilä et al., 2016; Carpenter et al., 2021), SA could be biogenic or /and anthropogenic. Further, the temperatures prevailing during this period may have facilitated the DMS oxidation at a higher rate, which forms the source of biogenic SA and MSA. However, this is not a very simple equation, since this fractional yield of ~~(~~biogenic~~)~~ SA from DMS oxidation additionally also depends on the atmospheric NO_x ($NO + NO_2$) and HO_x ($OH + HO_2$) levels and on the scavenging of SO_2 by sea salt or cloud droplets (Hoffmann et al., 2016). The anthropogenic sources of SA for this site could also include~~s~~ vehicular or ship traffic especially considering that there is a city road just 250 m and a harbor 6 km away from the measurement site. We explored the correlations of SA to a biogenic proxy, MSA and correlation with NO_x (anthropogenic proxy) to have a clear source apportionment of SA (Fig.4). SO_2 could not be treated entirely as anthropogenic proxy as it can be sourced from DMS oxidation as well.

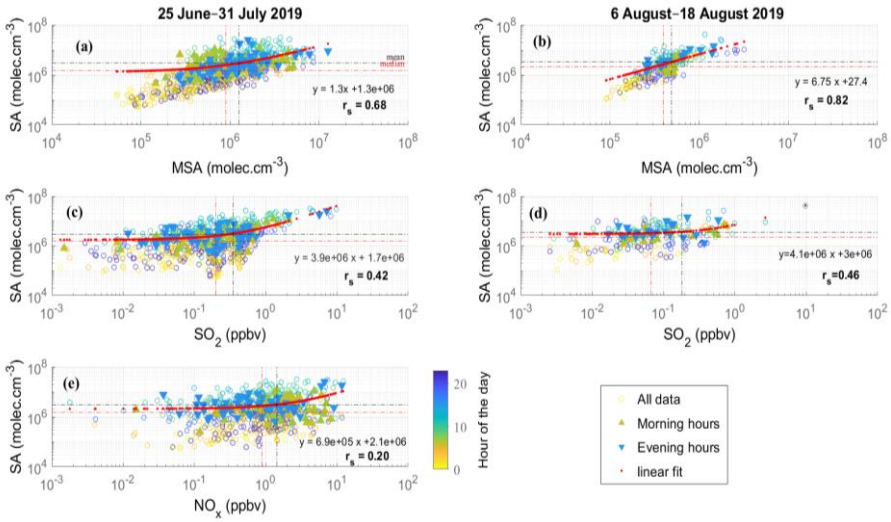

Figure 4: Correlation of SA with MSA (a,b), SO_2 (c,d) and NO_x (e) for June–July. The black dashed lines for both axis represent the mean of the gas concentration, red dashed line represent the median value the gas concentrations and red solid line represents the linear fit. Spearmann's coefficient (r_s) was used to test the correlation, at significance level, 0.001. The circles represent data points at different hours of the day. The upward pointing green triangles represent the morning rush hours (6:00–8:00 h) and the downward pointing blue triangles represent the evening rush hours (15:00–17:00 h). The yellow hollow circles represent all data. NO_x data unavailable of August.

The good correlations (r_s >0.6, Fig. 4a and 4b) between SA and MSA during the study period (June–August) could suggest that they were sourced from a common biogenic source, the DMS emission from the cyanobacterial bloom. Good correlations of SA and MSA was also found in August (r_s = 0.8, Fig. 4b) when the air mass was mostly marine (and/or from the Finnish coastline, Fig. 3). Another observation was that SO_2 also shows some correlations with SA in both June-July and August study periods (r_s = 0.4, Fig. 4c and 4d), but not as significant as SA and MSA correlations. SO_2 can have different sources unlike MSA which is mostly biogenic. However some emissions could be sourced from agriculture and other terrestrial sources, Bates et al., 1992, hence these observations could possibly indicate SA was more biogenic than from other sources. But we cannot be very accurate in this estimation only by analyzing the correlation coefficients since both MSA and SA can have a similar daily cycles due to the oxidation pathways.

Both SO_2 and MSA are the oxidation products of DMS (produced by phytoplanktons, including some cyanobacteria), oxidized through OH and NO_3 radical (Chen et al., 2000). Some of the previous chamber studies have confirmed that SO_2 is the major intermediate products formed from DMS oxidation (Sørensen et al., 1996; Berresheim et al., 1995). The SO_2 could be oxidized to SA (OH/O_2 oxidation) during the transport. Since our experimental site was surrounded by water bodies and the summer season had enriched most of these freshwater and marine waters with abundant cyanobacterial blooms, this biogenic SA contribution to the study site has to be accounted when analyzing the sources of SA. However, SO_2 can also be sourced from various anthropogenic activities and can be oxidized to SA. In Finland the major sources of anthropogenic SO_2 is the public power industries contributing to almost 90% to the total SO_2 emissions in Finland in the year 2019, while transport contributing to less than 1% according to the emission inventory prepared by Finnish Environment Institute, SYKE (Finnish Air Pollution Inventory; ymparisto.fi/en-US/Maps_and_statistics/Air_pollutant_emissions). Further the maximum data points of high concentrations of SO_2 (~ 10^7 molec. cm^{-3}) were not observed during the traffic hours in June-July-August (Fig. 4c and 4d) another possible indication that biogenic sources could be contributing to the SO_2 concentrations and thus SA concentrations near the study site.

The emission inventory of Finland for the year 2019 indicated that sources of NO_x as NO_2 were mainly the power industries (41.5%) and the transport sources (41%) (ymparisto.fi/en-US/Maps_and_statistics/Air_pollutant_emissions). These sources are indeed the most significant sources of NO_x globally (Meixner and Yang, 2006). NO_x, definitive proxy of anthropogenic influence shows a poor correlation with SA (r_s=0.28, Fig. 4e) during June-July ~~also suggest~~which could suggest insignificant effect of traffic on the SA concentrations. Unfortunately, the NO_x data from August was unavailable due to instrument malfunction so we cannot provide any correlations for this month.

~~After carefully analyzing~~ ~~the~~ The data presented in Figure 3, where we observe high SA concentrations even when the air mass was marine and the good correlations of SA-MSA (inclusive of insignificant correlations of SA-NO_x) (Fig. 4) indicate towards a greater possibility of the influence of biogenic emissions on the concentrations of SA as compared to the anthropogenic emissions.

3.3 Types of nucleation events during the study

During, 25 June 2019–19 August 2019, we observe a number of NPF events characterized by a short appearance of ultrafine particles in the number size distribution lasting for less than one hour. These so-called bursts /spikes appearing at small sizes (sub-3 nm) are indicative of local clustering ~~and NPF~~ processes in contrast to regional events, where it is possible to follow the growing particle mode for several hours (Dada et al., 2018; Dal Maso et al., 2005). Local clustering here means that the molecules could be transported from elsewhere but the actual clustering could have taken place near the experimental site, indicated by a small bump of clusters (with absolutely little or no growth) as seen in the NAIS spectra. We do observe transported events (events with a growing particle mode, but no small particles forming at the site) and non-events days but they are not included in the analysis. This section discusses the occurrence of local and regional new particle formation events with the focus on: 1) trace gases variability during the event days, 2) the evolution of different sized particles during these events, 3) the impact of meteorological parameters and 4) the effect of cyanobacterial bloom on the events.

Table 1: Timing and maximum concentration of SA, MSA and IA during local and burst/spike nucleation events during the study period

Dates	**Type of Event**	**time of NPF (UTC+02:00 h)**	**SA (max)** molec. cm^{-3}	**MSA (max)** molec. cm^{-3}	**IA(max)** molec. cm^{-3}
30.06.2019	Regional/ local	8:45-13:23 14:00-16:30	7.9×10^6	5.6×10^5	2.3×10^6
30.07.2019	Regional/ local	7:45 -11:16	1.2×10^7	1.2×10^6	5.3×10^6
11.08.2019	Ion Burst (Spike)	13:40-14:32	1.0×10^7	1×10^6	3.2×10^7

14.08.2019	Ion Burst (Spikes)	8:00-8:20	4.2×10^6	5.3×10^5	8.5×10^6
15.08.2019	Multiple Ion Bursts (Spikes)	6:00, 8:58, 14:00-16:00	6.4×10^6 6.3×10^6 7.0×10^6	5.8×10^5 4.6×10^5 6.8×10^5	2.5×10^6 3.1×10^6 1.5×10^6

3.3.1 Nucleation: Regional and Local events

A regional NPF event was observed on 30 June 2019, which starts at 08:45 h and ends at 13:23 h (Fig 5a). The negative ion clusters start to increase in concentration first at 08:45 h (Fig. 5b) concurrent with the increase in concentration of the smallest particles (<3nm) from 10^2 to 10^3 cm^{-3} (Fig. 5c). Preceding the NPF event the SA concentrations were steadily increasing and ~~Subsequently~~subsequently at 09:00 h, SA concentration doubles from 2×10^6 to 4×10^6 molec. cm^{-3} (Fig. 5d), while the particle formation rate at 1.5 nm ($J_{1.5}$) increasing from 0.3 cm^{-3} s^{-1} to 0.6 cm^{-3} s^{-1}. $J_{1.5}$ was much higher than either of $J_{+1.5}$ and $J_{-1.5}$, thus indicating a neutral formation pathway rather than ~~an~~ ion mediated ~~one~~. Further we also observe local clustering event at 15:00 h with simultaneous increase of concentration of SA and HOMs along with increase in the smallest particle concentration. This possibly indicates the role of SA and HOMs in the nucleation initiation. The high normalized signals of DMA-SA cluster seen during the entire event (increasing from the start of NPF event) possibly indicates that SA clusters initiate the event (Fig. S4a). DMA inclusive of other main methylamines like mono and tri methylamines (Bergman et al., 2015) in the global inventory (Schade and Crutzen, 1995) is contributed through the animal husbandry and other agricultural practices, biomass burning and some contributions from marine and terrestrial sources. Although among these methylamine emissions, generally the trimethylamine dominates (Schade and Crutzen, 1995). Although no estimates of DMA measurements are available from Helsinki region, the DMA in a boreal forest site in Finland has been estimated to be below ~ 150 ppqV (Sipilä et al., 2015), measured through a NO_3^- CIMS. Their work also stated that DMA was unlikely the playing an important role in the nucleation process observed at the site.

The increase of HOMs is also clearly observed during the event Fig. S4b. Therefore we suggest that nucleation and growth of particles was possibly due to SA-organics which ensures that particles reach the CCN and thus climate relevant diameters. The work of Okuljar et al. (2021) also report an increase in sub-3 nm particles with a simultaneous increase in SA concentration at the SMEAR III site, supporting our observations. However, the role of HOMs in nucleation initiation has not been explored at this site.

Formatted ...

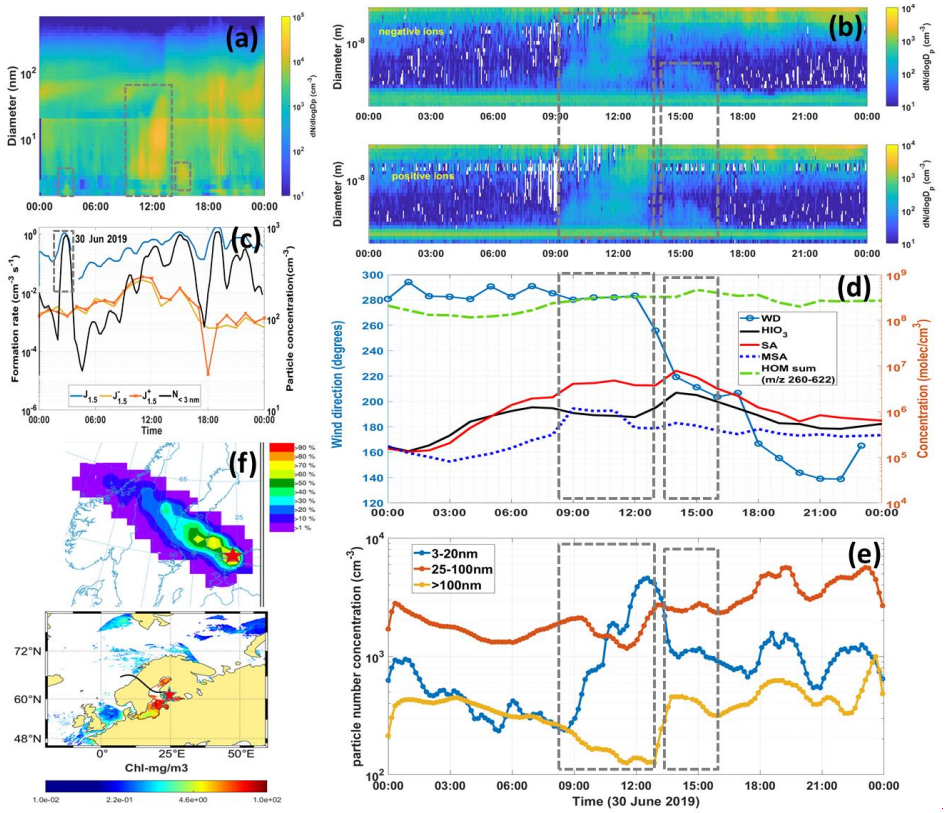
(a)
Diameter (nm)
00:00
06:00
12:00
18:00
00:00
(b)
negative ions
positive ions
Diameter (m)
(c)
30 Jun 2019
Formation rate (cm⁻³ s⁻¹)
Particle concentration(cm⁻³)
Time
(d)
WD
HIO3
SA
MSA
HOM sum
(m/z 260-622)
Wind direction (degrees)
Concentration (molec/cm³)
(e)
3-20nm
25-100nm
>100nm
particle number concentration (cm⁻³)
Time (30 June 2019)
(f)
72°N
60°N
48°N
0°
25°E
50°E
Chl-mg/m3
1.0e-02
2.2e-01
4.6e+00
1.0e+02

598

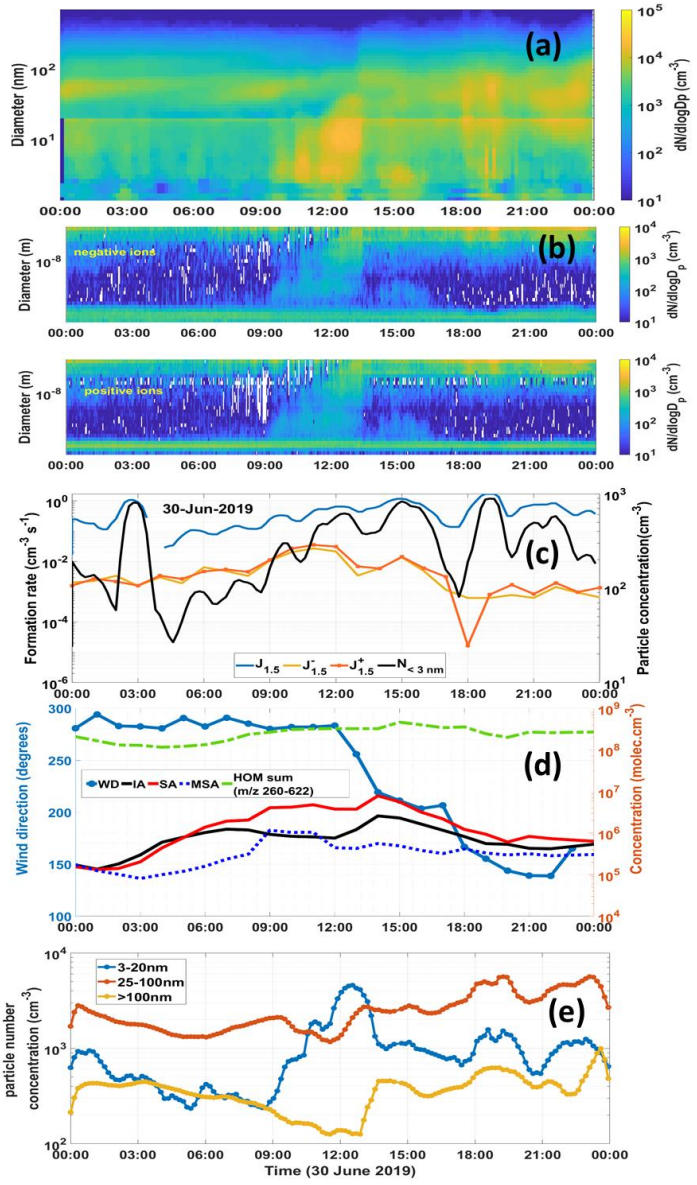

Figure 5: NPF Event (Regional and local events), 30 June 2019~~, the large dashed rectangle denotes the regional event, the small dashed rectangles show local cluster formation events~~. (a) Number size distribution of particles (data from PSM, NAIS and DMPS; size range: sub-3–100nm). (b) Charged

particles number size distribution (negative: upper, positive: lower) obtained from the NAIS. (c) Diurnal variation of formation rates ($J_{1.5}$) of 1.5 nm particles and ions ($J^{-}_{1.5}$ and $J^{+}_{1.5}$) on the left axis and particle number concentrations (1.5–3 nm) on the right axis. (d) Diurnal variation of HOMs SA, IA and MSA with wind direction (WD). (e) The diurnal variation of particle concentration in nucleation:3–20 nm; aitken: 25–100 nm and accumulation: >100nm) mode particles during the event (Data from DMPS).

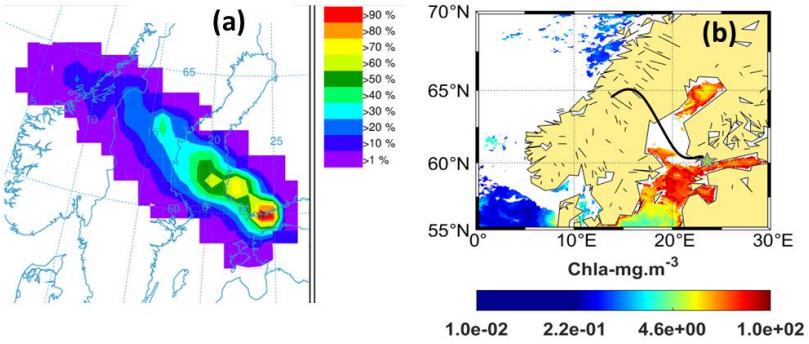

Figure 6: (a) Trajectory frequency plot (100 a.g.l, arrival time of trajectories at the meaurement site: 20:00 h) for 24 h back trajectory using GDAS meterological input data (frequency grid resolution: 1.0° × 1.0°) (b) Chl-*a* concentrations (GlobColour level-3); Black line shows the trajectory direction and the star point denotes the measurement site ~~(f) Trajectory frequency plot (100 a.g.l, arrival time of trajectories at the meaurement site: 20:00 h) for 24 h back trajectory using GDAS meterological input data (frequency grid resolution: 1.0° × 1.0°) and Chl-*a* concentrations (MODIS); Black line shows the trajectory direction and the red-star point denotes the measurement site~~.

A clear increase in nucleation mode particles is seen during the event, starting at 08:45 h (234 cm^{-3}) and reaching its maximum at 12:30 h (4589 cm^{-3}). This increase in concentration of the nucleation mode particles was followed by the increase in concentration of Aitken mode and accumulation mode particles and continues for a couple of hours, indicating growth of particles (Fig. 5e), possibly reaching to CCN relevant sizes. However, we also observe a drop in Aitken particles before NPF which also continues during NPF. We speculate it could be due to the change in wind direction (Väkevä et al., 2000) before NPF. The wind direction relatively remains constant throughout the NPF so the low concentration of Aitken mode continues. Wind direction changes abruptly at 12:00h and the Aitken mode particle concentrations increases soon after this change of wind direction ~~The growth~~

Formatted: Font: Bold

Formatted: Indent: First line: 0 cm, Space After: Auto

~~continues until the wind direction suddenly changed after 12:00 h~~ (Fig. 5d). This shows the particles must be the process of growth mostly elsewhere, which is not evident in the changed air mass, however we still observe almost the same (or even slightly higher) precursor vapor concentrations, since the wind still passed over the bloom areas before entering our study site.~~, that apparently discontinued the precursor vapor source to our site~~. After the change in local wind direction, the observed SA and IA slightly increase, and we still observe ~~local~~ clustering (formation of small ions and particles), but no continuous growth typical for regional events. Figure ~~5f~~ 6a shows that >40% of the trajectories passes above the Swedish island of Gotland towards southern part of Bothnian Sea. The ~~MODIS~~ satellite data shows that the bloom was present in the Bothnian Sea, but not quite dense as compared to the southern Baltic Sea (south of Gotland island) and the northern part of the Gulf of Finland (Fig. 6b). The majority of the trajectories did not pass over the dense cyanobacterial bloom patch during this day (Fig. ~~5F~~6b). The calculated ~~(~~normalized~~)~~ residence time was higher over the neighboring cities of Helsinki (Southwestern side) and parts of Bothnian Sea during the event time (see Fig. S3). Thus the land based anthropogenic activities and biogenic sources both can be contributing to SA concentrations for this event; here we cannot exactly quantify the source types for SA. However, the source of SA from the local sources such as vehicular traffic around our measurement site is small (as discussed above) but cannot be completely ignored (Olin et al., 2020).

Formatted: Font color: Red

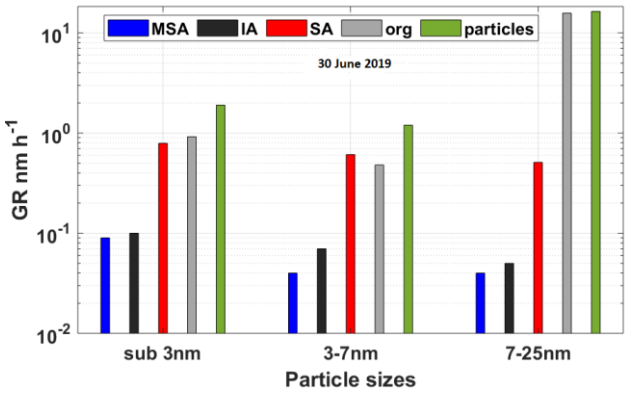

Figure ~~6~~7: Particle growth rates calculated from the kinetic condensation of gases (data from CI-APi-ToF) and the measured ~~observed~~ particle GRs (data from NAIS) in different size classes on 30 June~~ly~~ 2019.

~~The high signals (normalized) of DMA-SA cluster seen during the entire event (rising from the start of NPF event) indicates SA clusters initiate the event (Fig.S4a). The increase of HOMs is also clearly~~

~~observed during the event Fig. S4b. Therefore we suggest that nucleation and growth of particles was possibly due to SA-organics which ensures that particles reach the CCN and thus climate relevant diameters.~~

The particle GR (7–25 nm) for this event was 16.5 nm h^{-1}, which is typical of a coastal site. Even when several condensing vapors participate in the growth process, growth rates typically do not exceed 20 nm h^{-1} (Kulmala et al., 2004). The GR for organics was calculated after subtracting the combined contribution of the GR of SA, IA and MSA from the measured particle GR (Fig.7). The GR for organics should be treated as an estimation since no separate GR calculations and assumptions were used. The calculated growth rates (GR) shows that SA can explain maximum 41% of the growth of sub-3 nm particles, while IA and MSA can explain only <1% of the GR in this size range. The GR by SA in the bigger size fraction (7–25 nm) was only 0.51 nm h^{-1} explaining only 3% of the measured growth rate of particles. This means that vapors other than SA, IA and MSA were responsible for 96% of the measured particle growth. These other vapors could include different organics since organics are known to contribute to growth of particles (Kulmala et al., 1998, 2004; Riipinen et al., 2012; Zheng et al., 2020) and explain particle growth in the boreal forest (Ehn et al., 2014).

Another example of regional event (neutral nucleation) probably driven by SA and organics was observed on 30 July 2019 (Fig. S5) which lasts for around four hours. The trajectory frequency plots showed that most of the trajectories were from the northern land areas (including urban cities and boreal forests) of Finland with highest residence times over these land regions (Fig. S6 and S7). Since, the precursor gases from the biogenic origin, IA and MSA, do not show a significant concentration increase as compared to SA, at the start of the event, their contribution towards the initiation of the NPF event may not be as significant as SA. The greater residence times over the land areas clearly support the high SA and organic concentrations seen during the event indicating a SA driven event ~~–~~with a possible contribution of HOMs ~~driven local event~~ (Fig. S~~7~~6). In this case, ~~the growth due to~~ SA explains 60% of growth of sub-3nm particles compared to 41% when the dominating trajectories passed over the Gulf of Finland (Fig. 5, 30 June 2019). Still, as for the previous case, a major fraction of the growth in the 3–7 nm range remains unexplained by the available acids (SA, IA, MSA) and is expected to be related to the contribution of organic~~s material being abundant~~. The GRs explained by SA in both sub-3 nm (1.93 nm h^{-1}) and 3–7 nm (1.46 nm h^{-1}) size ranges are 58-59% higher than on 30 June 2019 (0.79 nm h^{-1} and 0.61 nm h^{-1} for sub-3 nm and 3–7 nm, respectively) which could be explained by the increase in SA by 52% on 30 July 2019. Thus, the events on 30 June and 30 July possibly occur via the nucleation of ~~sulfuric acid~~SA (possibly stabilized by bases eg. ammonia or amines) and the HOMs contribute to growth of particles and possibly in nucleation as well.

Field Code Changed

3.3.2 Nucleation: Burst events

Case 1: Biogenic IA nucleation- burst/spike events, 11 August.2019

Intense burst events are frequently observed at coastal sites accompanied with high concentrations of IA (O'Dowd et al., 2002; Rong et al., 2020; Sipilä et al., 2016). Two of such bursts or spike events were observed on 11 August 2019 at 04:00 h and 13:00 h (Fig. ~~7a~~8a). Only the second spike event was observed in the NAIS size distribution with a higher intensity in the negative mode at 13:00 h (Fig. ~~7b~~8b). During both these spike events we observe the formation of clusters (1.5 nm) and the formation rate ($J_{1.5}$) increases from 0.2 to 3.7 $cm^{-3}s^{-1}$ during the event with a simultaneous significant increase in the sub-3 nm particle concentrations from ~100 to >2000 cm^{-3} (Fig. ~~7c~~8c). $J_{1.5}^{+}$ and $J_{1.5}^{-}$ remain lower than the total formation rate indicating this event to be a case of neutral nucleation. At the same time, IA shows increase in concentration from 9~~.2~~$\times 10^5$ molec. cm^{-3} at 03:00 h to 1~~.2~~$\times 10^6$ molec. cm^{-3} at 04:00 h. During this event the air masses changes from 160° to 140° i.e the direction of the airmass is changed to the Gulf of Finland. In the second burst (at 13:00 h), the IA concentration increases from 2~~.3~~ $\times 10^6$ to 7~~.3~~ $\times 10^6$ molec. cm^{-3} from 13:00 h to 14:00 h (Fig. ~~7d~~8d) with a slight change in wind direction from 151° to 166° Most of these air masses are from the Gulf of Finland. SA concentration also increased but remained lower than IA during both the burst/spike events indicating a possibility that iodine oxoacid formation initiates cluster formation (He et al., 2021). We observe a growth of particles until 15:00 h in the particle modes (NAIS data, Fig. ~~7B~~7b). However the particles are seen reaching sizes up to size 100 nm (DMPS data , Fig. ~~7A~~8a). The organics almost remain constant within the range of 2~~.5~~–3~~.1~~ $\times 10^8$ molec. cm^{-3}. A further increase in IA concentration, 3~~.18~~ $\times 10^7$ molec. cm^{-3} occurs at 15:00 h, and the concentration remains in the range of 10^7 molec. cm^{-3} for another two hours (Fig. ~~7d~~8d). This was the highest observed IA concentration in the entire measurement period. A recent study by He et al., 2021, indicate that ~~HIO_3~~ IA concentrations above 1 $\times 10^7$ molec. cm^{-3} leads to rapid new particle formation at +10° C. At such concentrations the efficacy of iodine oxoacids to form new particles exceeds that of the H_2SO_4-NH_3 system at the same acid concentrations. Thus, the concentration of IA found in this event (two times higher than SA during the start of the event), the high formation rates (>1 cm^{-3} s^{-1}) and an unchanged concentration of SA during the event, as compared to the event on 30 June 2019, strongly suggests that it could be an IA driven-NPF event. ~~is capable of initiating nucleation, especially since the concentration of IA being two times higher than SA during the start of the event~~. In addition, a clear increase in the normalized signal of deprotonated IO_3^- with no significant increase in DMA-SA cluster during the event at 13:00 h (Fig. S~~8~~7a). However, HNO_3-IO_3^- cluster was the most abundant followed by the H_2O-IO_3^- cluster indicating this event to be IA-driven nucleation. Further, between 14:00–15:00 h, when we observe the highest IA concentrations a subsequent growth of particles is noted. We also observe an increasing

Formatted: Space After: Auto

number concentration of nucleation mode particles from 13:40 h (~650 cm^{-3}) to 14:40 h (~1800 cm^{-3}). After this one hour of intense clustering, the Aitken mode particles also begin to increase in concentration from ~1300 cm^{-3} to ~4800 cm^{-3} during 15:00 h–18:00 h (Fig. ~~7E~~8e). The total particle concentration increased from ~2400 cm^{-3} to ~6400 cm^{-3} within an hour during this burst event. We suggest that this burst event was possibly capable of producing particles big enough to act as CCN. Since it was an intense burst event with no proper horizontal growth (as seen in "banana" type events), we were not able to calculate the growth rate for this particular event. Therefore we are unable to quantify the contribution of IA towards the growth of particles reaching CCN sizes.

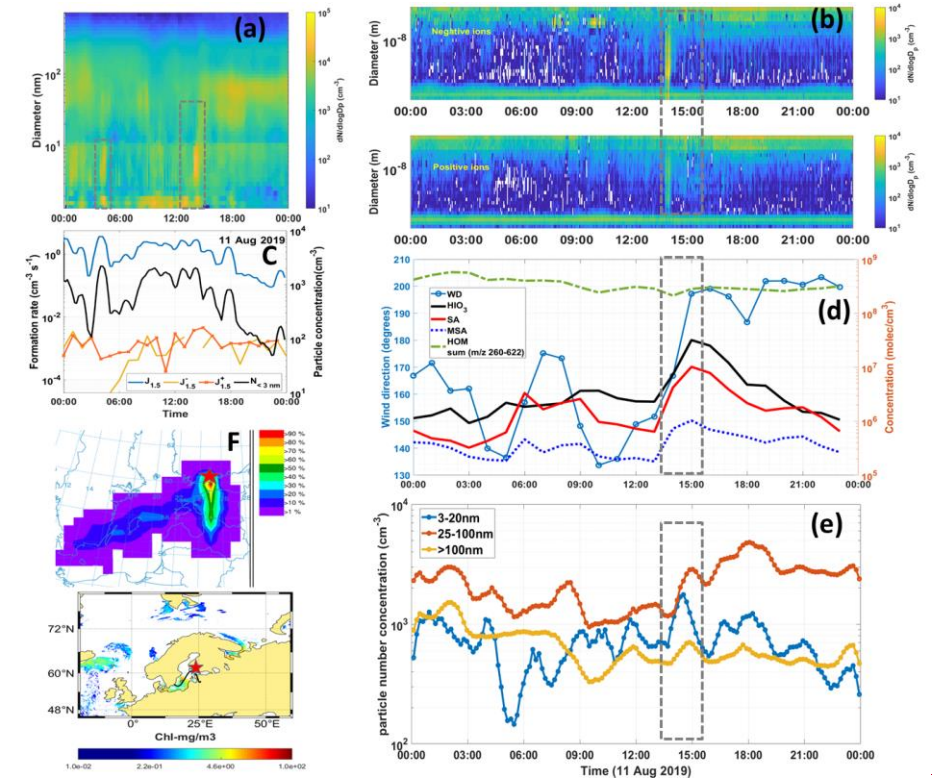

Formatted: English (United States)

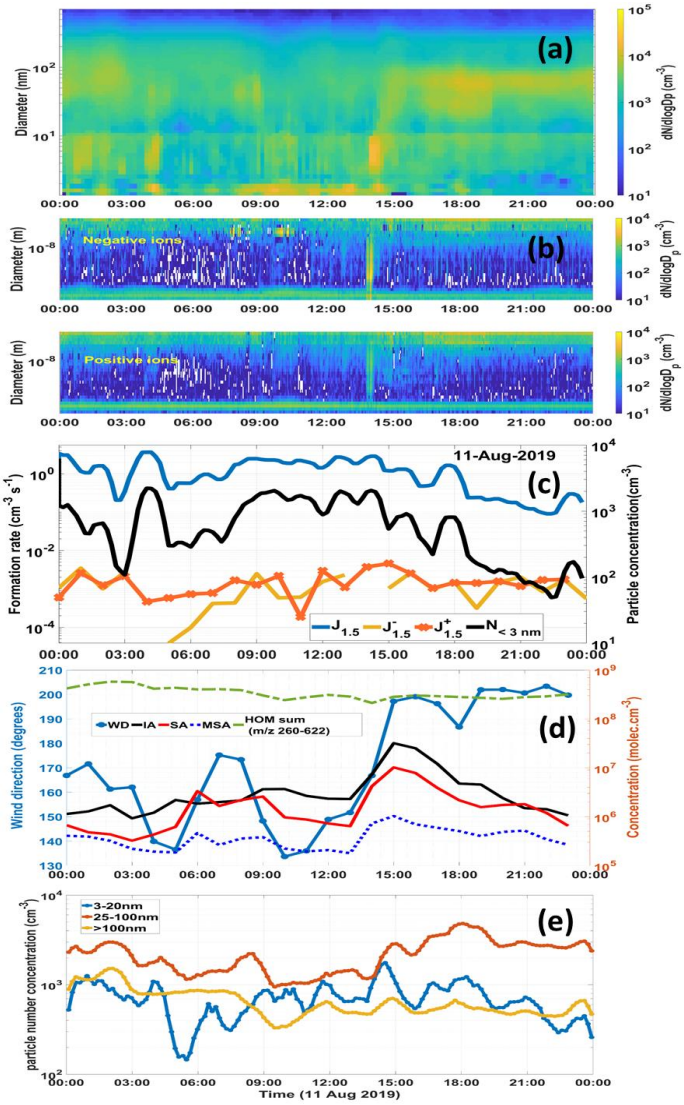

Figure 78: Burst/Event, 11 August 2019. The dashed grey rectangles denote the time stamp of the nucleation events. (a) Number size distribution of particles (data from PSM, NAIS and DMPS; size range: 1–100 nm). (b) Charged particles number size distribution (negative: upper, positive: lower) obtained from the NAIS. (c) Diurnal variation of formation rates ($J_{1.5}$) of 1.5 nm particles and ions ($J^-_{1.5}$ and $J^+_{1.5}$) and total number concentrations of particles (<3 nm, PSM). (d) Diurnal variation of HOMs, SA, IA and MSA with wind direction (WD). (e) The diurnal variation of particle

Formatted: Centered

concentration in nucleation (3–20 nm), Aitken (25–100 nm) and accumulation mode (>100 nm) particles (DMPS data).

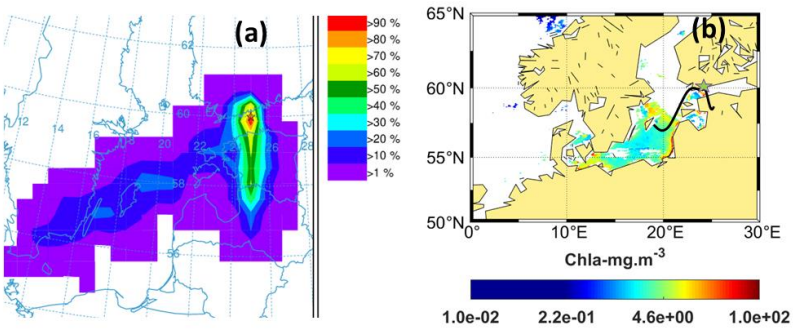

Figure: 9 (~~f~~a) Trajectory frequency plot (100 a.g.l, arrival time of trajectories at measurement site: 22:00 h) for 24 hour back trajectory using GDAS meteorological input data (frequency grid resolution: 1.0° × 1.0°) (b) ~~and~~ Chl-*a* concentrations (GlobColour level-3~~MODIS~~); Black line shows the trajectory direction and the ~~red~~ star point denotes the measurement site.

The global radiation and brightness parameter suggest that 11 August 2019 was an overall a cloudy day until 12:30 h (Fig. ~~S8~~S9). The weather starts to turn into clear-sky after 13:00 h when the brightness parameter increases from <0.3 to ~0.7 (Fig. ~~S8~~S9). Impact of brightness parameter on NPF is also observed in a previous study (Dada et al. 2017). The clearing of the sky could explain the intense spike at 13:00 h in the particle number size distribution as well as in the acid concentrations. For this particular case, we investigated further the source of such high IA concentrations and we found that during this day, the cyanobacterial bloom was observed in three intense patches in the central Baltic sea, southern Gulf of Finland (ship transect route between Helsinki and Tallinn) and Gulf of Riga (Fig. 9b~~7f~~). The trajectory frequency analysis clearly shows that the maximum frequency of trajectories was observed over southern Gulf of Finland (inclusive of the coastal waters of Suomenlinna island) however we do see the air masses coming in from the central Baltic sea as well which was characterized by intense bloom during this day (Fig. 9a~~7f~~). The sea level was also low as it was observed to be 0.8–0.9 m in the coastal waters in around the measurement site (Suomenlinna and Gulf of Finland coastal measurements sites), supporting the exposure of the macro ~~algae~~ to sunlight which can be a good source of iodine precursors.

Formatted: Centered

Formatted: Font: Bold

The residence time of the airmasses coming from the Gulf of Finland and Northern Baltic Sea were longer than the residence time of the airmasses coming from the neighboring land areas (Fig. ~~S9~~S10) clearly explaining the source of high IA observed during the event, which is through the blooms. Further, the airmass was completely marine at 15:00 h when the highest IA is recorded supportive of the marine biogenic source of IA and its transport to the measurement site. The distance from the Gulf of Finland to the measurement site is approximately 5-10 km. With the wind speed of 5 m s^{-1} recorded during the event, it takes less than one hour for the emission to transfer to our measurement site. By the time the air mass reached our measurement site from the emission source, ~~all~~ a fraction of the emitted I_2 could have ~~was~~ oxidized to IA. However, at this point we cannot differentiate between the sources of IA from neighboring coastal waters and the central Baltic Sea but can speculate that most of the IA observed could be sourced from the nearest coastal locations of Gulf of Finland.

Another burst/spike event driven by IA occurred on 14 August 2019 (Fig. S1~~0~~) when the IA concentration was found to be 8~~.54~~ × 10^6 molec.cm^{-3} which was 2~~.3~~ times higher than SA concentration (4~~.2~~ × 10^6 molec.cm^{-3}). The event did not last more than 30 minutes. The precursor vapor concentration was not large enough for the event to continue or the particles to grow further. The meteorological conditions were very much similar to this event (11 August 2019). For this event also, the airmass was marine with maximum residence times over the Gulf of Finland and Baltic Sea regions. Vicinity of the emissions to the measurement site enabled the detection of these fast-forming clusters ~~(from the emissions)~~.

Case 2: Biogenic SA nucleation –multiple bursts events

Another kind of event was observed on 15 August 2019 (Fig. ~~8a~~10a) where multiple particle bursts are observed and the particles grow to sizes > 50 nm.

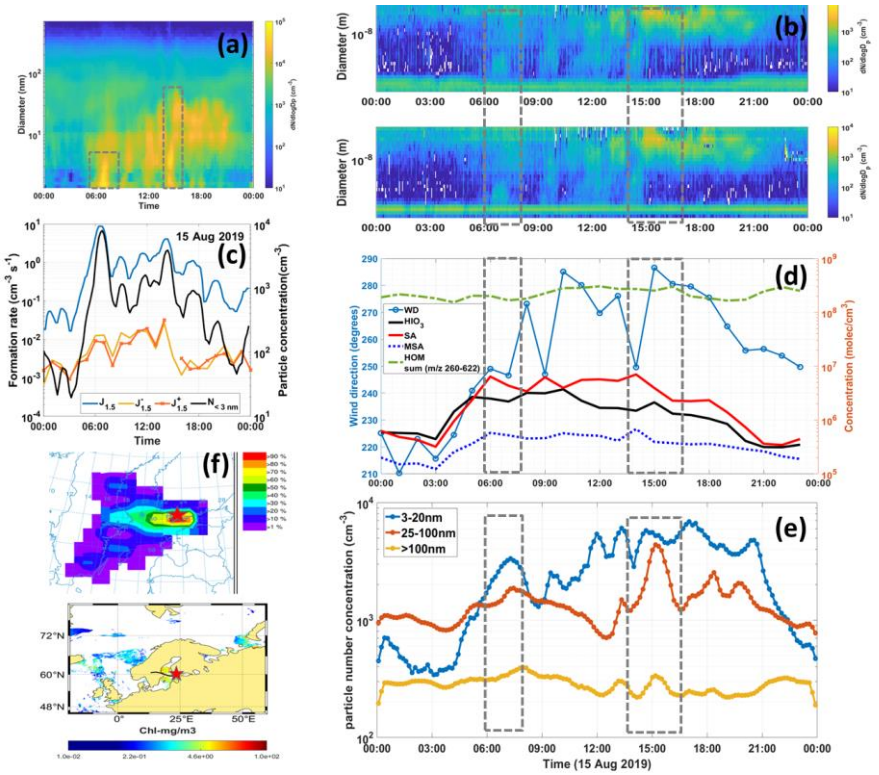
(a)
Diameter (nm)
Time
(b)
Diameter (m)
(c)
15 Aug 2019
Formation rate (cm-3 s-1)
Particle concentration(cm-3)
Time
(d)
WD
HIO3
SA
MSA
HOM sum (m/z 260-622)
Wind direction (degrees)
Concentration (molec/cm3)
(e)
3-20nm
25-100nm
>100nm
particle number concentration (cm-3)
Time (15 Aug 2019)
(f)
72°N
60°N
48°N
0°
25°E
50°E
Chl-mg/m3

785

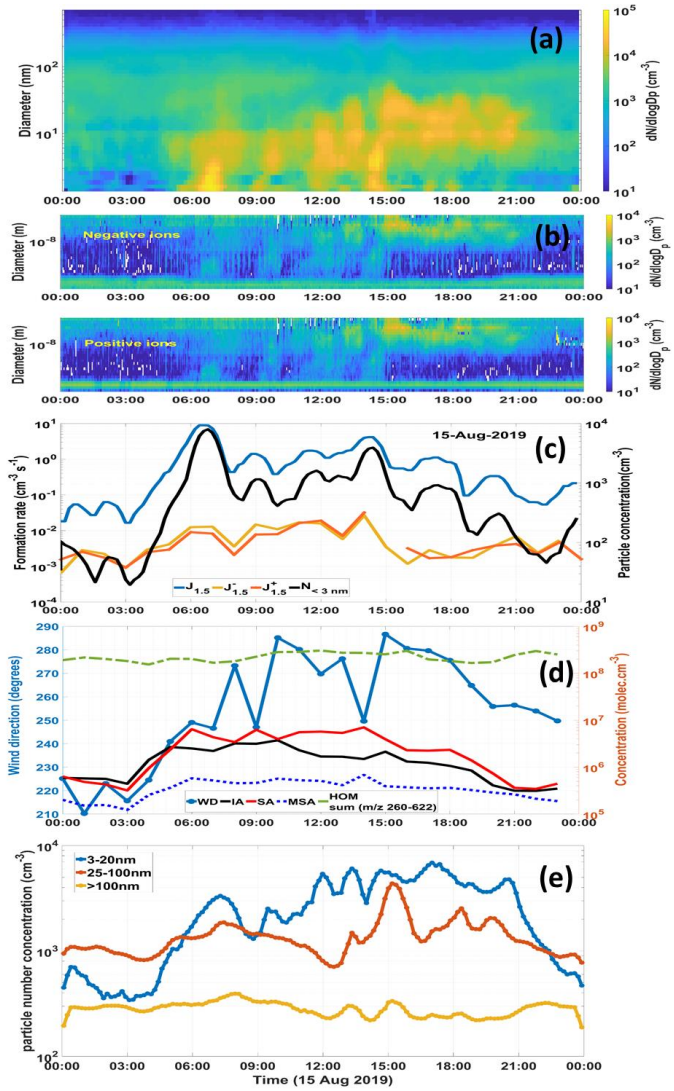

Figure ~~8~~10: Multiple Burst/Spikes, 15 August 2019~~, The dashed grey rectangles denote the time stamp of the nucleation events.~~ (a) Number size distribution of particles (data from PSM, NAIS and DMPS; size range: 1–100nm). (b) Charged particles number size distribution (negative: upper, positive: lower) obtained from the NAIS. (c) Diurnal variation of formation rates ($J_{1.5}$) of 1.5 nm particles and ions ($J^{-}_{1.5}$ and $J^{+}_{1.5}$) and total number concentrations of particles (<3 nm, PSM). (d) Diurnal variation of HOMs SA, IA and MSA with wind direction (WD). (e) The diurnal variation of

particle concentration in nucleation (3–20 nm), Aitken (25–100 nm) and accumulation mode (>100 nm) particles (DMPS data).

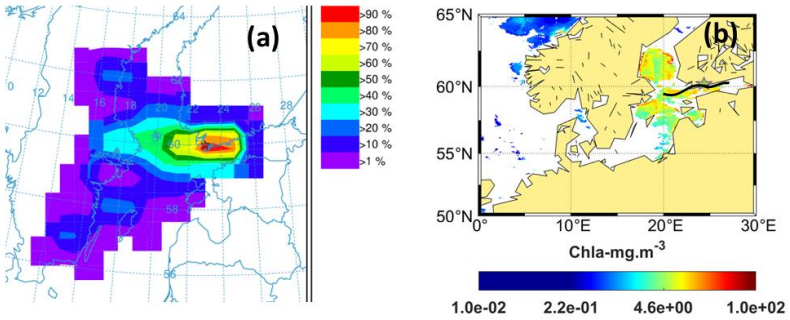

Figure 11: (~~f~~a) Trajectory frequency plot (100 a.g.l, arrival time of trajectories at the measurement site: 22:00 h) for 24 h back trajectory using GDAS meterological input data (frequency grid resolution: 1.0° × 1.0°) ~~and~~ (b) Chl-*a* concentrations (GlobColour level-3~~MODIS~~); Black line shows the trajectory direction and the ~~red~~ star point denotes the measurement site.

The formation rates for the smallest clusters for both the polarities were the same ($J_{1.5}^{+}$ and $J_{1.5}^{-}$) (Fig. 10~~8~~b and c). This was also a case of neutral nucleation as inferred from the relatively high (as compared to ions) $J_{1.5}$ (neutrals). On 15 August there was a sudden change of wind direction from the 180°–215° (prominent wind direction during 11–14 August) to 280° and a series of bursts is triggered with the intense formation of clusters (<3 nm) at each burst (Fig. 10~~8~~d). The two most intense burst events ~~(marked as dashed rectangles in Fig. 8a, b, d and e~~) were associated with an increase in SA from 2~~.~~4 to 6~~.43~~ × 10^6 molec. cm^{-3} at 06:00 h, and 5~~.~~3 to 7~~.03~~ ×10^6 molec. cm^{-3} at 14:00 h (Fig. ~~8d~~10d). A third burst at 09:00 h showed an increase in SA from 3~~.~~4 to 6~~.25~~×10^6 molec. cm^{-3} at 09:00 h interestingly with IA_{max}: 3.~~14~~ ×10^6 molec. cm^{-3}. In all the three bursts a simultaneous increase in IA and MSA from 03:00 h to 12:00 h is observed, but the SA concentration was two to three times higher than IA and four to five times higher than MSA concentrations. The most intensive burst was at 14:00 h (as compared burst to 6:00 h) when the SA was 3 times higher than IA. This burst was associated with a significant increase in Aitken mode particle concentration (from 1490 at 14:00 h to 4300 cm^{-3} at 15:00 h). The increase in accumulation particle concentration was seen just after one hour from the start of the bursts for both events (06:00 h and 14:00 h). However the increase in accumulation mode particle concentration for these two events was not very significant (~100cm^{-3}) although particles reaching a size more than 80 nm (CCN relevant sizes) was observed. We saw

Formatted: Centered

Formatted: Font: Bold

DMA-SA clusters during the event (Fig. ~~S11~~S12) which supports the observation that this a SA-driven NPF event.

During both these events (in fact, all the smaller burst events observed during this day), the trajectories were originating from Sweden (24 h prior to arrival). However, before entering the measurement site the trajectories passed over the Southern part of Gulf of Bothnia and the trajectory frequency was >70% when the wind passed over the cyanobacterial bloom region (Fig. 11a and b~~8f~~). To confirm our findings we checked a day where there was less intense bloom in the Gulf of Finland and Northern Baltic Sea and the dominant airmass did not pass over the bloom patch in Gulf of Finland (Fig. S13) before entering our experimental site. We did not observe an NPF event on this day, thereby suggesting that the airmasses passing over the bloom patches before arriving at our study site were capable of bringing in biogenic precursor vapors capable of initiating NPF events.

3.4 Possible contributions of biogenic emissions to Precursor gaseous vapors

Assuming insignificant anthropogenic SA contribution as discussed in section 3.2, we investigated the other possible sources of SA by evaluating the type of algae present in the water bodies from where the air masses travelled during the events. The marine algae produces dimethylsulfoniopropionate (DMSP), which is capable of forming DMS, which subsequently oxidizes into SA and MSA. While very few cyanobacterial species are capable of producing DMSP (Karsten et al., 1996; Jonkers et al., 1998), and its concentration can vary considerably from one species to another (Keller et al., 1989). Moreover, blooms could be well-mixed with other algal species (ESA report, 2000) which are capable of producing DMSP. A recent experiment identified *Aphanizomenon* as the only cyanobacteria producing DMS (Steinke et al., 2018). The Gulfs of Bothnia and Riga are dominated by the genus *Aphanizomenon* (Kownacka et al., 2020). In addition, the Bothnian Sea and Gulf of Finland were found to be rich in cyanobacterial genera of *Aphanizomenon* along with *Nodularia* and *Dolichospermum* (Kownacka et al., 2020~~SYKE 2020~~). As per the previous studies which were carried out as part of the Baltic-wide monitoring (Kowancka et al., 2020 and the references mentioned therein), bloom composition is fairly consistent for different regions and seasons from year to year, which makes it possible for us to make close estimations of the species present during our study in a particular region (from where the airmass travels and the residence time over a particular region).

A recent study also indicated that the abundance of DMS producing cyanobacteria, *Aphanizomenon* has increased in the Bothnian Sea due to decreasing salinity (Olofsson et al., 2020). Moreover, marine waters themselves are a large source of DMS (Kettle and Andreae, 2000)

852 explaining the contribution of biogenic SA in the above-mentioned burst events (15 August 2019).
853 Hence to conclude, the marinegulf regions surrounding the experimental site could be potential
854 sources of biogenic SA. Moreover, high iodine emissions could be expected over the Baltic Sea
855 proper region due to the presence of the macroalgal species which are well established and adapted
856 in the Baltic Sea despite its low salinity (Kautsky and Kautsky, 2000; Schagerström et al., 2014) (high
857 IA on 11 August 2019 event day). The rocky shorelines of the northern Baltic Sea provides ample
858 habitat for several species of macroalgae, including *F. vesiculosus* (Kautsky & Kautsky 2000, Torn
859 et al., 2006). Previous studies have documented that certain macroalgae contain high levels of iodine
860 (Ar Gall et al., 2004), of which the kelp *Laminaria digitata* stores the highest amount (Ar Gall et al.,
861 2004; Küpper et al., 1998).
862 However recent chamber experiments comparing different species of brown algae
863 found that emission rate of I_2 was higher in the case of *F. vesiculosus* when compared to other species
864 like *L. digitata* (Huang et al., 2013). This could possibly explain the high IA concentration recorded
865 by the CI-APi-TOF when the air mass was coming from the Northern Baltic Sea region (11 August
866 2019 and 14 August 2019). High production of macroalgal species is common along the extensive
867 archipelago coastlines of the northern Baltic Sea, and particularly *F. vesiculosus* is likely to contribute
868 with high emission rates, especially when during peak production times when exposed to low sea-
869 levels and direct sunlight. However, partitioning the influence of macroalgae and other microalage
870 requires further mechanistic studies. We suggestconclude that marine and coastal regions surrounding
871 the measurement site are capable of producing SA and IA during bloom period, which can initiate
872 NPF.
873
874 **4 Conclusions**
875 We studied the composition, concentrations and sources of precursor vapors forming aerosols in
876 Helsinki, Finland during the summer of 2019. The source of precursor gases causing responsible for
877 new particle formations were assessed by analyzing the meteorological parameters, situation of
878 cyanobacterial/algal bloom in the Baltic Sea. Our study recorded several regional, local and burst
879 events and we found that they were connected to elevated concentrations of SA and IA. The burst
880 /spike events occurred simultaneously with high intensity cyanobacterial/algal blooms in the Baltic
881 Sea.
882 The study draws the following conclusions. 1) Constantly changing algal conditions in
883 Gulf of Bothnia, Gulf of Finland and Baltic Sea are could be a significant source for the emission of
884 iodine precursors and DMS. These gases produced by these emissionsemission further oxidize in the
885 atmosphere to form IA and SA, which can be detected by mass spectrometric methods. Interestingly,

during marine air mass intrusion with higher residence time over the algal blooms, the gaseous precursors formed from the biological emissions possibly exceeded the gaseous precursors sourced from anthropogenic emissions at the measurement site. In fact, an overall higher impact of biogenic emissions was noted in this semi-urban site particularly during end of July and mid-August when the bloom intensity decreases and the cyanobacteria/macroalgae start to decay and die (while being exposed to sunlight) and consequently produce more emissions (biogenic SA and IA). 2) Moreover, the meteorological conditions like wind direction ~~(biogenic and anthropogenic source sectors)~~ and possibly wind speed were identified as the most important parameters influencing the precursor vapor concentration reaching the measurement site and thus determining if NPF occurred. ~~These factors will become more important if the measurement site is distant from the coast.~~ Further we also infer that that the wind direction played an important role in determining the particle concentrations at the study site. Our study ~~infers~~reports, that when the air mass travelled over the land with higher residence time of the air mass over the urban areas, it was enriched with SA and organics from proximal-local sources leading to the occurrence of regional and local events (30 June 2019 and 30 July 2019). In contrast, when the air mass travelled over the water bodies, with higher residence times over the cyanobacterial blooms, the air mass was enriched with biogenic IA and/or SA initiating a burst/spike event at the measurement site (11, 14, 15 August 2019). This observation is comparable to other coastal sites like Mace Head, although the NPF events are much stronger in Mace Head, since the measurement site is just at the coast with intensive low tide–high tide periods. 3) The formation rates of 1.5 nm particle and ions suggest that both IA-driven and SA-driven NPF events were neutral nucleation events. 4) The type of phytoplankton species, intensity of the bloom and distance of the bloom from the experimental site is speculated to play~~s~~ an ~~very~~ important role in determining the concentrations of precursor gases and thus influence the duration and type of NPF. The IA driven nucleation occurred when the air mass travelled from over the Baltic Sea region, where the coasts are dominated by several species of macroalgae, including *F. vesiculosus.* The SA rich burst events occurred when air mass travelled over the Gulf of Bothnia which was mainly dominated by the cyanobacteria species *Aphanizomenon* 5) Burst/spike events, connected to high IA concentrations, likely led to fast growth of particles potentially to CCN sizes. The role of stabilizing the IA clusters by SA and ammonia in a semi-urban coastal place needs to be further explored. The growth rate of particles was not fully explained by the SA, IA and MSA alone, this applies especially for 3–7 nm or larger particles, indicating that organics might be playing a critical role in the growth of particles in this semi-urban location. We have significantly high ambient concentrations of HOMs in this study, although the detailed descriptions is beyond the scope of this work.

The role of organics (HOM) in the growth of particles is an active research question. Exploring the sources and characterizing them during a bloom period, when the emission of biogenic volatile organics increase with temperature, is crucial to understand the climate linkages of aerosol formation. In order to r~~R~~esolv~~e~~~~ing~~ these links require more quantitative studies are required, which aims to understand the correlation between the~~linking~~ ~~of the~~ quality and quantity of cyanobacterial blooms and~~to~~ the strength of emissions ~~and to production~~ of aerosol precursors. More systematic studies, partitioning the influence of pelagic cyanobacterial blooms and ~~influence of~~ coastal macroalgae on new particle formations, would need to be undertaken.

Data availability

Mass spectrometer and air ion spectrometer data related to this article are available upon request to the corresponding author. Rest of the data are available for download from https://avaa.tdata.fi/web/smart/smear.

Supplement

The supplement related to this article is available online at:

Author contributions

RCT and TJ, MS designed the experiment, MS, LB, NS, YJT, TC, YJ, JL, ML were involved in the instrument installations and performed calibrations, RCT, collected, processed, analyzed and interpreted the mass spectrometric data. TC, JS, JL, RCT and ML collected and processed the particle data. RCT, LD and KL interpreted the particle data. LD, LB, LQ and XCH preformed the calculations. MS, RCT, TJ and MK conceptualized the idea of connecting marine biology and atmospheric processes. AN improvised the marine biology section of the paper. CX carried out Flexpart analysis. MM contributed to the satellite data procurement and its interpretation. All authors contributed commented on the manuscript and improvised the data interpretation.

Acknowledgements

We thank the ACTRIS CiGAS-UHEL calibration center for providing facility for CI-APi-TOF calibration and INAR technical staff for support during the entire experiment. We acknowledge Finnish Meteorological Institute for providing open access to oceanographic data used in this study.

Financial support: This work was supported by the European Research Council (ERC) under the European Union's Horizon 2020 research and innovation programme (GASPARCON, grant agreement no. 714621) and by the Finnish Academy (grant agreement no. 334514). We also acknowledge Jane and Aatos Erkko Foundation, ERC ATM-GTP, Flagship ACCC and Aerosols, clouds and trace gases infrastructure (ACTRIS) for funding support. The authors gratefully

Field Code Changed

Formatted: English (United States)

Formatted: Font: (Default) Times New Roman, 12 pt, Not Italic, Font color: Auto, English (United States), Pattern: Clear

acknowledge the NOAA Air Resources Laboratory (ARL) for the provision of the HYSPLIT transport and dispersion model and/or READY website (https://www.ready.noaa.gov) used in this publication. We also acknowledge Finnish Meteorological Institute for the provision of the wave height data in used this study through the website https://en.ilmatieteenlaitos.fi/wave-height. We humbly acknowledge the useful discussion and data reference obtained from Finnish Environmental Institute.

References

Allan, J. D., Williams, P. I., Najera, J., Whitehead, J. D., Flynn, M. J., Taylor, J. W., Liu, D., Darbyshire, E., Carpenter, L. J., Chance, R., Andrews, S. J., Hackenberg, S. C. and McFiggans, G.: Iodine observed in new particle formation events in the Arctic atmosphere during ACCACIA, Atmos. Chem. Phys., 15(10), 5599–5609, doi:10.5194/acp-15-5599-2015, 2015.

Almeida, J., Schobesberger, S., Kürten, A., Ortega, I. K., Kupiainen-Määttä, O., Praplan, A. P., Adamov, A., Amorim, A., Bianchi, F., Breitenlechner, M., David, A., Dommen, J., Donahue, N. M., Downard, A., Dunne, E., Duplissy, J., Ehrhart, S., Flagan, R. C., Franchin, A., Guida, R., Hakala, J., Hansel, A., Heinritzi, M., Henschel, H., Jokinen, T., Junninen, H., Kajos, M., Kangasluoma, J., Keskinen, H., Kupc, A., Kurtén, T., Kvashin, A. N., Laaksonen, A., Lehtipalo, K., Leiminger, M., Leppä, J., Loukonen, V., Makhmutov, V., Mathot, S., McGrath, M. J., Nieminen, T., Olenius, T., Onnela, A., Petäjä, T., Riccobono, F., Riipinen, I., Rissanen, M., Rondo, L., Ruuskanen, T., Santos, F. D., Sarnela, N., Schallhart, S., Schnitzhofer, R., Seinfeld, J. H., Simon, M., Sipilä, M., Stozhkov, Y., Stratmann, F., Tomé, A., Tröstl, J., Tsagkogeorgas, G., Vaattovaara, P., Viisanen, Y., Virtanen, A., Vrtala, A., Wagner, P. E., Weingartner, E., Wex, H., Williamson, C., Wimmer, D., Ye, P., Yli-Juuti, T., Carslaw, K. S., Kulmala, M., Curtius, J., Baltensperger, U., Worsnop, D. R., Vehkamäki, H. and Kirkby, J.: Molecular understanding of sulphuric acid-amine particle nucleation in the atmosphere, Nature, 502(7471), 359–363, doi:10.1038/nature12663, 2013.

Andersen, J. H., Carstensen, J., Conley, D. J., Dromph, K., Fleming-Lehtinen, V., Gustafsson, B. G., Josefson, A. B., Norkko, A., Villnäs, A. and Murray, C.: Long-term temporal and spatial trends in eutrophication status of the Baltic Sea, Biol. Rev., doi:10.1111/brv.12221, 2017.

Ar Gall, E., Küpper, F. C. and Kloareg, B.: A survey of iodine content in Laminaria digitata, Bot. Mar., doi:10.1515/BOT.2004.004, 2004.

Artaxo, P., Rizzo, L. V., Brito, J. F., Barbosa, H. M. J., Arana, A., Sena, E. T., Cirino, G. G., Bastos, W., Martin, S. T. and Andreae, M. O.: Atmospheric aerosols in Amazonia and land use change: From natural biogenic to biomass burning conditions, Faraday Discuss., 165, 203–235, doi:10.1039/c3fd00052d, 2013.

Attard, K. M., Rodil, I. F., Berg, P., Norkko, J., Norkko, A. and Glud, R. N.: Seasonal metabolism and carbon export potential of a key coastal habitat: The perennial canopy-forming macroalga Fucus vesiculosus,

Limnol. Oceanogr., doi:10.1002/lno.11026, 2019.

Baalbaki, R., Pikridas, M., Jokinen, T., Laurila, T., Dada, L., Bezantakos, S., Ahonen, L., Neitola, K., Maisser, A., Bimenyimana, E., Christodoulou, A., Unga, F., Savvides, C., Lehtipalo, K., Kangasluoma, J., Biskos, G., Petäjä, T., Kerminen, V. M., Sciare, J. and Kulmala, M.: Towards understanding the characteristics of new particle formation in the Eastern Mediterranean, Atmos. Chem. Phys., doi:10.5194/acp-21-9223-2021, 2021.

Baccarini, A., Karlsson, L., Dommen, J., Duplessis, P., Vüllers, J., Brooks, I. M., Saiz-Lopez, A., Salter, M., Tjernström, M., Baltensperger, U., Zieger, P. and Schmale, J.: Frequent new particle formation over the high Arctic pack ice by enhanced iodine emissions, Nat. Commun., doi:10.1038/s41467-020-18551-0, 2020.

Bates, T.S., Lamb, B.K., Guenther, A., Dignon, J. and Stoiber, R.E.: Sulfur emissions to the atmosphere from natural sources., J Atmos Chem., 14, 315–337, https://doi.org/10.1007/BF00115242, 1992.

Beck, L. J., Sarnela, N., Junninen, H., Hoppe, C. J. M., Garmash, O., Bianchi, F., Riva, M., Rose, C., Peräkylä, O., Wimmer, D., Kausiala, O., Jokinen, T., Ahonen, L., Mikkilä, J., Hakala, J., He, X. C., Kontkanen, J., Wolf, K. K. E., Cappelletti, D., Mazzola, M., Traversi, R., Petroselli, C., Viola, A. P., Vitale, V., Lange, R., Massling, A., Nøjgaard, J. K., Krejci, R., Karlsson, L., Zieger, P., Jang, S., Lee, K., Vakkari, V., Lampilahti, J., Thakur, R. C., Leino, K., Kangasluoma, J., Duplissy, E. M., Siivola, E., Marbouti, M., Tham, Y. J., Saiz-Lopez, A., Petäjä, T., Ehn, M., Worsnop, D. R., Skov, H., Kulmala, M., Kerminen, V. M. and Sipilä, M.: Differing Mechanisms of New Particle Formation at Two Arctic Sites, Geophys. Res. Lett., doi:10.1029/2020GL091334, 2021.

Benson, D. R., Young, L. H., Kameel, F. R. and Lee, S. H.: Laboratory-measured nucleation rates of sulfuric acid and water binary homogeneous nucleation from the SO2 + OH reaction, Geophys. Res. Lett., 35(11), 1–6, doi:10.1029/2008GL033387, 2008.

Bergman, T., Laaksonen, A., Korhonen, H., Malila, J., Dunne, E. M., Mielonen, T., Lehtinen, K. E. J., Kühn, T., Arola, A. and Kokkola, H.: Geographical and diurnal features of amine-enhanced boundary layer nucleation, J. Geophys. Res. Atmos., 120, 9606–9624, doi:10.1002/ 2015JD023181, 2015.

Berresheim, H., Elste, T., Tremmel, H. G., Allen, A. G., Hansson, H. C., Rosman, K., Dal Maso, M., Mäkelä, J. M., Kulmala, M. and O'Dowd, C. D.: Gas-aerosol relationships of H2so4, MSA, and OH: Observations in the coastal marine boundary layer at Mace Head, Ireland, J. Geophys. Res. Atmos., 107(19), 1–12, doi:10.1029/2000JD000229, 2002.

Bianchi, F., Tröstl, J., Junninen, H., Frege, C., Henne, S., Hoyle, C. R., Molteni, U., Herrmann, E., Adamov, A., Bukowiecki, N., Chen, X., Duplissy, J., Gysel, M., Hutterli, M., Kangasluoma, J., Kontkanen, J., Kürten, A., Manninen, H. E., Münch, S., Peräkylä, O., Petäjä, T., Rondo, L., Williamson, C., Weingartner, E., Curtius, J., Worsnop, D. R., Kulmala, M., Dommen, J. and Baltensperger, U.: New particle formation in the free troposphere: A question of chemistry and timing, Science (80-.)., 352(6289), 1109–1112, doi:10.1126/science.aad5456, 2016.

Bianchi, F., Junninen, H., Bigi, A., Sinclair, V. A., Dada, L., Hoyle, C. R., Zha, Q., Yao, L., Ahonen, L. R.,

Bonasoni, P., Buenrostro Mazon, S., Hutterli, M., Laj, P., Lehtipalo, K., Kangasluoma, J., Kerminen, V. M., Kontkanen, J., Marinoni, A., Mirme, S., Molteni, U., Petäjä, T., Riva, M., Rose, C., Sellegri, K., Yan, C., Worsnop, D. R., Kulmala, M., Baltensperger, U. and Dommen, J.: Biogenic particles formed in the Himalaya as an important source of free tropospheric aerosols, Nat. Geosci., doi:10.1038/s41561-020-00661-5, 2020.

Bigg, E. K. and Turvey, D. E.: Sources of atmospheric particles over Australia, Atmos. Environ., 12(8), 1643–1655, doi:10.1016/0004-6981(78)90313-X, 1978.

Boy, M., Karl, T., Turnipseed, A., Mauldin, R. L., Kosciuch, E., Greenberg, J., Rathbone, J., Smith, J., Held, A., Barsanti, K., Wehner, B., Bauer, S., Wiedensohler, A., Bonn, B., Kulmala, M. and Guenther, A.: New particle formation in the front range of the Colorado Rocky Mountains, Atmos. Chem. Phys., 8(6), 1577–1590, doi:10.5194/acp-8-1577-2008, 2008.

Buenrostro Mazon, S., Kontkanen, J., Manninen, H. E., Nieminen, T., Kerminen, V. M. and Kulmala, M.: A long-term comparison of nighttime cluster events and daytime ion formation in a boreal forest, Boreal Environ. Res., 21(3–4), 242–261, 2016.

Cai, R. and Jiang, J.: A new balance formula to estimate new particle formation rate: Reevaluating the effect of coagulation scavenging, Atmos. Chem. Phys., 17(20), 12659–12675, doi:10.5194/acp-17-12659-2017, 2017.

Carbone, M. S., Park Williams, A., Ambrose, A. R., Boot, C. M., Bradley, E. S., Dawson, T. E., Schaeffer, S. M., Schimel, J. P. and Still, C. J: Cloud shading and fog drip influence the metabolism of a coastal pine ecosystem Global Change Biol., 19, 484–97, 2013.

Chan, T., Cai, R., Ahonen, L. R., Liu, Y., Zhou, Y., Vanhanen, J., Dada, L., Chao, Y., Liu, Y., Wang, L., Kulmala, M. and Kangasluoma, J.: Assessment of particle size magnifier inversion methods to obtain the particle size distribution from atmospheric measurements, Atmos. Meas. Tech., 13(9), 4885–4898, doi:10.5194/amt-13-4885-2020, 2020.

Chen, D., Wang, W., Li, D. and Wang, W.: Atmospheric implication of synergy in methanesulfonic acid-base trimers: A theoretical investigation, RSC Adv., 10(9), 5173–5182, doi:10.1039/c9ra08760e, 2020.

Chen, H., Ezell, M. J., Arquero, K. D., Varner, M. E., Dawson, M. L., Gerber, R. B. and Finlayson-Pitts, B. J.: New particle formation and growth from methanesulfonic acid, trimethylamine and water, Phys. Chem. Chem. Phys., 17(20), 13699–13709, doi:10.1039/c5cp00838g, 2015.

Chen, H., Varner, M. E., Gerber, R. B. and Finlayson-Pitts, B. J.: Reactions of Methanesulfonic Acid with Amines and Ammonia as a Source of New Particles in Air, J. Phys. Chem. B, 120(8), 1526–1536, doi:10.1021/acs.jpcb.5b07433, 2016.

Croft, B., Martin, R. V., Richard Leaitch, W., Tunved, P., Breider, T. J., D'Andrea, S. D. and Pierce, J. R.: Processes controlling the annual cycle of Arctic aerosol number and size distributions, Atmos. Chem. Phys., 16(6), 3665–3682, doi:10.5194/acp-16-3665-2016, 2016.

Dada, L., Paasonen, P., Nieminen, T., Buenrostro Mazon, S., Kontkanen, J., Peräkylä, O., Lehtipalo, K., Hussein, T., Petäjä, T., Kerminen, V. M., Bäck, J. and Kulmala, M.: Long-term analysis of clear-sky

new particle formation events and nonevents in Hyytiälä, Atmos. Chem. Phys., doi:10.5194/acp-17-6227-2017, 2017.

Dada, L., Chellapermal, R., Buenrostro Mazon, S., Paasonen, P., Lampilahti, J., E Manninen, H., Junninen, H., Petäjä, T., Kerminen, V. M. and Kulmala, M.: Refined classification and characterization of atmospheric new-particle formation events using air ions, Atmos. Chem. Phys., 18(24), 17883–17893, doi:10.5194/acp-18-17883-2018, 2018.

Dada, L., Lehtipalo, K., Kontkanen, J., Nieminen, T., Baalbaki, R., Ahonen, L., Duplissy, J., Yan, C., Chu, B., Petäjä, T., Lehtinen, K., Kerminen, V. M., Kulmala, M. and Kangasluoma, J.: Formation and growth of sub-3-nm aerosol particles in experimental chambers, Nat. Protoc., 15(3), 1013–1040, doi:10.1038/s41596-019-0274-z, 2020a.

Dada, L., Ylivinkka, I., Baalbaki, R., Li, C., Guo, Y., Yan, C., Yao, L., Sarnela, N., Jokinen, T., Daellenbach, K. R., Yin, R., Deng, C., Chu, B., Nieminen, T., Wang, Y., Lin, Z., Thakur, R. C., Kontkanen, J., Stolzenburg, D., Sipilä, M., Hussein, T., Paasonen, P., Bianchi, F., Salma, I., Weidinger, T., Pikridas, M., Sciare, J., Jiang, J., Liu, Y., Petäjä, T., Kerminen, V. M. and Kulmala, M.: Sources and sinks driving sulfuric acid concentrations in contrasting environments: Implications on proxy calculations, Atmos. Chem. Phys., doi:10.5194/acp-20-11747-2020, 2020b.

Dal Maso, M., Kulmala, M., Lehtinen, K. E. J., Mkelä, J. M., Aalto, P. and O'Dowd, C. D.: Condensation and coagulation sinks and formation of nucleation mode particles in coastal and boreal forest boundary layers, J. Geophys. Res. Atmos., 107(19), 1–22, doi:10.1029/2001JD001053, 2002.

Dal Maso, M., Kulmala, M., Riipinen, I., Wagner, R., Hussein, T., Aalto, P. P. and Lehtinen, K. E. J.: Formation and growth of fresh atmospheric aerosols: Eight years of aerosol size distribution data from SMEAR II, Hyytiälä, Finland, Boreal Environ. Res., 10(5), 323–336, 2005.

Dal Maso, M., Liao, L., Wildt, J., Kiendler-Scharr, A., Kleist, E., Tillmann, R., Sipilä, M., Hakala, J., Lehtipalo, K., Ehn, M., Kerminen, V. M., Kulmala, M., Worsnop, D. and Mentel, T.: A chamber study of the influence of boreal BVOC emissions and sulfuric acid on nanoparticle formation rates at ambient concentrations, Atmos. Chem. Phys., 16(4), 1955–1970, doi:10.5194/acp-16-1955-2016, 2016.

Deng, C., Fu, Y., Dada, L., Yan, C., Cai, R., Yang, D., Zhou, Y., Yin, R., Lu, Y., Li, X., Qiao, X., Fan, X., Nie, W., Kontkanen, J., Kangasluoma, J., Chu, B., Ding, A., Kerminen, V. M., Paasonen, P., Worsnop, D. R., Bianchi, F., Liu, Y., Zheng, J., Wang, L., Kulmala, M. and Jiang, J.: Seasonal characteristics of new particle formation and growth in urban Beijing, Environ. Sci. Technol., 54(14), 8547–8557, doi:10.1021/acs.est.0c00808, 2020.

Dowd, C. D. O., Lowe, J. A., Smith, M. H., Davison, B., Hewitt, C. N. and Harrison, R. M.: Biogenic sulphur emissions and inferred non-sea-salt-sulphate particularly during Events of new particle formation were Instrumentation and Cruise Summary, Atlantic, 102(Dll), 1997.

Du, W., Dada, L., Zhao, J., Chen, X., Daellenbach, K. R., Xie, C., Wang, W., He, Y., Cai, J., Yao, L., Zhang, Y., Wang, Q., Xu, W., Wang, Y., Tang, G., Cheng, X., Kokkonen, T. V., Zhou, W., Yan, C., Chu, B., Zha, Q., Hakala, S., Kurppa, M., Järvi, L., Liu, Y., Li, Z., Ge, M., Fu, P., Nie, W., Bianchi, F., Petäjä,

T., Paasonen, P., Wang, Z., Worsnop, D. R., Kerminen, V. M., Kulmala, M. and Sun, Y.: A 3D study on the amplification of regional haze and particle growth by local emissions, npj Clim. Atmos. Sci., doi:10.1038/s41612-020-00156-5, 2021.

Duplissy, J., Merikanto, J., Franchin, A., Tsagkogeorgas, G., Kangasluoma, J., Wimmer, D., Vuollekoski, H., Schobesberger, S., Lehtipalo, K., Flagan, R. C., Brus, D., Donahue, N. M., Vehkamäki, H., Almeida, J., Amorim, A., Barmet, P., Bianchi, F., Breitenlechner, M., Dunne, E. M., Guida, R., Henschel, H., Junninen, H., Kirkby, J., Kürten, A., Kupc, A., Määttänen, A., Makhmutov, V., Mathot, S., Nieminen, T., Onnela, A., Praplan, A. P., Riccobono, F., Rondo, L., Steiner, G., Tome, A., Walther, H., Baltensperger, U., Carslaw, K. S., Dommen, J., Hansel, A., Petäjä, T., Sipilä, M., Stratmann, F., Vrtala, A., Wagner, P. E., Worsnop, D. R., Curtius, J. and Kulmala, M.: Journal of Geophysical Research : Atmospheres, , 1752–1775, doi:10.1002/2015JD023538.Effect, 2016.

Eisele, Fred L; Tanner, D. .: Measurement of the gas phase concentrationof H2SO4 and Methane sulphonic acid and estimates of H2SO4 production and Loss in Atmosphere, , 98(93), 9001–9010, 1993.

Eisele, F. L., Lovejoy, E. R., Kosciuch, E., Moore, K. F., Mauldin, I. L., Smith, J. N., McMurry, P. H. and Iida, K.: Negative atmospheric ions and their potential role in ion-induced nucleation, J. Geophys. Res. Atmos., 111(4), doi:10.1029/2005JD006568, 2006.

Ehn, M., Thornton, J. A., Kleist, E., Sipilä, M., Junninen, H., Pullinen, I., Springer, M., Rubach, F., Tillmann, R., Lee, B., Lopez-Hilfiker, F., Andres, S., Acir, I.-H. H., Rissanen, M., Jokinen, T., Schobesberger, S., Kangasluoma, J., Kontkanen, J., Nieminen, T., Kurtén, T., Nielsen, L. B., Jørgensen, S., Kjaergaard, H. G., Canagaratna, M., Maso, M. D., Berndt, T., Petäjä, T., Wahner, A., Kerminen, V.-M. M., Kulmala, M., Worsnop, D. R., Wildt, J. and Mentel, T. F.: A large source of low-volatility secondary organic aerosol, Nature, 506(7489), 476–479, doi:10.1038/nature13032, 2014.

Emery, N. C., D'Antonio, C .M. and Still, C. J.: Fog and live fuel moisture in coastal California shrublands Ecosphere, 9, e02167, https://doi.org/10.1002/ecs2.2167 ,2018.

Fiedler, V., Dal Maso, M., Boy, M., Aufmhoff, H., Hoffmann, J., Schuck, T., Birmili, W., Hanke, M., Uecker, J., Arnold, F. and Kulmala, M.: The contribution of sulphuric acid to atmospheric particle formation and growth: A comparison between boundary layers in Northern and Central Europe, Atmos. Chem. Phys., 5(7), 1773–1785, doi:10.5194/acp-5-1773-2005, 2005.

Flanagan, R. J., Geever, M. and O'Dowd, C. D.: Direct measurements of new-particle fluxes in the coastal environment, Environ. Chem., 2(4), 256–259, doi:10.1071/EN05069, 2005.

Funkey, C. P., Conley, D. J., Reuss, N. S., Humborg, C., Jilbert, T. and Slomp, C. P.: Hypoxia sustains cyanobacteria blooms in the Baltic Sea, Environ. Sci. Technol., doi:10.1021/es404395a, 2014.

Glasoe, W. A., Volz, K., Panta, B., Freshour, N., Bachman, R., Hanson, D. R., McMurry, P. H. and Jen, C.: Sulfuric acid nucleation: An experimental study of the effect of seven bases, J. Geophys. Res., doi:10.1002/2014JD022730, 2015.

He, X. C., Iyer, S., Sipilä, M., Ylisirniö, A., Peltola, M., Kontkanen, J., Baalbaki, R., Simon, M., Kürten, A.,

Tham, Y. J., Pesonen, J., Ahonen, L. R., Amanatidis, S., Amorim, A., Baccarini, A., Beck, L., Bianchi, F., Brilke, S., Chen, D., Chiu, R., Curtius, J., Dada, L., Dias, A., Dommen, J., Donahue, N. M., Duplissy, J., El Haddad, I., Finkenzeller, H., Fischer, L., Heinritzi, M., Hofbauer, V., Kangasluoma, J., Kim, C., Koenig, T. K., Kubečka, J., Kvashnin, A., Lamkaddam, H., Lee, C. P., Leiminger, M., Li, Z., Makhmutov, V., Xiao, M., Marten, R., Nie, W., Onnela, A., Partoll, E., Petäjä, T., Salo, V. T., Schuchmann, S., Steiner, G., Stolzenburg, D., Stozhkov, Y., Tauber, C., Tomé, A., Väisänen, O., Vazquez-Pufleau, M., Volkamer, R., Wagner, A. C., Wang, M., Wang, Y., Wimmer, D., Winkler, P. M., Worsnop, D. R., Wu, Y., Yan, C., Ye, Q., Lehtinen, K., Nieminen, T., Manninen, H. E., Rissanen, M., Schobesberger, S., Lehtipalo, K., Baltensperger, U., Hansel, A., Kerminen, V. M., Flagan, R. C., Kirkby, J., Kurtén, T. and Kulmala, M.: Determination of the collision rate coefficient between charged iodic acid clusters and iodic acid using the appearance time method, Aerosol Sci. Technol., doi:10.1080/02786826.2020.1839013, 2021a.

He, X. C., Tham, Y. J., Dada, L., Wang, M., Finkenzeller, H., Stolzenburg, D., Iyer, S., Simon, M., Kürten, A., Shen, J., Rörup, B., Rissanen, M., Schobesberger, S., Baalbaki, R., Wang, D. S., Koenig, T. K., Jokinen, T., Sarnela, N., Beck, L. J., Almeida, J., Amanatidis, S., Amorim, A., Ataei, F., Baccarini, A., Bertozzi, B., Bianchi, F., Brilke, S., Caudillo, L., Chen, D., Chiu, R., Chu, B., Dias, A., Ding, A., Dommen, J., Duplissy, J., Haddad, I. El, Carracedo, L. G., Granzin, M., Hansel, A., Heinritzi, M., Hofbauer, V., Junninen, H., Kangasluoma, J., Kemppainen, D., Kim, C., Kong, W., Krechmer, J. E., Kvashin, A., Laitinen, T., Lamkaddam, H., Lee, C. P., Lehtipalo, K., Leiminger, M., Li, Z., Makhmutov, V., Manninen, H. E., Marie, G., Marten, R., Mathot, S., Mauldin, R. L., Mentler, B., Möhler, O., Müller, T., Nie, W., Onnela, A., Petäjä, T., Pfeifer, J., Philippov, M., Ranjithkumar, A., Saiz-Lopez, A., Salma, I., Scholz, W., Schuchmann, S., Schulze, B., Steiner, G., Stozhkov, Y., Tauber, C., Tomé, A., Thakur, R. C., Väisänen, O., Vazquez-Pufleau, M., Wagner, A. C., Wang, Y., Weber, S. K., Winkler, P. M., Wu, Y., Xiao, M., Yan, C., Ye, Q., Ylisirniö, A., Zauner-Wieczorek, M., Zha, Q., Zhou, P., Flagan, R. C., Curtius, J., Baltensperger, U., Kulmala, M., Kerminen, V. M., Kurtén, T., et al.: Role of iodine oxoacids in atmospheric aerosol nucleation, Science (80-.)., doi:10.1126/science.abe0298, 2021b.

Hoffmann, E. H., Tilgner, A., Schrödner, R., Bräuer, P., Wolke, R. and Herrmann, H.: An advanced modeling study on the impacts and atmospheric implications of multiphase dimethyl sulfide chemistry, Proc. Natl. Acad. Sci. U. S. A., doi:10.1073/pnas.1606320113, 2016.

Huang, R.-J., Seitz, K., Buxmann, J., Poehler, D., Hornsby, K. E., Carpenter, L. J., Platt, U. and Hoffmann, T.: In situ measurements of molecular iodine in the marine boundary layer: the link to macroalgae and the implications for O₃, IO, OIO and NO_x, Atmos. Chem. Phys. Discuss., 10(1), 361–390, doi:10.5194/acpd-10-361-2010, 2010.

Huang, R. J., Thorenz, U. R., Kundel, M., Venables, D. S., Ceburnis, D., Ho, K. F., Chen, J., Vogel, A. L., Küpper, F. C., Smyth, P. P. A., Nitschke, U., Stengel, D. B., Berresheim, H., O'Dowd, C. D. and Hoffmann, T.: The seaweeds Fucus vesiculosus and Ascophyllum nodosum are significant contributors to coastal iodine emissions, Atmos. Chem. Phys., 13(10), 5255–5264, doi:10.5194/acp-13-5255-2013,

Formatted: Justified, Space Before: 0 pt, No widow/orphan control, Don't adjust space between Latin and Asian text, Don't adjust space between Asian text and numbers, Pattern: Clear

2013.
Humborg, C., Geibel, M.C., Sun, X., McCrackin, M, Mörth, C-M., Stranne. C., Jakobsson, M., Gustafsson, B., Sokolov, A., Norkko, A. and Norkko, J.: High Emissions of Carbon Dioxide and Methane From the Coastal Baltic Sea at the End of a Summer Heat Wave. Front. Mar. Sci. 6, https://doi.org/10.3389/fmars.2019.00493, 2019.
Iida, K., Stolzenburg, M. R., McMurry, P. H. and Smith, J. N.: Estimating nanoparticle growth rates from size-dependent charged fractions: Analysis of new particle formation events in Mexico City, J. Geophys. Res. Atmos., 113(5), 1–15, doi:10.1029/2007JD009260, 2008.
Jang, E., Park, K. T., Jun Yoon, Y., Kim, T. W., Hong, S. B., Becagli, S., Traversi, R., Kim, J. and Gim, Y.: New particle formation events observed at the King Sejong Station, Antarctic Peninsula - Part 2: Link with the oceanic biological activities, Atmos. Chem. Phys., 19(11), 7595–7608, doi:10.5194/acp-19-7595-2019, 2019.
Jokinen, T., Sipilä, M., Junninen, H., Ehn, M., Lönn, G., Hakala, J., Petäjä, T., Mauldin, R. L., Kulmala, M. and Worsnop, D. R.: Atmospheric sulphuric acid and neutral cluster measurements using CI-APi-TOF, Atmos. Chem. Phys., 12(9), 4117–4125, doi:10.5194/acp-12-4117-2012, 2012.
Jokinen, T., Sipilä, M., Kontkanen, J., Vakkari, V., Tisler, P., Duplissy, E. M., Junninen, H., Kangasluoma, J., Manninen, H. E., Petäjä, T., Kulmala, M., Worsnop, D. R., Kirkby, J., Virkkula, A. and Kerminen, V. M.: Ion-induced sulfuric acid–ammonia nucleation drives particle formation in coastal Antarctica, Sci. Adv., 4(11), 1–7, doi:10.1126/sciadv.aat9744, 2018.
Jokinen, T., Kontkanen, J., Lehtipalo, K. et al. Solar eclipse demonstrating the importance of photochemistry in new particle formation. Sci Rep 7, 45707, https://doi.org/10.1038/srep45707, 2017.
Junninen, H., Ehn, M., Petäjä, T., Luosujärvi, L., Kotiaho, T., Kostiainen, R., Rohner, U., Gonin, M., Fuhrer, K., Kulmala, M. and Worsnop, D. R.: A high-resolution mass spectrometer to measure atmospheric ion composition, Atmos. Meas. Tech. Discuss., 3(1), 599–636, doi:10.5194/amtd-3-599-2010, 2010.
Kahru, M. and Elmgren, R.: Multidecadal time series of satellite-detected accumulations of cyanobacteria in the Baltic Sea, Biogeosciences, doi:10.5194/bg-11-3619-2014, 2014.
Kautsky, L. and Kautsky, N.: The Baltic Sea, including Bothnian Sea and Bothnian Bay, Seas Millenn. - an Environ. Eval. - Vol. 1, 2000.
Keller, M. D., Bellows, W. K. and Guillard, R. R. L.: Dimethyl Sulfide Production in Marine Phytoplankton., 1989.
Kettle, A. J. and Andreae, M. O.: Flux of dimethylsulfide from the oceans: A comparison of updated data sets and flux models, J. Geophys. Res. Atmos., doi:10.1029/2000JD900252, 2000.
Kirkby, J., Curtius, J., Almeida, J., Dunne, E., Duplissy, J., Ehrhart, S., Franchin, A., Gagné, S., Ickes, L., Kürten, A., Kupc, A., Metzger, A., Riccobono, F., Rondo, L., Schobesberger, S., Tsagkogeorgas, G., Wimmer, D., Amorim, A., Bianchi, F., Breitenlechner, M., David, A., Dommen, J., Downard, A., Ehn, M., Flagan, R. C., Haider, S., Hansel, A., Hauser, D., Jud, W., Junninen, H., Kreissl, F., Kvashin, A., Laaksonen, A., Lehtipalo, K., Lima, J., Lovejoy, E. R., Makhmutov, V., Mathot, S., Mikkilä, J.,

Minginette, P., Mogo, S., Nieminen, T., Onnela, A., Pereira, P., Petäjä, T., Schnitzhofer, R., Seinfeld, J. H., Sipilä, M., Stozhkov, Y., Stratmann, F., Tomé, A., Vanhanen, J., Viisanen, Y., Vrtala, A., Wagner, P. E., Walther, H., Weingartner, E., Wex, H., Winkler, P. M., Carslaw, K. S., Worsnop, D. R., Baltensperger, U. and Kulmala, M.: Role of sulphuric acid, ammonia and galactic cosmic rays in atmospheric aerosol nucleation, Nature, 476(7361), 429–435, doi:10.1038/nature10343, 2011.

Kirkby, J., Duplissy, J., Sengupta, K., Frege, C., Gordon, H., Williamson, C., Heinritzi, M., Simon, M., Yan, C., Almeida, J., Trostl, J., Nieminen, T., Ortega, I. K., Wagner, R., Adamov, A., Amorim, A., Bernhammer, A. K., Bianchi, F., Breitenlechner, M., Brilke, S., Chen, X., Craven, J., Dias, A., Ehrhart, S., Flagan, R. C., Franchin, A., Fuchs, C., Guida, R., Hakala, J., Hoyle, C. R., Jokinen, T., Junninen, H., Kangasluoma, J., Kim, J., Krapf, M., Kurten, A., Laaksonen, A., Lehtipalo, K., Makhmutov, V., Mathot, S., Molteni, U., Onnela, A., Perakyla, O., Piel, F., Petaja, T., Praplan, A. P., Pringle, K., Rap, A., Richards, N. A. D., Riipinen, I., Rissanen, M. P., Rondo, L., Sarnela, N., Schobesberger, S., Scott, C. E., Seinfeld, J. H., Sipila, M., Steiner, G., Stozhkov, Y., Stratmann, F., Tomé, A., Virtanen, A., Vogel, A. L., Wagner, A. C., Wagner, P. E., Weingartner, E., Wimmer, D., Winkler, P. M., Ye, P., Zhang, X., Hansel, A., Dommen, J., Donahue, N. M., Worsnop, D. R., Baltensperger, U., Kulmala, M., Carslaw, K. S. and Curtius, J.: Ion-induced nucleation of pure biogenic particles, Nature, 533(7604), 521–526, doi:10.1038/nature17953, 2016.

Knutson, E. O. and Whitby, K. T.: Aerosol classification by electric mobility: apparatus, theory, and applications, J. Aerosol Sci., 6(6), 443–451, doi:10.1016/0021-8502(75)90060-9, 1975.

Knutson, E. O., Whitby, K. T., Fiedler, V., Dal Maso, M., Boy, M., Aufmhoff, H., Hoffmann, J., Schuck, T., Birmili, W., Hanke, M., Uecker, J., Arnold, F., Kulmala, M., Petäjä, T., Nieminen, T., Sipilä, M., Manninen, H. E., Lehtipalo, K., Dal Maso, M., Aalto, P. P., Junninen, H., Paasonen, P., Riipinen, I., Lehtinen, K. E. J., Laaksonen, A., Kerminen, V. M., Croft, B., Martin, R. V., Richard Leaitch, W., Tunved, P., Breider, T. J., D'Andrea, S. D., Pierce, J. R., Glasoe, W. A., Volz, K., Panta, B., Freshour, N., Bachman, R., Hanson, D. R., McMurry, P. H., Jen, C., Suikkanen, S., Pulina, S., Engström-Öst, J., Lehtiniemi, M., Lehtinen, S., Brutemark, A., Berresheim, H., Elste, T., Tremmel, H. G., Allen, A. G., Hansson, H. C., Rosman, K., Dal Maso, M., Mäkelä, J. M., Kulmala, M., O'Dowd, C. D., Lehtinen, K. E. J., Kulmala, M., Manninen, H. E., Nieminen, T., Asmi, E., Gagné, S., Häkkinen, S., Lehtipalo, K., Aalto, P. P., Vana, M., Mirme, A., Mirme, S., Hõrrak, U., Plass-Dülmer, C., Stange, G., Kiss, G., Hoffer, A., Töro, N., Moerman, M., Henzing, B., De Leeuw, G., Brinkenberg, M., Kouvarakis, G. N., Bougiatioti, A., Mihalopoulos, N., O'Dowd, C. D., Ceburnis, D., Arneth, A., Svenningsson, B., Swietlicki, E., Tarozzi, L., Decesari, S., Facchini, M. C., Birmili, W., Sonntag, A., Wiedensohler, A., Boulon, J., Sellegri, K., Laj, P., Gysel, M., Bukowiecki, N., Weingartner, E., et al.: Quantification of the volatility of secondary organic compounds in ultrafine particles during nucleation events, Atmos. Chem. Phys., 10(4), 1–10, doi:10.1039/c9ra08760e, 2016.

Kownacka, J., Całkiewicz, J. and Kornijów, R.: A turning point in the development of phytoplankton in the Vistula Lagoon (southern Baltic Sea) at the beginning of the 21st century, Oceanologia,

doi:10.1016/j.oceano.2020.08.004, 2020.

Kulmala, M., Toivonen, A., Mäkelä, J. M. and Laaksonen, A.: Analysis of the growth of nucleation mode particles observed in Boreal forest, Tellus, Ser. B Chem. Phys. Meteorol., doi:10.3402/tellusb.v50i5.16229, 1998.

Kulmala, M., Laakso, L., Lehtinen, K. E. J., Riipinen, I., Dal Maso, M., Anttila, T., Kerminen, V.-M., Hõrrak, U., Vana, M. and Tammet, H.: Initial steps of aerosol growth, Atmos. Chem. Phys., doi:10.5194/acp-4-2553-2004, 2004.

Kulmala, M., Petäjä, T., Mönkkönen, P., Koponen, I. K., Dal Maso, M., Aalto, P. P., Lehtinen, K. E. J. and Kerminen, V. M.: On the growth nucleation mode particles: Source rates of condensable vapor in polluted and clean environments, Atmos. Chem. Phys., 5(2), 409–416, doi:10.5194/acp-5-409-2005, 2005.

Kulmala, M., Petäjä, T., Nieminen, T., Sipilä, M., Manninen, H. E., Lehtipalo, K., Dal Maso, M., Aalto, P. P., Junninen, H., Paasonen, P., Riipinen, I., Lehtinen, K. E. J., Laaksonen, A. and Kerminen, V. M.: Measurement of the nucleation of atmospheric aerosol particles, Nat. Protoc., 7(9), 1651–1667, doi:10.1038/nprot.2012.091, 2012.

Kulmala, M., Kontkanen, J., Junninen, H., Lehtipalo, K., Manninen, H. E., Nieminen, T., Petäjä, T., Sipilä, M., Schobesberger, S., Rantala, P., Franchin, A., Jokinen, T., Järvinen, E., Äijälä, M., Kangasluoma, J., Hakala, J., Aalto, P. P., Paasonen, P., Mikkilä, J., Vanhanen, J., Aalto, J., Hakola, H., Makkonen, U., Ruuskanen, T., Mauldin, R. L., Duplissy, J., Vehkamäki, H., Bäck, J., Kortelainen, A., Riipinen, I., Kurtén, T., Johnston, M. V., Smith, J. N., Ehn, M., Mentel, T. F., Lehtinen, K. E. J., Laaksonen, A., Kerminen, V. M. and Worsnop, D. R.: Direct observations of atmospheric aerosol nucleation, Science (80)., 339(6122), 943–946, doi:10.1126/science.1227385, 2013.

Kulmala, M., Petäjä, T., Kerminen, V. M., Kujansuu, J., Ruuskanen, T., Ding, A., Nie, W., Hu, M., Wang, Z., Wu, Z., Wang, L. and Worsnop, D. R.: On secondary new particle formation in China, Front. Environ. Sci. Eng., 10(5), 1–10, doi:10.1007/s11783-016-0850-1, 2016.

Kulmala, M., Kerminen, V. M., Petäjä, T., Ding, A. J. and Wang, L.: Atmospheric gas-to-particle conversion: Why NPF events are observed in megacities?, Faraday Discuss., 200, 271–288, doi:10.1039/c6fd00257a, 2017.

Kuosa, H., Fleming-Lehtinen, V., Lehtinen, S., Lehtiniemi, M., Nygård, H., Raateoja, M., Raitaniemi, J., Tuimala, J., Uusitalo, L. and Suikkanen, S.: A retrospective view of the development of the Gulf of Bothnia ecosystem, J. Mar. Syst., 167, 78–92, doi:10.1016/j.jmarsys.2016.11.020, 2017.

Küpper, F. C., Schweigert, N., Ar Gall, E., Legendre, J. M., Vilter, H. and Kloareg, B.: Iodine uptake in Laminariales involves extracellular, haloperoxidase-mediated oxidation of iodide, Planta, doi:10.1007/s004250050469, 1998.

Kürten, A., Jokinen, T., Simon, M., Sipilä, M., Sarnela, N., Junninen, H., Adamov, A., Almeida, J., Amorim, A., Bianchi, F., Breitenlechner, M., Dommen, J., Donahue, N. M., Duplissy, J., Ehrhart, S., Flagan, R. C., Franchin, A., Hakala, J., Hansel, A., Heinritzi, M., Hutterli, M., Kangasluoma, J., Kirkby, J.,

Laaksonen, A., Lehtipalo, K., Leiminger, M., Makhmutov, V., Mathot, S., Onnela, A., Petäjä, T., Praplan, A. P., Riccobono, F., Rissanen, M. P., Rondo, L., Schobesberger, S., Seinfeld, J. H., Steiner, G., Tomé, A., Tröstl, J., Winkler, P. M., Williamson, C., Wimmer, D., Ye, P., Baltensperger, U., Carslaw, K. S., Kulmala, M., Worsnop, D. R. and Curtius, J.: Neutral molecular cluster formation of sulfuric acid-dimethylamine observed in real time under atmospheric conditions, Proc. Natl. Acad. Sci. U. S. A., 111(42), 15019–15024, doi:10.1073/pnas.1404853111, 2014.

Kürten, A., Münch, S., Rondo, L., Bianchi, F., Duplissy, J., Jokinen, T., Junninen, H., Sarnela, N., Schobesberger, S., Simon, M., Sipilä, M., Almeida, J., Amorim, A., Dommen, J., Donahue, N. M., Dunne, E. M., Flagan, R. C., Franchin, A., Kirkby, J., Kupc, A., Makhmutov, V., Petäjä, T., Praplan, A. P., Riccobono, F., Steiner, G., Tomé, A., Tsagkogeorgas, G., Wagner, P. E., Wimmer, D., Baltensperger, U., Kulmala, M., Worsnop, D. R. and Curtius, J.: Thermodynamics of the formation of sulfuric acid dimers in the binary (H2SO4-H2O) and ternary (H2SO4-H2O-NH3) system, Atmos. Chem. Phys., 15(18), 10701–10721, doi:10.5194/acp-15-10701-2015, 2015.

Kürten, A., Bianchi, F., Almeida, J., Kupiainen-Määttä, O., Dunne, E. M., Duplissy, J., Williamson, C., Barmet, P., Breitenlechner, M., Dommen, J., Donahue, N. M., Flagan, R. C., Franchin, A., Gordon, H., Hakala, J., Hansel, A., Heinritzi, M., Ickes, L., Jokinen, T., Kangasluoma, J., Kim, J., Kirkby, J., Kupc, A., Lehtipalo, K., Leiminger, M., Makhmutov, V., Onnela, A., Ortega, I. K., Petäjä, T., Praplan, A. P., Riccobono, F., Rissanen, M. P., Rondo, L., Schnitzhofer, R., Schobesberger, S., Smith, J. N., Steiner, G., Stozhkov, Y., Tomé, A., Tröstl, J., Tsagkogeorgas, G., Wagner, P. E., Wimmer, D., Ye, P., Baltensperger, U., Carslaw, K., Kulmala, M. and Curtius, J.: Experimental particle formation rates spanning tropospheric sulfuric acid and ammonia abundances, ion production rates, and temperatures, J. Geophys. Res., doi:10.1002/2015JD023908, 2016.

Kurten, T., Petäjä, T., Smith, J., Ortega, I. K., Sipilä, M., Junninen, H., Ehn, M., Vehkamäki, H., Mauldin, L., Worsnop, D. R. and Kulmala, M.: The effect of H_2SO_4 – amine clustering on chemical ionization mass spectrometry (CIMS) measurements of gas-phase sulfuric acid, Atmos. Chem. Phys., 11, 3007–3019, doi:10.5194/acp-11-3007-2011, 2011.

Kyrö, E. M., Väänänen, R., Kerminen, V. M., Virkkula, A., Petäjä, T., Asmi, A., Dal Maso, M., Nieminen, T., Juhola, S., Shcherbinin, A., Riipinen, I., Lehtipalo, K., Keronen, P., Aalto, P. P., Hari, P. and Kulmala, M.: Trends in new particle formation in eastern Lapland, Finland: Effect of decreasing sulfur emissions from Kola Peninsula, Atmos. Chem. Phys., 14(9), 4383–4396, doi:10.5194/acp-14-4383-2014, 2014.

Lawson, D. M., Clemesha, R.E.S., Vanderplank, S., Gershunov, A. and Cayan, D.: Impacts and influences of coastal low clouds and fog on biodiversity in San Diego California's Fourth Climate Change Assessment CCCA4-EXT-2018-010 69–89, https://www.energy.ca.gov/ sites/default/files/2019-12/Biodiversity_CCCA4-EXT-2018-010_ada_0.pdf, 2018.

Lehtipalo, K., Yan, C., Dada, L., Bianchi, F., Xiao, M., Wagner, R., Stolzenburg, D., Ahonen, L. R., Amorim, A., Baccarini, A., Bauer, P. S., Baumgartner, B., Bergen, A., Bernhammer, A. K., Breitenlechner, M., Brilke, S., Buchholz, A., Mazon, S. B., Chen, D., Chen, X., Dias, A., Dommen, J., Draper, D. C.,

Formatted: Left, Widow/Orphan control, Adjust space between Latin and Asian text, Adjust space between Asian text and numbers, Pattern: Clear (White)

Formatted: Font: 11 pt, English (United States)

Duplissy, J., Ehn, M., Finkenzeller, H., Fischer, L., Frege, C., Fuchs, C., Garmash, O., Gordon, H., Hakala, J., He, X., Heikkinen, L., Heinritzi, M., Helm, J. C., Hofbauer, V., Hoyle, C. R., Jokinen, T., Kangasluoma, J., Kerminen, V.-M., Kim, C., Kirkby, J., Kontkanen, J., Kürten, A., Lawler, M. J., Mai, H., Mathot, S., Mauldin III, R. L., Molteni, U., Nichman, L., Nie, W., Nieminen, T., Ojdanic, A., Onnela, A., Passananti, M., Petäjä, T., Piel, F., Pospisilova, V., Quéléver, L. L. J., Rissanen, M. P., Rose, C., Sarnela, N., Schallhart, S., Schuchmann, S., Sengupta, K., Simon, M., Sipilä, M., Tauber, C., Tomé, A., Tröstl, J., Väisänen, O., Vogel, A. L., Volkamer, R., Wagner, A. C., Wang, M., Weitz, L., Wimmer, D., Ye, P., Ylisirniö, A., Zha, Q., Carslaw, K. S., Curtius, J., Donahue, N. M., Flagan, R. C., Hansel, A., Riipinen, I., Virtanen, A., Winkler, P. M., Baltensperger, U., Kulmala, M., and Worsnop, D. R.: Multicomponent new particle formation from sulfuric acid, ammonia, and 979 biogenic vapors, Sci. Adv., 12, doi: 10.1126/sciadv.aau5363, 2018.

Lehtipalo, K., Leppä, J., Kontkanen, J., Kangasluoma, J., Franchin, A., Wimmer, D., Schobesberger, S., Junninen, H., Petäjä, T., Sipilä, M., Mikkilä, J., Vanhanen, J., Worsnop, D. R. and, Kulmala, M.:, Lehtipalo, K., Mikkilä, J., Vanhanen, J., Leppä, J. and Worsnop, D. R.: Methods for determining particle size distribution and growth rates between 1 and 3 nm using the Particle Size Magnifier, Boreal Environ. Res., 19(September), 215–236, 2014.

Leino, K., Nieminen, T., Manninen, H. E., Petäjä, T., Kerminen, V. M. and Kulmala, M.: Intermediate ions as a strong indicator of new particle formation bursts in boreal forest, Boreal Environ. Res., 21(3–4), 274–286, 2016.

Mahajan, A. S., Oetjen, H., Saiz-Lopez, A., Lee, J. D., McFiggans, G. B. and Plane, J. M. C.: Reactive iodine species in a semi-polluted environment, Geophys. Res. Lett., 36(16), 6–11, doi:10.1029/2009GL038018, 2009.

Mahajan, A. S., Sorribas, M., Martín, J. C. G., MacDonald, S. M., Gil, M., Plane, J. M. C. and Saiz-Lopez, A.: Concurrent observations of atomic iodine, molecular iodine and ultrafine particles in a coastal environment, Atmos. Chem. Phys., 11(6), 2545–2555, doi:10.5194/acp-11-2545-2011, 2011.

Manninen, H. E., Nieminen, T., Asmi, E., Gagné, S., Häkkinen, S., Lehtipalo, K., Aalto, P., Vana, M., Mirme, A., Mirme, S., Hõrrak, U., Plass-Dülmer, C., Stange, G., Kiss, G., Hoffer, A., Töro, N., Moerman, M., Henzing, B., De Leeuw, G., Brinkenberg, M., Kouvarakis, G. N., Bougiatioti, A., Mihalopoulos, N., O'Dowd, C., Ceburnis, D., Arneth, A., Svenningsson, B., Swietlicki, E., Tarozzi, L., Decesari, S., Facchini, M. C., Birmili, W., Sonntag, A., Wiedensohler, A., Boulon, J., Sellegri, K., Laj, P., Gysel, M., Bukowiecki, N., Weingartner, E., Wehrle, G., Laaksonen, A., Hamed, A., Joutsensaari, J., Petäjä, T., Kerminen, V. M. and Kulmala, M.: EUCAARI ion spectrometer measurements at 12 European sites-analysis of new particle formation events, Atmos. Chem. Phys., 10(16), 7907–7927, doi:10.5194/acp-10-7907-2010, 2010.

Mauldin, R. L., Eisele, F. L., Kosciuch, E., Shetter, R., Lefer, B., Buhr, M., Chen, G., Wang, P. and Davis, D.: Oil] andjO (' D), , 28(19), 3629–3632, 2001.

McFiggans, G., Coe, H., Burgess, R., Allan, J., Cubison, M., Alfarra, M. R., Saunders, R., Saiz-Lopez, A.,

Plane, J. M. C., Wevill, D. J., Carpenter, L. J., Rickard, A. R. and Monks, P. S.: Direct evidence for coastal iodine particles from Laminaria macroalgae - Linkage to emissions of molecular iodine, Atmos. Chem. Phys., 4(3), 701–713, doi:10.5194/acp-4-701-2004, 2004.

McFiggans, G., Bale, C. S. E., Ball, S. M., Beames, J. M., Bloss, W. J., Carpenter, L. J., Dorsey, J., Dunk, R., Flynn, M. J., Furneaux, K. L., Gallagher, M. W., Heard, D. E., Hollingsworth, A. M., Hornsby, K., Ingham, T., Jones, C. E., Jones, R. L., Kramer, L. J., Langridge, J. M., Leblanc, C., LeCrane, J. P., Lee, J. D., Leigh, R. J., Longley, I., Mahajan, A. S., Monks, P. S., Oetjen, H., Orr-Ewing, A. J., Plane, J. M. C., Potin, P., Shillings, A. J. L., Thomas, F., Von Glasow, R., Wada, R., Whalley, L. K. and Whitehead, J. D.: Iodine-mediated coastal particle formation: An overview of the Reactive Halogens in the Marine boundary layer (RHaMBLe) Roscoff coastal study, Atmos. Chem. Phys., 10(6), 2975–2999, doi:10.5194/acp-10-2975-2010, 2010.

Meixner, F. X. and Yang, W. X.: Biogenic emissions of nitric oxide and nitrous oxide from arid and semi-arid land, in Dryland Ecohydrology., 2006.

Mirme, S. and Mirme, A.: The mathematical principles and design of the NAIS - A spectrometer for the measurement of cluster ion and nanometer aerosol size distributions, Atmos. Meas. Tech., 6(4), 1061–1071, doi:10.5194/amt-6-1061-2013, 2013.

~~Nieminen, T., Manninen, H. E., Sihto, S. L., Yli-Juuti, T., Mauldin, R. L., Petäjä, T., Riipinen, I., Kerminen, V. M. and Kulmala, M.: Connection of sulfuric acid to atmospheric nucleation in boreal forest, Environ. Sci. Technol., 43(13), 4715–4721, doi:10.1021/es803152j, 2009.~~

~~Nieminen, T., Lehtinen, K. E. J. and Kulmala, M.: Sub-10 nm particle growth by vapor condensation-effects of vapor molecule size and particle thermal speed, Atmos. Chem. Phys., doi:10.5194/acp-10-9773-2010, 2010.~~

Nieminen, T., Asmi, A., Aalto, P. P., Keronen, P., Petäjä, T., Kulmala, M., Kerminen, V. M., Nieminen, T. and Dal Maso, M.: Trends in atmospheric new-particle formation: 16 years of observations in a boreal-forest environment, Boreal Environ. Res., 19(September), 191–214, 2014.

O'dowd, C. D., Jimenez, J. L., Bahreini, R., Flagan, R. C., Seinfeld, J. H., Hämerl, K., Pirjola, L., Kulmala, M. and Hoffmann, T.: Marine aerosol formation from biogenic iodine emissions, Nature, 417(6889), 632–636, doi:10.1038/nature00775, 2002.

Okuljar, M., Kuuluvainen, H., Kontkanen, J., Garmash, O., Olin, M., Niemi, J. V., Timonen, H., Kangasluoma, J., Tham, Y. J., Baalbaki, R., Sipilä, M., Salo, L., Lintusaari, H., Portin, H., Teinilä, K., Aurela, M., Dal Maso, M., Rönkkö, T., Petäjä, T. and Paasonen, P.: Measurement report: The influence of traffic and new particle formation on the size distribution of 1-800nm particles in Helsinki-a street canyon and an urban background station comparison, Atmos. Chem. Phys., doi:10.5194/acp-21-9931-2021, 2021.

Olin, M., Kuuluvainen, H., Aurela, M., Kalliokoski, J., Kuittinen, N., Isotalo, M., Timonen, H. J., Niemi, J. V., Rönkkö, T. and Dal Maso, M.: Traffic-originated nanocluster emission exceeds H2SO4-driven photochemical new particle formation in an urban area, Atmos. Chem. Phys., 20(1), 1–13, doi:10.5194/acp-20-1-2020, 2020.

Paasonen, P., Nieminen, T., Asmi, E., Manninen, H. E., Petäjä, T., Plass-Dülmer, C., Flentje, H., Birmili, W., Wiedensohler, A., Hõrrak, U., Metzger, A., Hamed, A., Laaksonen, A., Facchini, M. C., Kerminen, V. M. and Kulmala, M.: On the roles of sulphuric acid and low-volatility organic vapours in the initial steps of atmospheric new particle formation, Atmos. Chem. Phys., 10(22), 11223–11242, doi:10.5194/acp-10-11223-2010, 2010.

Peters, C., Pechtl, S., Stutz, J., Hebestreit, K., Hönninger, G., Heumann, K. G., Schwarz, A., Winterlik, J. and Platt, U.: Reactive and organic halogen species in three different European coastal environments, Atmos. Chem. Phys., 5(12), 3357–3375, doi:10.5194/acp-5-3357-2005, 2005.

Pierce, J. R., Riipinen, I., Kulmala, M., Ehn, M., Petäjä, T., Junninen, H., Worsnop, D. R. and Donahue, N. M.: Quantification of the volatility of secondary organic compounds in ultrafine particles during nucleation events, Atmos. Chem. Phys., 11(17), 9019–9036, doi:10.5194/acp-11-9019-2011, 2011.

~~Pisso, I., Sollum, E., Grythe, H., Kristiansen, N. I., Cassiani, M., Eckhardt, S., Arnold, D., Morton, D., Thompson, R. L., Groot Zwaaftink, C. D., Evangeliou, N., Sodemann, H., Haimberger, L., Henne, S., Brunner, D., Burkhart, J. F., Fouilloux, A., Brioude, J., Philipp, A., Seibert, P. and Stohl, A.: The Lagrangian particle dispersion model FLEXPART version 10.4, Geosci. Model Dev., doi:10.5194/gmd-12-4955-2019, 2019.~~

Raso, A. R. W., Custard, K. D., May, N. W., Tanner, D., Newburn, M. K., Walker, L., Moore, R. J., Huey, L. G., Alexander, L., Shepson, P. B. and Pratt, K. A.: Active molecular iodine photochemistry in the Arctic, Proc. Natl. Acad. Sci. U. S. A., 114(38), 10053–10058, doi:10.1073/pnas.1702803114, 2017.

Riipinen, I., Yli-Juuti, T., Pierce, J. R., Petäjä, T., Worsnop, D. R., Kulmala, M. and Donahue, N. M.: The contribution of organics to atmospheric nanoparticle growth, Nat. Geosci., 5(7), 453–458, doi:10.1038/ngeo1499, 2012.

Riipinen, I., Yli-Juuti, T., Pierce, J. R., Petäjä, T., Worsnop, D. R., Kulmala, M. and Donahue, N. M.: The contribution of organics to atmospheric nanoparticle growth, Nat. Geosci., doi:10.1038/ngeo1499, 2012b.

~~Rolph, G., Stein, A. and Stunder, B.: Real-time Environmental Applications and Display sYstem: READY, Environ. Model. Softw., 95, 210–228, doi:10.1016/j.envsoft.2017.06.025, 2017.~~

Rong, H., Liu, J., Zhang, Y., Du, L., Zhang, X. and Li, Z.: Nucleation mechanisms of iodic acid in clean and polluted coastal regions, Chemosphere, 253, 126743, doi:10.1016/j.chemosphere.2020.126743, 2020.

Rose, C., Zha, Q., Dada, L., Yan, C., Lehtipalo, K., Junninen, H., Mazon, S. B., Jokinen, T., Sarnela, N., Sipilä, M., Petäjä, T., Kerminen, V. M., Bianchi, F. and Kulmala, M.: Observations of biogenic ion-induced cluster formation in the atmosphere, Sci. Adv., 4(4), 1–11, doi:10.1126/sciadv.aar5218, 2018.

Saiz-Lopez, A. and Plane, J. M. C.: Novel iodine chemistry in the marine boundary layer, Geophys. Res. Lett., 31(4), 1999–2002, doi:10.1029/2003GL019215, 2004.

Saiz-Lopez, A., Plane, J. M. C., Baker, A. R., Carpenter, L. J., Von Glasow, R., Gómez Martín, J. C., McFiggans, G. and Saunders, R. W.: Atmospheric chemistry of iodine, Chem. Rev., 112(3), 1773–1804, doi:10.1021/cr200029u, 2012.

Schade, G. W. and P. J. Crutzen.: Emission of aliphatic-amines from animal husbandry and their reactions: Potential source of N_2O and HCN, *J. Atmos. Chem.*, **22**(3), 319– 346, doi:10.1007/BF00696641, 1995.

Schagerström, E., Forslund, H., Kautsky, L., Pärnoja, M. and Kotta, J.: Does thalli complexity and biomass affect the associated flora and fauna of two co-occurring Fucus species in the Baltic Sea?, Estuar. Coast. Shelf Sci., doi:10.1016/j.ecss.2014.08.022, 2014.

Sipilä, M., Sarnela, N., Jokinen, T., Junninen, H., Hakala, J., Rissanen, M. P., Praplan, A., Simon, M., Kürten, A., Bianchi, F., Dommen, J., Curtius, J., Petäjä, T., and Worsnop, D. R.: Bisulfate – cluster based atmospheric pressure chemical ionization mass spectrometer for high-sensitivity (< 100 ppqV) detection of atmospheric dimethyl amine: proof-of-concept and first ambient data from boreal forest, Atmos. Meas. Tech., 8, 4001–4011, https://doi.org/10.5194/amt-8-4001-2015, 2015.

Sipila, M., Berndt, T., Petaja, T., Brus, D., Vanhanen, J., Stratmann, F., Patokoski, J., Mauldin, R. L., Hyvärinen, A. P., Lihavainen, H. and Kulmala, M.: The role of sulfuric acid in atmospheric nucleation, Science (80-.)., 327(5970), 1243–1246, doi:10.1126/science.1180315, 2010.

Sipilä, M.: Insights Into Atmospheric Nucleation. [online] Available from: https://helda.helsinki.fi/bitstream/handle/10138/154171/insights.pdf?sequence=1, 2010.

Sipilä, M., Sarnela, N., Jokinen, T., Henschel, H., Junninen, H., Kontkanen, J., Richters, S., Kangasluoma, J., Franchin, A., Peräkylä, O., Rissanen, M. P., Ehn, M., Vehkamäki, H., Kurten, T., Berndt, T., Petäjä, T., Worsnop, D., Ceburnis, D., Kerminen, V. M., Kulmala, M. and O'Dowd, C.: Molecular-scale evidence of aerosol particle formation via sequential addition of HIO3, Nature, 537(7621), 532–534, doi:10.1038/nature19314, 2016.

~~Stein, A. F., Draxler, R. R., Rolph, G. D., Stunder, B. J. B., Cohen, M. D. and Ngan, F.: Noaa's hysplit atmospheric transport and dispersion modeling system, Bull. Am. Meteorol. Soc., 96(12), 2059–2077, doi:10.1175/BAMS-D-14-00110.1, 2015.~~

Steinke, M., Hodapp, B., Subhan, R., Bell, T. G. and Martin-Creuzburg, D.: Flux of the biogenic volatiles isoprene and dimethyl sulfide from an oligotrophic lake, Sci. Rep., doi:10.1038/s41598-017-18923-5, 2018.

~~Stohl, A., Forster, C., Frank, A., Seibert, P. and Wotawa, G.: Technical note: The Lagrangian particle dispersion model FLEXPART version 6.2, Atmos. Chem. Phys., doi:10.5194/acp-5-2461-2005, 2005.~~

Stolzenburg, D., Stolzenburg, D., Simon, M., Ranjithkumar, A., Kürten, A., Lehtipalo, K., Lehtipalo, K., Gordon, H., Ehrhart, S., Finkenzeller, H., Pichelstorfer, L., Nieminen, T., He, X. C., Brilke, S., Xiao, M., Amorim, A., Baalbaki, R., Baccarini, A., Beck, L., Bräkling, S., Murillo, L. C., Chen, D., Chu, B., Dada, L., Dias, A., Dommen, J., Duplissy, J., El Haddad, I., Fischer, L., Carracedo, L. G., Heinritzi, M., Kim, C., Kim, C., Koenig, T. K., Kong, W., Lamkaddam, H., Lee, C. P., Leiminger, M., Leiminger, M., Li, Z., Makhmutov, V., Manninen, H. E., Marie, G., Marten, R., Müller, T., Nie, W., Partoll, E., Petäjä, T., Pfeifer, J., Philippov, M., Rissanen, M. P., Rissanen, M. P., Rörup, B., Schobesberger, S., Schuchmann, S., Shen, J., Sipilä, M., Steiner, G., Stozhkov, Y., Tauber, C., Tham, Y. J., Tomé, A., Vazquez-Pufleau, M., Wagner, A. C., Wagner, A. C., Wang, M., Wang, Y., Weber, S. K., Wimmer, D.,

Wimmer, D., Wlasits, P. J., Wu, Y., Ye, Q., Zauner-Wieczorek, M., Baltensperger, U., Carslaw, K. S., Curtius, J., Donahue, N. M., Flagan, R. C., Hansel, A., Hansel, A., Kulmala, M., Lelieveld, J., Volkamer, R., Kirkby, J., Kirkby, J. and Winkler, P. M.: Enhanced growth rate of atmospheric particles from sulfuric acid, Atmos. Chem. Phys., doi:10.5194/acp-20-7359-2020, 2020.

Suikkanen, S., Laamanen, M. and Huttunen, M.: Long-term changes in summer phytoplankton communities of the open northern Baltic Sea, Estuar. Coast. Shelf Sci., 71(3–4), 580–592, doi:10.1016/j.ecss.2006.09.004, 2007.

Suikkanen, S., Pulina, S., Engström-Öst, J., Lehtiniemi, M., Lehtinen, S. and Brutemark, A.: Climate Change and Eutrophication Induced Shifts in Northern Summer Plankton Communities, PLoS One, 8(6), 1–10, doi:10.1371/journal.pone.0066475, 2013.

SYKE press release (29 August 2019), Summary of algal bloom monitoring June-August 2019: Cyanobacteria were mostly mixed in the water in the Finnish sea areas, in lakes the cyanobacteria situation varied a lot. https://www.syke.fi/enUS/Current/Press_releases/Summary_of_algal_bloom_monitoring_JuneAu(51391).

Torn, K., Krause-Jensen, D. and Martin, G.: Present and past depth distribution of bladderwrack (Fucus vesiculosus) in the Baltic Sea, Aquat. Bot., 84(1), 53–62, doi:10.1016/j.aquabot.2005.07.011, 2006.

Väkevä, M., Hämeri, K., Puhakka, T., Nilsson, E. D., Hohti, H. and Mäkelä, J. M.: Effects of meteorological processes on aerosol particle size distribution in an urban background area, J. Geophys. Res. Atmos., 105(D8), 9807–9821, doi:10.1029/1999JD901143, 2000.

Vanhanen, J., Mikkilä, J., Lehtipalo, K., Sipilä, M., Manninen, H. E., Siivola, E., Petäjä, T. and Kulmala, M.: Particle size magnifier for nano-CN detection, Aerosol Sci. Technol., 45(4), 533–542, doi:10.1080/02786826.2010.547889, 2011.

Wagner, R., Manninen, H.E., Franchin, A., Lehtipalo, K., Mirme, S., Steiner, G., Petäjä, T., Kulmala, M.: On the accuracy of ion measurements using a Neutral cluster and Air Ion Spectrometer, Boreal Environ. Res., 21, pp. 230-241, 2016.

Wang, Z., Wu, Z., Yue, D., Shang, D., Guo, S., Sun, J., Ding, A., Wang, L., Jiang, J., Guo, H., Gao, J., Cheung, H. C., Morawska, L., Keywood, M. and Hu, M.: New particle formation in China: Current knowledge and further directions, Sci. Total Environ., doi:10.1016/j.scitotenv.2016.10.177, 2017.

Wang, Z. B., Hu, M., Yue, D. L., Zheng, J., Zhang, R. Y., Wiedensohler, A., Wu, Z. J., Nieminen, T. and Boy, M.: Evaluation on the role of sulfuric acid in the mechanisms of new particle formation for Beijing case, Atmos. Chem. Phys., 11(24), 12663–12671, doi:10.5194/acp-11-12663-2011, 2011.

Weber, R. J., McMurry, P. H., Mauldin, L., Tanner, D. J., Eisele, F. L., Brechtel, F. J., Kreidenweis, S. M., Kok, G. L., Schillawski, R. D. and Baumgardner, B.: A study of new particle formation and growth involving biogenic and trace gas species measured during ACE 1, J. Geophys. Res. Atmos., 103(D13), 16385–16396, doi:10.1029/97JD02465, 1998.

Weber, R. J., McMurry, P. H., Mauldin, R. L., Tanner, D. J., Eisele, F. L., Clarke, A. D. and Kapustin, V. N.:

Formatted: Left, Widow/Orphan control, Adjust space between Latin and Asian text, Adjust space between Asian text and numbers, Pattern: Clear (White)

New particle formation in the remote troposphere: A comparison of observations at various sites, Geophys. Res. Lett., 26(3), 307–310, doi:10.1029/1998GL900308, 1999.

Wimmer, D., Buenrostro Mazon, S., Elina Manninen, H., Kangasluoma, J., Franchin, A., Nieminen, T., Backman, J., Wang, J., Kuang, C., Krejci, R., Brito, J., Goncalves Morais, F., Turnbull Martin, S., Artaxo, P., Kulmala, M., Kerminen, V. M. and Petäjä, T.: Ground-based observation of clusters and nucleation-mode particles in the Amazon, Atmos. Chem. Phys., 18(17), 13245–13264, doi:10.5194/acp-18-13245-2018, 2018.

Yan, C., Yin, R., Lu, Y., Dada, L., Yang, D., Fu, Y., Kontkanen, J., Deng, C., Garmash, O., Ruan, J., Baalbaki, R., Schervish, M., Cai, R., Bloss, M., Chan, T., Chen, T., Chen, Q., Chen, X., Chen, Y., Chu, B., Dällenbach, K., Foreback, B., He, X., Heikkinen, L., Jokinen, T., Junninen, H., Kangasluoma, J., Kokkonen, T., Kurppa, M., Lehtipalo, K., Li, H., Li, H., Li, X., Liu, Y., Ma, Q., Paasonen, P., Rantala, P., Pileci, R. E., Rusanen, A., Sarnela, N., Simonen, P., Wang, S., Wang, W., Wang, Y., Xue, M., Yang, G., Yao, L., Zhou, Y., Kujansuu, J., Petäjä, T., Nie, W., Ma, Y., Ge, M., He, H., Donahue, N. M., Worsnop, D. R., Veli-Matti, K., Wang, L., Liu, Y., Zheng, J., Kulmala, M., Jiang, J. and Bianchi, F.: The Synergistic Role of Sulfuric Acid, Bases, and Oxidized Organics Governing New-Particle Formation in Beijing, Geophys. Res. Lett., doi:10.1029/2020GL091944, 2021.

Yao, L., Garmash, O., Bianchi, F., Zheng, J., Yan, C., Kontkanen, J., Junninen, H., Mazon, S. B., Ehn, M., Paasonen, P., Sipilä, M., Wang, M., Wang, X., Xiao, S., Chen, H., Lu, Y., Zhang, B., Wang, D., Fu, Q., Geng, F., Li, L., Wang, H., Qiao, L., Yang, X., Chen, J., Kerminen, V. M., Petäjä, T., Worsnop, D. R., Kulmala, M. and Wang, L.: Atmospheric new particle formation from sulfuric acid and amines in a Chinese megacity, Science (80-.)., 361(6399), 278–281, doi:10.1126/science.aao4839, 2018.

Yu, H., Ren, L., Huang, X., Xie, M., He, J. and Xiao, H.: Iodine speciation and size distribution in ambient aerosols at a coastal new particle formation hotspot in China, Atmos. Chem. Phys., doi:10.5194/acp-19-4025-2019, 2019.

Zhang, R., Wang, L., Khalizov, A. F., Zhao, J., Zheng, J., McGraw, R. L. and Molina, L. T.: Formation of nanoparticles of blue haze enhanced by anthropogenic pollution, Proc. Natl. Acad. Sci. U. S. A., 106(42), 17650–17654, doi:10.1073/pnas.0910125106, 2009.

Zheng, G., Kuang, C., Uin, J., Watson, T. and Wang, J.: Large contribution of organics to condensational growth and formation of cloud condensation nuclei (CCN) in the remote marine boundary layer, Atmos. Chem. Phys., doi:10.5194/acp-20-12515-2020, 2020.

Formatted: English (United States)

Supplementary Information

An evaluation of new particle formation events in Helsinki during a Baltic Sea cyanobacterial summer bloom

Roseline C. Thakur[1], Lubna Dada[1,2,3], Lisa J. Beck[1], Lauriane L.J. Quéléver[1], Tommy Chan[1], Marjan Marbouti[1,12], Xu-Cheng He[1], Carlton Xavier[1], Juha Sulo[1], Janne Lampilahti[1], Markus Lampimäki[1], Yee Jun Tham[1,11], Nina Sarnela[1], Katrianne Lehtipalo[1,4], Alf Norkko[8,9], Markku Kulmala[1,5,6,7], Mikko Sipilä[1], Tuija Jokinen[1,10]

[1]Institute for Atmospheric and Earth System Research/Physics, Faculty of Science, 00014 University of Helsinki, Helsinki, Finland.

[2]School of Architecture, Civil and Environmental Engineering, École Polytechnique Fédérale de Lausanne, Lausanne, Switzerland

[3]Laboratory of Atmospheric Chemistry, Paul Scherrer Institute, 5232 Villigen PSI, Switzerland

[4]Finnish Meteorological Institute, Helsinki, Finland.

[5]Aerosol and Haze Laboratory, Beijing Advanced Innovation Center for Soft Matter Science and Engineering, Beijing University of Chemical Technology, 100089 Beijing, China.

[6]Joint International Research Laboratory of Atmospheric and Earth System Sciences, Nanjing University, 210023 Nanjing, China.

[7]Lomonosov Moscow State University, Faculty of Geography, 119991, Moscow, GSP-1, 1 Leninskiye Gory.

[8]Tvärminne Zoological Station, University of Helsinki, J.A. Palméns väg 260, FI-10900 Hangö, Finland .

[9]Baltic Sea Centre, Stockholm University, Stockholm, Sweden

[10]Climate & Atmosphere Research Centre (CARE-C), The Cyprus Institute, P.O. Box 27456, Nicosia, CY-1645, Cyprus.

[11]School of Marine Sciences, Sun Yat-Sen University, Zhuhai 519082, China.

[12] Department of Electronics and Nano-engineering, Aalto University, 00076 Aalto, Finland.

Back trajectory calculations

Back trajectories of the different NPF event days were calculated using the data from the Global data Assimilation System (GDAS) as input into the NOAA Hybrid Single-Particle Lagrangian Integrated Trajectory (HYSPLIT) model (http://www.arl.noaa.gov/ready/, Rolph et al., 2017; Stein et al., 2015). We used the isentropic trajectories as they incorporate vertical transport components. The 24 h back trajectories were calculated at an arrival height of 100 m a.g.l. The new trajectory starts every 6 hours. The frequency (%) of trajectory was calculated with the following equation (Eq. (1)).

$$\text{Traj. Freq.} = \frac{100 \times number\ of\ trajectories\ passing\ through\ each\ grid\ square}{number\ of\ trajectories} \quad (1)$$

The trajectory analysis was also performed using the Lagrangian particle dispersion model Flexpart v10.4 (Pisso et al., 2019; Stohl et al., 2005) mainly to assess the residence times of the air masses. Flexpart is a stochastic model used to compute trajectories of hypothetical particles, based on mean as well as turbulent and diffusive flow (Pisso et al., 2019). We have used Flexpart along with ECMWF ERA-Interim wind-fields which has a spatial resolution of 1°×1° at three hour temporal resolution (Pisso et al., 2019). Flexpart was used to simulate 3-day backward trajectories starting from the particle release point located at SMEAR III (24.5° E, 60.1° N) for the event days. The residence times were normalized for clarity in the all the figures and is shown on a scale of 0 to 1.

Meteorological and other supporting data

The meteorological data such as wind speed, wind direction, temperature, pressure, relative humidity and other supporting datasets e.g chlorophyll (Chl-*a*), SO_2, O_3 concentration and sea level information was additionally used to interpret the NPF events and support the observations of this work (See table S1 for details). All the meteorological parameters are measured by sensors installed on the roof of the physicum building (where CI-APiTOF was housed). Thus we can say that the precursor vapor concentrations measured by the CI-APiTOF was not influenced by any vertical mixing of airmasses since the sensors for meterological parameters (installed on the roof of 5th floor, physicum building and CI-APiTOF (installed on the 4th floor, physicum building) was almost at the same height. However, the measurements for particle size distributions was carried out at SMEAR III, which is 25 m a.m.sl and the wind vane at the physicum building was situated roughly at 50 m a.m.s.l. ,we state that the particle size distribution data might not be completely free from downward vertical mixing of airmass and should be treated with certain uncertainty. However, near the SMEAR III station, the

Formatted: Not Highlight

Field Code Changed

Formatted: Not Highlight

mixing usually affected the larger particles, decreasing their number concentration (Järvi et al., 2009). So we can assume that the uncertainties in the number concentration of nucleation and Aitken mode particles would be negligible in this study.

The Chl-*a* satellite images were mapped through the GlobColour level-3. The GlobColour level-3 mapped products present merged data from SeaWIFS, MERIS, MODIS AQUA, VIIRS (0'Reily et al., 2000) sensors to provide robust and high coverage data for Chl-*a* measurements. The merging processes are described in Mangin and d'Andon, 2017. In this study, weighted average method (AVW) for retrieving daily Chl-*a* concentration (mg m^{-3}) for latitude: 45 °N to 80 °N and longitude: 20 °W to 60 °E was used. The GlobColour level-3 binned products have a resolution of 1/24° at the equator (i.e. around 4.63 km) for global products (Mangin and d'Andon, 2017). The details of these additional supporting data given in SI (Table S1). However this resolution is not high enough to demarcate the contribution of Chla from cyanobacteria and macroalgae in the marine region. Nonetheless, the contribution of macrolagae to Chl*a* still holds a significant place since the Baltic Sea and other regions of Gulf of Finland are abundant in microalgae.

Formatted: Font: (Default) Times New Roman, 12 pt, Font color: Auto, English (United States), Pattern: Clear

Formatted: Font: (Default) Times New Roman, 12 pt, Italic

Formation and growth rate calculations

The growth rates (GRs) were calculated based on the 50% appearance time method using the NAIS ion data from both polarities, depending on the better quality polarity (Dada et al., 2020; Dal Maso et al., 2016; Lehtipalo et al., 2014). This method uses particle number concentration at different size bins (D*p*), which are recorded as a function of time. The "appearance time" of particles of size D*p* is the time when their number concentration reaches 50% of its maximum value during the NPF event. To estimate the maximum GR (kinetic) that can be explained by the condensation of certain vapors, two parametrization methods were used, first by Nieminen et al., 2010 for IA and MSA and the second by Stolzenburg et al., 2020 for SA. The growth estimation from SA condensation recently provided by Stolzenburg et al., 2020 also takes into account the hydration of SA particles and dipole-dipole enhancement which is responsible for increasing the collision rate between neutral molecules and neutral particles. As these parameters were not known for IA and MSA, we used the method by Nieminen et al. (2010) for them. The growth due to MSA could be slightly overestimation by this method (Beck et al., 2021) since the parameterization is based on the assumption of irreversible condensation, but MSA rapidly partitions between gas and particle phases if suitable meteorological conditions prevail. The calculated kinetic GR was compared with the total measured particle GR to determine the contribution of each vapor to the growth process (discussed in further sections).

Formatted: Not Highlight

Field Code Changed

Field Code Changed

Formatted: Not Highlight

Formatted: Not Highlight

Formatted: Not Highlight

The formation rate of the total particles of mobility diameter 1.5 nm is calculated using the time derivative of the particle number concentration measured using the PSM in the size range 1.5– 3 nm. The formation rate was corrected for the coagulation losses and growth out of the bin following the method explained by Kulmala et al. 2012. The formation rate of the charged particles was calculated from the time derivative of ions measured using the NAIS in ion mode in size range 1.5–3 nm from both polarities. The formation rate of ions was corrected for coagulation sink, growth outside of the bin, ion-ion recombination and ion-neutral attachment as previously discussed in Kulmala et al. 2012.

Formatted: Not Highlight

Table S1 Details of Instruments and other supporting data

Parameter measured	**Technique**	**Instrument**	**Resolution and detection limits**	**Site of Measurement**
SO_2	UV-fluorescence technique	Horiba APSA 360	60 s detection limit: 0.2 ppb	a
NO_x	Chemiluminescence technique + thermal (molybdenum) converter	TEI42S	60 s detection limit: 0.2 ppb	a
~~O_2~~O_3	IR-absorption photometer	TEI 49	60 s detection limit: 0.5 ppb	a
Air Temperature	Platinum resistance thermometer	Pt-100	60 s	b
Wind direction	2-D ultrasonic anemometer	Thies Clima ver. 2.1x	10 s	b
Wind Speed	Platinum resistance thermometer + thin film polymer sensor	Vaisala DPA500	4 min	b
Relative humidity	Platinum resistance thermometer + thin film polymer sensor	Vaisala DPA500	4 min	b
Global Radiation	Net radiometer	Kipp & Zonen CNR1	60s	b
Tidal Height	wave buoys		c	Helsinki Suomenlina, Gulf of Bothnia, Northern Baltic Sea

[a] SMEAR III station

[b]roof of university of Helsinki (UHEL) Building (kumpula campus)

[c]Wave height is the vertical difference between the wave through and the wave crest. The significant wave height is calculated as the average of one third of the highest waves from the energy spectrum.

The cloudiness parameter

It is defined as is the ratio of measured global radiation (R_d) divided by the theoretical global irradiance (Rg):

$$P = \frac{R_d}{R_g}$$

The theoretical maximum of global radiation (R_g) is calculated by taking into consideration the latitude of the measurement station and the seasonal solar cycle. P < 0.3 defines a complete cloud coverage and P > 0.7 defines clear-sky conditions .This classification is followed by man previous studies (Perez et al., 1990; Sogacheva et al., 2008; Sánchez et al., 2012).

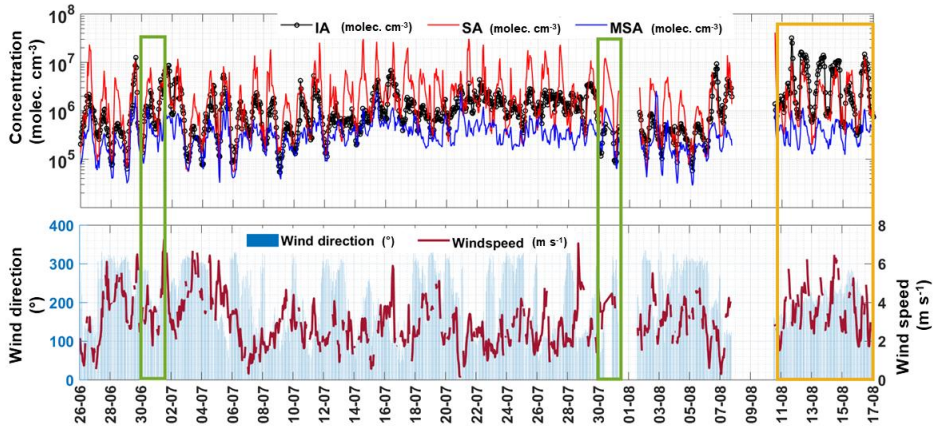

Figure S1: Time series concentration of SA, MSA and IA (60min averaged data) and their variability with changing wind speed and wind direction (30min averaged data). The Green boxes denote the local events and yellow box is covers the time period when the burst/spike events were observed during the study.

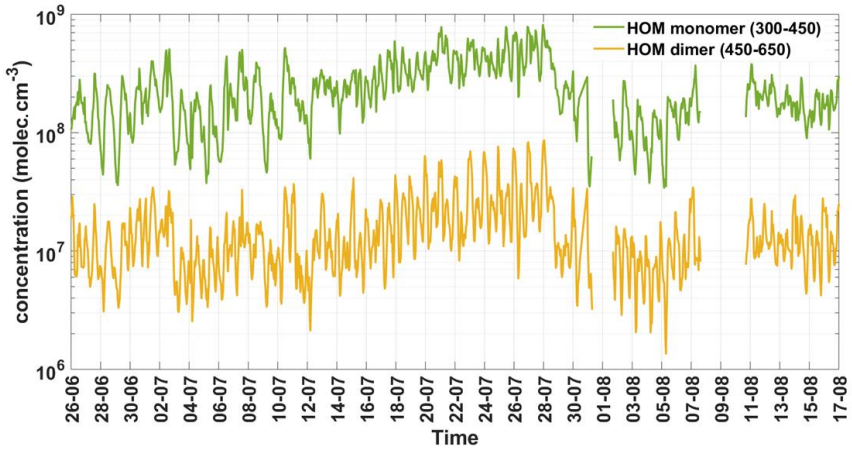

Figure S2: Time series variability in HOM monomer (sum of mass range 300-450 m/z) and dimer (sum of mass range 450-650 m/z) concentration during the study period (60min averaged data from CI-Api-ToF)**.** Note the concentrations are plotted using the unit mass resolution data.

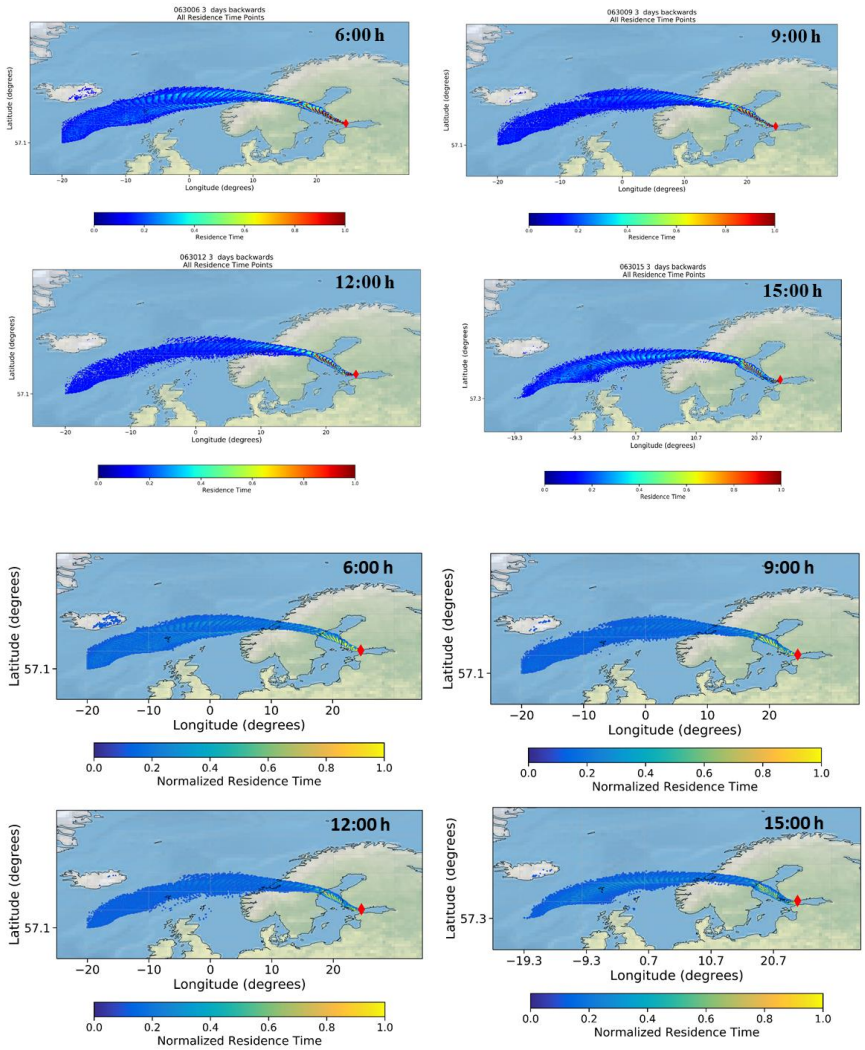

Figure S3: **Normalized** residence times of air masses (3-day backwards) arriving at the experimental site on 30 June 2019. The color bar indicates the normalized residence times for each subplot. The residence time of particles originating 3 days before reaching SMEAR III is shown for ~~3~~6:00 h, ~~6~~9:00 h, ~~9~~12:00 h and ~~12~~15:00 h. The red shaded areas indicate the latitude/longitude pairs having the maximum residence time.

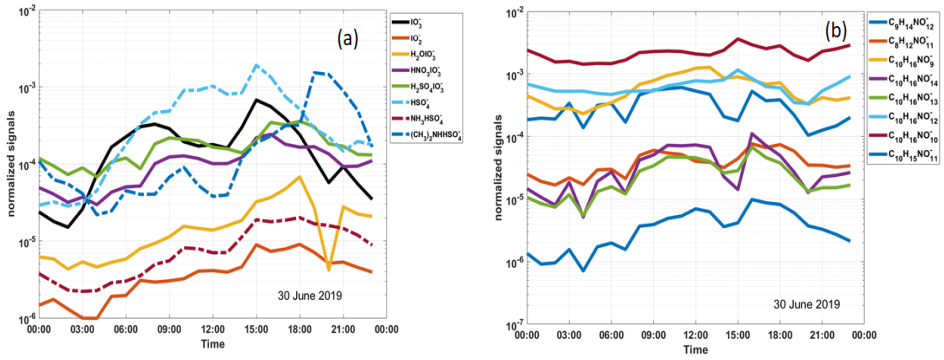

Figure S4: Diurnal variation of the inorganic clusters (a) and organic clusters (b) observed during the NPF event on 30th June 2019 as seen from the spectrum of CI-ApiToF.

Local/regional event 30 July 2019

Another local/regional event ~~probably driven by SA~~ was observed on 30 July 2019 (Fig. S5a), forming particles, which grew to almost CCN relevant sizes. The growth of ions and particles actually occurred from 07:45 h-11:15 h (Fig. S5a and S5b). By this time, the particles had reached around 50 nm in size (lower limit of CCN).The highest $J_{1.5}$ was 3.7 cm^{-3} s^{-1} was observed at 09:00 h, significantly higher than *J* (ions), indicative of a neutral dominated nucleation event (Fig. S5c). After 11:30 h, we observe a group of fragmented burst or spike events without clear growth pattern. No significant variation in formation rates was observed in the positive and the negative mode (Fig. S5b). A clear increase in sub-3 nm (1.25–3.1 nm) particle concentration (from 10^2 to $>10^3$) is seen during this event and formation rate of the smallest particles ($J_{1.5}$) increases from 0.9 cm^{-3} s^{-1} to 3.8 cm^{-3} s^{-1} between 06:00 -09:00 h indicating cluster formation (neutral nucleation) (Fig. S5c). A 10 times increase in sub 3nm particles is observed once the cluster formation initiated (07:45 h, local time UTC+2 h) when the concentration of SA increases from 8.2×10^6 to 1.2×10^7molec. cm^{-3} and ~~The~~ the nucleation mode particles how a signifiacnt increase from ~2000 cm^{-3} to ~10 000 cm^{-3} during the event, however we do not see any significant increase in Aitken and accumulation mode particles~~.~~ (Fig. S5e). The aitken mode particle concentration starts to increase after a time lag of 40 min. Unfortunately, in this case we cannot discuss on the SA concentration after 12:00 h as data recording was disrupted between 12:30-20:30 h. The highest SA concentration during this event was 1.22×10^7 molec cm^{-3} as compared to IA and MSA which were one order of magnitude lower than SA (1.15×10^6 and 5.28×10^6 molec. cm^{-3}, respectively) (Fig. S5d). The particles reached the size of 40 nm at around 11:30 h after which

the event ceases. The ~~condensation sink and the~~ accumulation mode particles remain more or less constantly low, yet we observe a disruption in the event. A change in wind direction from 120° to 200° was observed between 11:30–12:30 h, which lead to the observation that we do not see regional NPF (growing particles) in the changed air mass. The cynobacteria bloom on 30 July 2019 was not much spread in the sea areas (Fig. S5f).

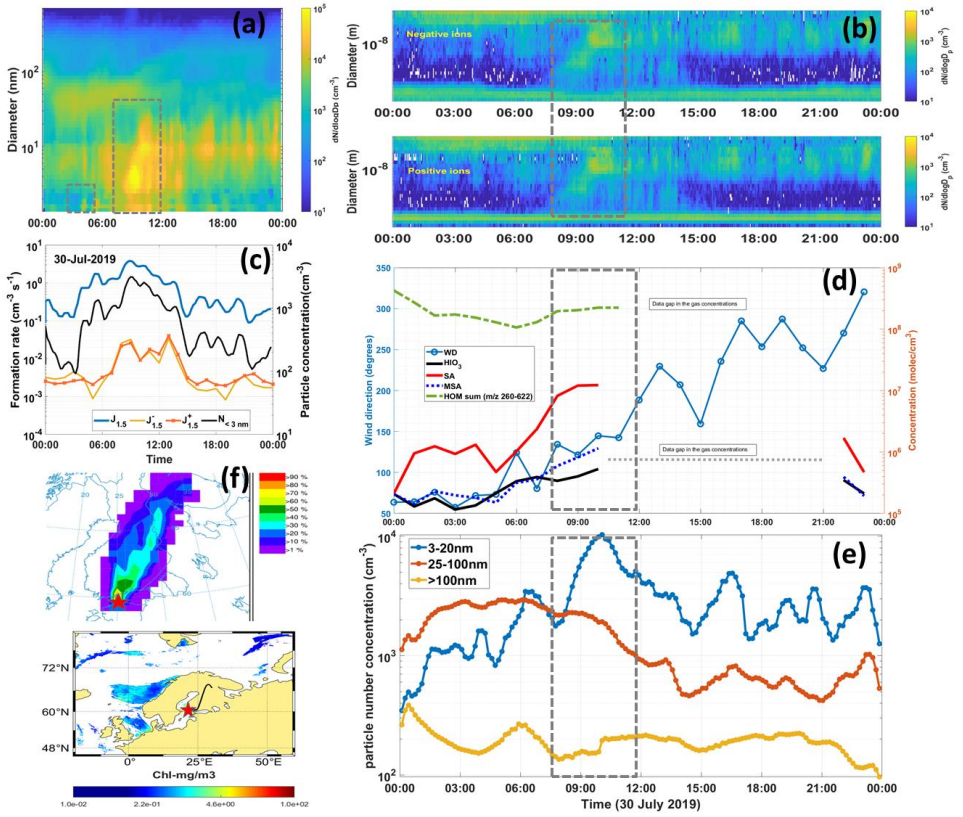

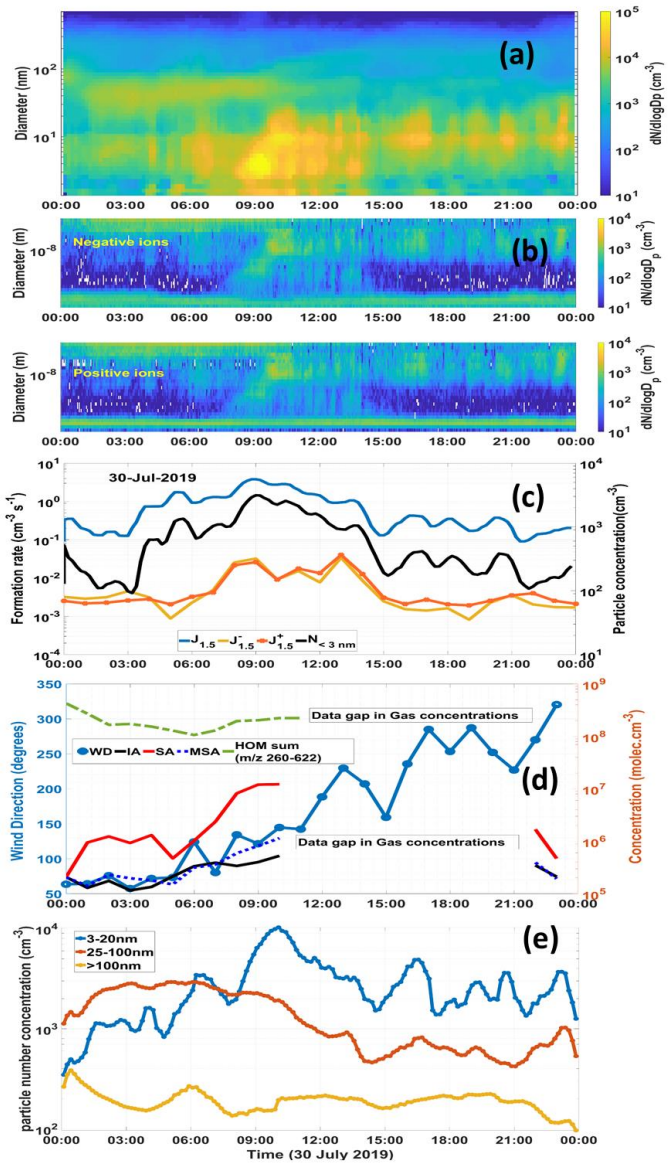

Figure S5: Local/regional Event, 30 July 2019. (a) Number size distribution of particles (data combined from PSM,NAIS and DMPS; size range: sub-3 nm–1000nm). (b) Charged particle number size distribution (negative: upper, positive: lower) obtained from the NAIS~~Size distribution of ions during the event (NAIS)~~. (c) formation rates ($J_{1.5}$) of 1.5 nm particles and ions ($J^-_{1.5}$ and $J^+_{1.5}$) particle

Formatted: Centered

number concentrations (<3 nm). (d) Dirunal variation of HOMs, SA, IA and MSA with wind direction (WD). (e) The concentration of nucleation (3–10 nm) Aitken (10–100 nm) and accumulation mode (>100nm) particles during the event.

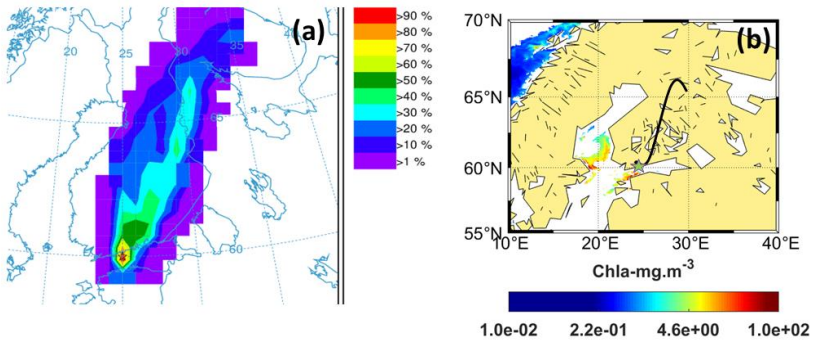

Figure S6: (a)~~(f)~~ Trajectory frequency plot (100 a.g.l, arrival time of trajectory at the measurement site: 22:00 h) for 24 h back trajectory using GDAS meterological input data (frequency grid resolution: 1.0° × 1.0°) ~~and~~ (b) Chl-*a* concentrations (GlobColour level-3~~MODIS~~); Black line shows the trajectory direction and the star point denotes the measurement site. ~~The dashed black lines show denote the time stamp of the nucleation events.~~

Even in lakes the abundance of cynobacteria was sparse. Only cynobacterial bloom was found in Southern edge of Gulf of Bothania and northern most part of the Baltic sea. The trajectory frequency plots showed that most of the trajectories were from the northern land areas (including urban cities and boreal forests) of Finland (Fig. S5f) with highest residence times over these land regions. Therefore, the precursor gases from the biogenic origin, IA and MSA do not show a significant concentration increase as compared to SA, during this event and hence their contribution towards the initation of the NPF event may not be as significant as SA~~Therefore the precursor gases from the cynobacteria bloom, IA and MSA do not show a significant concentration increase during this event and hence are assumed to be contributing insignificantly to this event~~. The greater residence times over the land areas clearly support SA-driven NPF with possible contribution of organics.

Formatted: Font: Bold

Formatted: Font: (Default) Times New Roman, 12 pt, Do not check spelling or grammar

Formatted: Font: (Default) Times New Roman, 12 pt, Do not check spelling or grammar

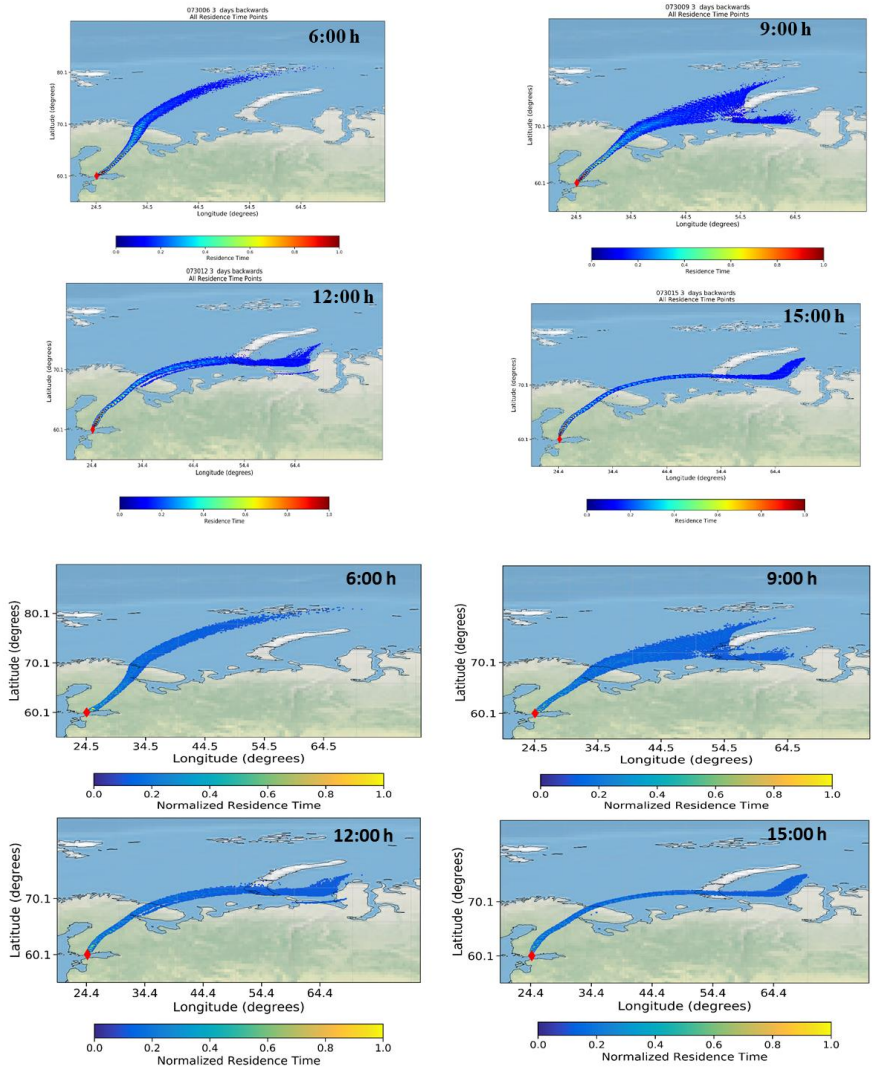

Figure ~~S6~~S7: Normalized ~~Residence~~ residence times of Air masses (3-day backwards) arriving at the experimental site on 30 July 2019. The color bar indicates the normalized residence times for each subplot. The residence time of particles originating 3 days before reaching SMEAR III is shown for 6:00 h, 9:00 h, 12:00 h and 15:00 h. The red shaded areas indicate the latitude/longitude pairs having the maximum residence time. Note the highest residence times over the land areas.

Formatted: Font: Not Bold

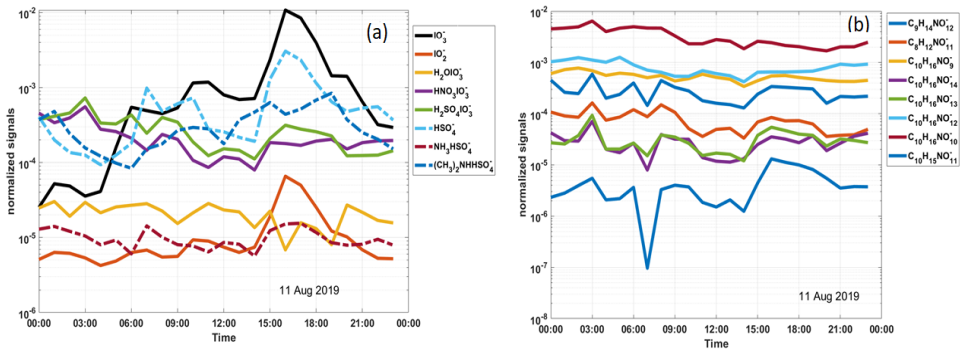

Figure ~~S7~~S8: Diurnal variation of the inorganic (a) and organic clusters (b) observed during the NPF event on 11 August 2019

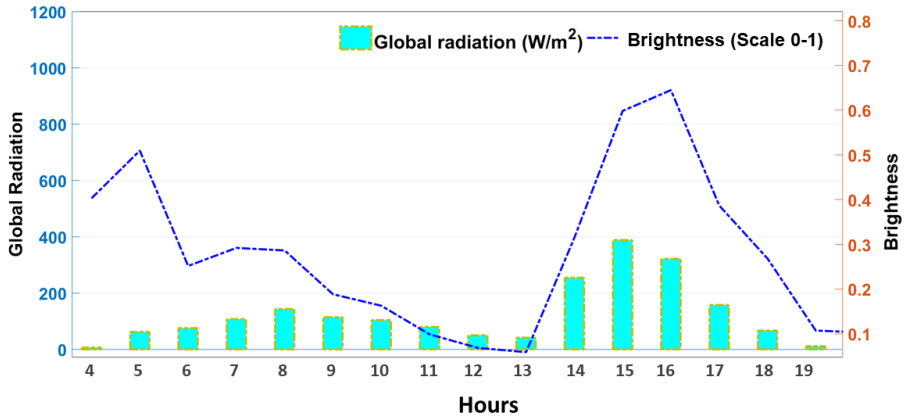

Figure ~~S8~~S9: Diurnal variability of global radiation and estimated cloudiness on 11 August 2019. Note the increased radiation and brightness from 14–16 h (time when NPF starts).

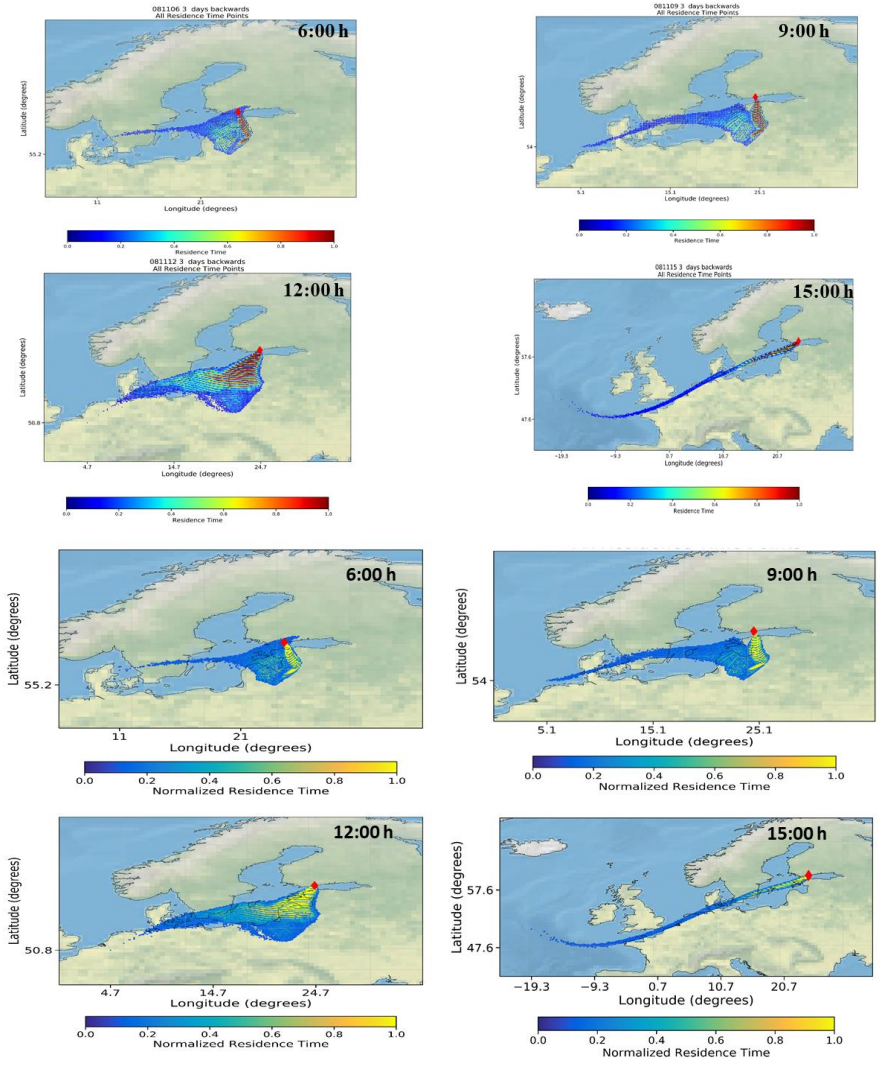

Figure ~~S9~~S10: Normalized r~~R~~esidence times of air masses (3-day backwards) arriving at the experimental site on 11 August 2019. The color bar indicates the normalized residence times for each subplot. The residence time of particles originating 3 days before reaching SMEAR III is shown for 6:00 h, 9:00 h, 12:00 h and 15:00 h. The red shaded areas indicate the latitude/longitude pairs having

the maximum residence time. Note the highest residence times over Baltic Sea region at 15:00 h (highest IA concentration was observed).

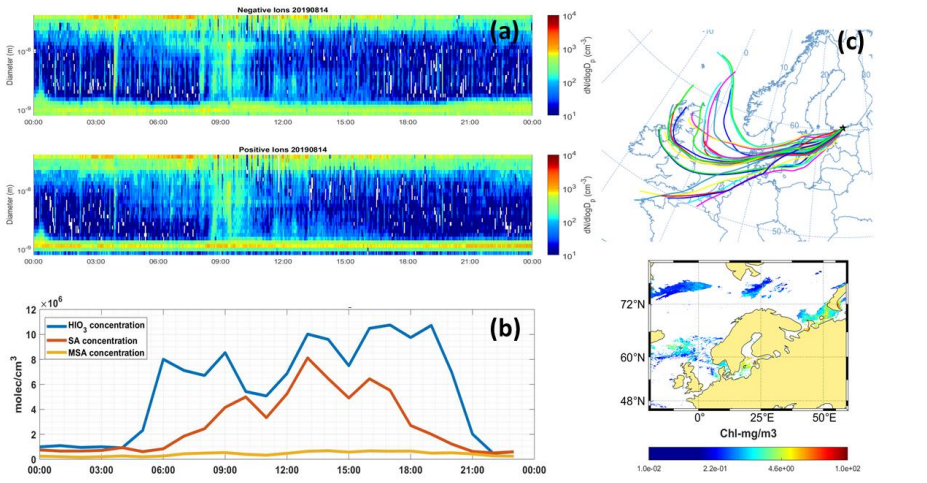

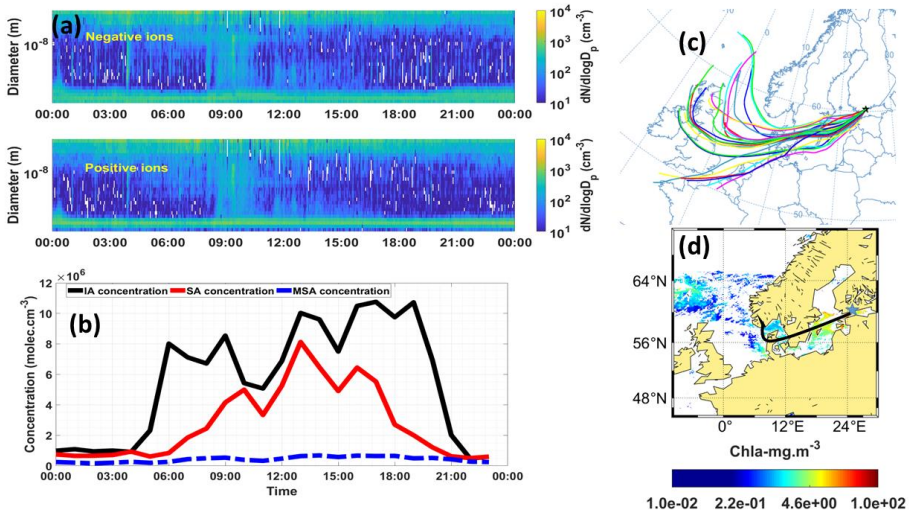

Figure ~~S10~~S11: (a) Charged particle number size distribution (negative: upper, positive: lower) obtained from the NAIS. (b) concentration of SA, IA and MSA. (c) Trajectory analyis plot (100 a.g.l) for 24 h back trajectory using GDAS meterological input data (frequency grid resolution: 1.0° × 1.0°)

and (d) Chl-*a* concentrations (GlobColour level-3MODIS) for 14 August 2019. Black line shows the trajectory direction and the star point denotes the measurement site.

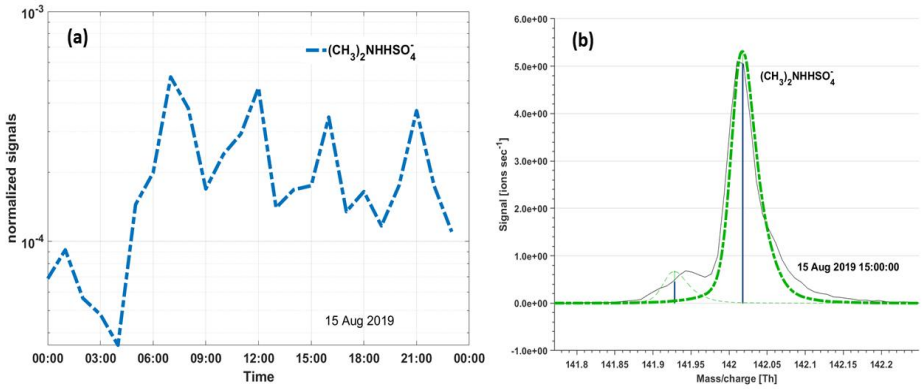

Figure S11S12: (a) Diurnal variation of the DMA-SA cluster (CI-ApiToF) observed during the NPF event on 15 August 2019. (b) The prominent peak of DMA-SA cluster seen at the peaktime of NPF at 15:00 h.

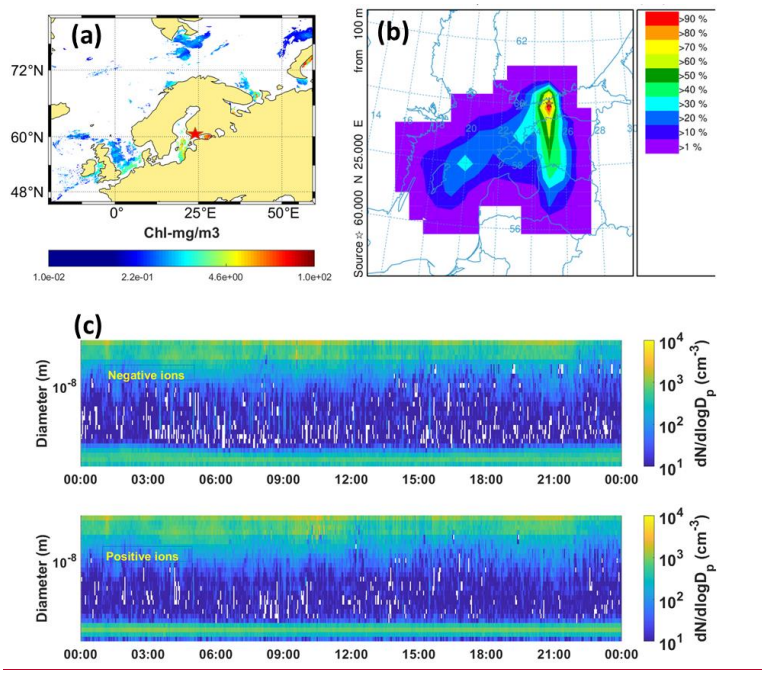

Figure S13: No event day, 17August 2019 (a): Satellite map showing Chl*a* concentrations (GlobColour level-3) (b) Trajectory analyis plot (100 a.g.l) for 24 h back trajectory using GDAS meterological input data (frequency grid resolution: 1.0° × 1.0°). (c) Charged particle number size distribution (negative: upper, positive: lower) obtained from the NAIS.

References:

Beck, L. J., Sarnela, N., Junninen, H., Hoppe, C. J. M., Garmash, O., Bianchi, F., Riva, M., Rose, C., Peräkylä, O., Wimmer, D., Kausiala, O., Jokinen, T., Ahonen, L., Mikkilä, J., Hakala, J., He, X. C., Kontkanen, J., Wolf, K. K. E., Cappelletti, D., Mazzola, M., Traversi, R., Petroselli, C., Viola, A. P., Vitale, V., Lange, R., Massling, A., Nøjgaard, J. K., Krejci, R., Karlsson, L., Zieger, P., Jang, S., Lee, K., Vakkari, V., Lampilahti, J., Thakur, R. C., Leino, K., Kangasluoma, J., Duplissy, E. M., Siivola, E., Marbouti, M., Tham, Y. J., Saiz-Lopez, A., Petäjä, T., Ehn, M., Worsnop, D. R., Skov, H., Kulmala, M., Kerminen, V. M. and Sipilä, M.: Differing Mechanisms of New Particle Formation at Two Arctic Sites, Geophys. Res. Lett., doi:10.1029/2020GL091334, 2021.

Dada, L., Lehtipalo, K., Kontkanen, J., Nieminen, T., Baalbaki, R., Ahonen, L., Duplissy, J., Yan, C., Chu, B., Petäjä, T., Lehtinen, K., Kerminen, V. M., Kulmala, M. and Kangasluoma, J.: Formation and

Formatted: Font: Bold

Formatted: Font: 11 pt

growth of sub-3-nm aerosol particles in experimental chambers, Nat. Protoc., 15(3), 1013–1040, doi:10.1038/s41596-019-0274-z, 2020.

Dal Maso, M., Liao, L., Wildt, J., Kiendler-Scharr, A., Kleist, E., Tillmann, R., Sipilä, M., Hakala, J., Lehtipalo, K., Ehn, M., Kerminen, V. M., Kulmala, M., Worsnop, D. and Mentel, T.: A chamber study of the influence of boreal BVOC emissions and sulfuric acid on nanoparticle formation rates at ambient concentrations, Atmos. Chem. Phys., 16(4), 1955–1970, doi:10.5194/acp-16-1955-2016, 2016.

Järvi, L., Hannuniemi, H., Hussein, T., Junninen, H., Aalto, P. P., Hillamo, R., Mäkelä, T., Keronen, P., Siivola, E., Vesala, T. and Kulmala, M.: The urban measurement station SMEAR III: continuous monitoring of air pollution and surface–atmosphere interactions in Helsinki, Finland. Boreal Environ. Res., 14 (suppl. A), 86–109, 2009.

Kulmala, M., Petäjä, T., Nieminen, T., Sipilä, M., Manninen, H. E., Lehtipalo, K., Dal Maso, M., Aalto, P. P., Junninen, H., Paasonen, P., Riipinen, I., Lehtinen, K. E. J., Laaksonen, A. and Kerminen, V. M.: Measurement of the nucleation of atmospheric aerosol particles, Nat. Protoc., 7(9), 1651–1667, doi:10.1038/nprot.2012.091, 2012.

Lehtipalo, K., Kontkanen, J., Kangasluoma, J., Franchin, A., Wimmer, D., Schobesberger, S., Junninen, H., Petäjä, T., Sipilä, M., Worsnop, D. R., Kulmala, M., Lehtipalo, K., Mikkilä, J., Vanhanen, J., Leppä, J. and Worsnop, D. R.: Methods for determining particle size distribution and growth rates between 1 and 3 nm using the Particle Size Magnifier, Boreal Environ. Res., 19(September), 215–236, 2014.

Mangin, A., and d'Andon., O.F.: GlobColour Product User Guide, GC-UM-ACR-PUG-01, Version 4.1, 2017.

Nieminen, T., Lehtinen, K. E. J. and Kulmala, M.: Sub-10 nm particle growth by vapor condensation-effects of vapor molecule size and particle thermal speed, Atmos. Chem. Phys., doi:10.5194/acp-10-9773-2010, 2010.

Perez, R., Ineichen, P., Seals, R., and Zelenka, A.: Making full use of the clearness index for parameterizing hourly insolation conditions, Solar Energ., 45, 111–114, doi:10.1016/0038- 092X(90)90036-C, 1990.

Pisso, I., Sollum, E., Grythe, H., Kristiansen, N. I., Cassiani, M., Eckhardt, S., Arnold, D., Morton, D., Thompson, R. L., Groot Zwaaftink, C. D., Evangeliou, N., Sodemann, H., Haimberger, L., Henne, S., Brunner, D., Burkhart, J. F., Fouilloux, A., Brioude, J., Philipp, A., Seibert, P. and Stohl, A.: The Lagrangian particle dispersion model FLEXPART version 10.4, Geosci. Model Dev., doi:10.5194/gmd-12-4955-2019, 2019.

Rolph, G., Stein, A. and Stunder, B.: Real-time Environmental Applications and Display sYstem: READY, Environ. Model. Softw., 95, 210–228, doi:10.1016/j.envsoft.2017.06.025, 2017.

Formatted: Font: (Default) Times New Roman, English (United States)

Formatted: Font: 11 pt

Formatted: Default Paragraph Font, Font: (Default) Times New Roman, English (United States), Border: : (No border), Pattern: Clear

Formatted: Font: 11 pt, English (United States)

Formatted: Font: 11 pt

Formatted: Font: (Default) Times New Roman, Font color: Auto, English (United States), Border: : (No border), Pattern: Clear

Formatted: Font: 11 pt

Formatted: Font: (Default) Times New Roman, Font color: Auto, English (United States), Pattern: Clear

Formatted: Font: 11 pt

Formatted: Font: (Default) Times New Roman

Sánchez, G., Serrano, A., and Cancillo, M.: Effect of cloudiness on solar global, solar diffuse and terrestrial downward radiation at Badajoz (Southwestern Spain), Optica pura y aplicada, 45, 33– 38, 2012.

Sogacheva, L., Saukkonen, L., Nilsson, E., Dal Maso, M., Schultz, D. M., De Leeuw, G., and Kulmala, M.: New aerosol particle formation in different synoptic situations at Hyytiälä, southern Finland, Tellus B, 60, 485–494, doi:10.1111/j.1600- 0889.2008.00364.x, 2008.

Stein, A. F., Draxler, R. R., Rolph, G. D., Stunder, B. J. B., Cohen, M. D. and Ngan, F.: Noaa's hysplit atmospheric transport and dispersion modeling system, Bull. Am. Meteorol. Soc., 96(12), 2059–2077, doi:10.1175/BAMS-D-14-00110.1, 2015.

Stohl, A., Forster, C., Frank, A., Seibert, P. and Wotawa, G.: Technical note: The Lagrangian particle dispersion model FLEXPART version 6.2, Atmos. Chem. Phys., doi:10.5194/acp-5-2461-2005, 2005.

Stolzenburg, D., Stolzenburg, D., Simon, M., Ranjithkumar, A., Kürten, A., Lehtipalo, K., Lehtipalo, K., Gordon, H., Ehrhart, S., Finkenzeller, H., Pichelstorfer, L., Nieminen, T., He, X. C., Brilke, S., Xiao, M., Amorim, A., Baalbaki, R., Baccarini, A., Beck, L., Bräkling, S., Murillo, L. C., Chen, D., Chu, B., Dada, L., Dias, A., Dommen, J., Duplissy, J., El Haddad, I., Fischer, L., Carracedo, L. G., Heinritzi, M., Kim, C., Kim, C., Koenig, T. K., Kong, W., Lamkaddam, H., Lee, C. P., Leiminger, M., Leiminger, M., Li, Z., Makhmutov, V., Manninen, H. E., Marie, G., Marten, R., Müller, T., Nie, W., Partoll, E., Petäjä, T., Pfeifer, J., Philippov, M., Rissanen, M. P., Rissanen, M. P., Rörup, B., Schobesberger, S., Schuchmann, S., Shen, J., Sipilä, M., Steiner, G., Stozhkov, Y., Tauber, C., Tham, Y. J., Tomé, A., Vazquez-Pufleau, M., Wagner, A. C., Wagner, A. C., Wang, M., Wang, Y., Weber, S. K., Wimmer, D., Wimmer, D., Wlasits, P. J., Wu, Y., Ye, Q., Zauner-Wieczorek, M., Baltensperger, U., Carslaw, K. S., Curtius, J., Donahue, N. M., Flagan, R. C., Hansel, A., Hansel, A., Kulmala, M., Lelieveld, J., Volkamer, R., Kirkby, J., Kirkby, J. and Winkler, P. M.: Enhanced growth rate of atmospheric particles from sulfuric acid, Atmos. Chem. Phys., doi:10.5194/acp-20-7359-2020, 2020.

Formatted: Font: 11 pt

Formatted: Font: (Default) Times New Roman

Formatted: Font: 11 pt

Formatted: Font: (Default) Times New Roman

Formatted: Font: 11 pt

Formatted: Font: 11 pt